Tunneling in Presence of Chaos and Interactions

Habilitationsschrift

zur Erlangung der Lehrbefähigung für Physik
in der Naturwissenschaftlichen Fakultät II – Physik
der Universität Regensburg

vorgelegt von

Peter Schlagheck

Regensburg 2006

Die Stimme des Intellekts ist leise,
aber sie ruht nicht,
ehe sie sich Gehör verschafft hat.

Sigmund Freud

Table of Contents

Introduction

Together with entanglement and interference, tunneling certainly belongs to the most spectacular implications of quantum theory. The possibility of a quantum particle to penetrate an energetic barrier, and thereby undergo a transition that is classically impossible, has led to a number of fascinating phenomena and experiments, resulting in various applications in atomic and molecular physics as well as in mesoscopic science. We mention for instance the scanning tunneling microscope [1] where electrons escape from the surface of a solid-state sample into a positively charged metallic tip, thereby providing detailed and sensitive information about the structure of the surface. Other relevant examples can be found in the field of superconductivity (the Josephson effect [2]) as well as in the context of modern device technology, e.g. resonant tunneling diodes [3] or the effect of tunneling magnetoresistance which permits spin-dependent currents through small ferromagnetic junctions [4]. Although the phenomenon of tunneling became apparent already in the very early days of quantum theory [5], it still stimulates active theoretical and experimental research in our time, as is documented by various reviews on the subject (e.g. [6–8]).

Throughout this thesis, we shall consider tunneling processes as transitions of quantum particles (in configuration space or phase space) that are not possible in the underlying classical description. This working definition necessarily implies that the quantum system under consideration exhibits a classical counterpart, and thereby excludes the manifestation of tunneling in "abstract" quantum setups composed, e.g., by two- or three-level systems. We remark that the notion of tunneling is sometimes used in a more general way: In the quantum dynamics within spatially periodic potentials, for instance, the transition between different bands is termed "Landau-Zener tunneling" [9], irrespective of whether the underlying classical process is allowed (in the case of small barriers of the periodic potential) or forbidden. Such processes are not discussed in this thesis.

Probably the most prominent textbook scenario for the manifestation of tunneling is the quantum dynamics of a particle in a symmetric double well potential

(see Figure 1.1(a)). Below the energy of the barrier that separates the two wells, the eigenspectrum of this system consists of pairs of energy levels that are nearly degenerate. The associated eigenstates are given by the symmetric and antisymmetric combinations of the left-well and right-well *quasi-modes*, i.e., of the wavefunctions that are semiclassically constructed upon the invariant phase-space orbits in the respective wells [10]. The energetic splitting of the doublets is induced by a small matrix element between those quasi-modes, which reflects the nonclassical coupling process through the barrier. Preparing the initial state of the system on, say, the energetically lowest quasi-mode in the left well consequently leads to Rabi oscillations between the wells, which take place on a time scale that is given by the inverse of the splitting between the lowest symmetric and antisymmetric eigenenergy.

This double-well scenario arises in a number of situations in the context of molecular dynamics. It was indeed considered in one of the first studies on tunneling [11], which focused on the motion of an outer electron in a diatomic molecule where the classical dynamics is characterized by an impenetrable barrier between the atoms. Another prominent example is the NH_3 molecule where the transition of the nitrogen atom through the triangle formed by the three hydrogen atoms is classically forbidden, but can be triggered quantum mechanically by an external field (what is used in the ammonium maser [12]).

Tunneling can also manifest in *open* systems, where a quantum particle that is confined to a metastable potential well can escape, by penetration through finite barriers, into the free space (see Figure 1.1(b)). In this case, the local quasi-mode within the well does not correspond to a bound state, but is embedded into the continuous spectrum of free, unbound motion outside the well. As a consequence, the continuum is "structured" due to the admixture of this bound-state component and exhibits a *spectral resonance* the width of which is given by the square modulus of the coupling matrix element across the barrier [13].

This classically forbidden decay process played an important role in the early history of quantum tunneling. The most prominent example in this context is the alpha decay of heavy nuclei, where the alpha particle escapes via penetration through the barrier that is formed by the combination of the strong nuclear interaction and the Coulomb repulsion. A semiclassical analysis of the problem, leading to the celebrated "Gamov factor", provided an excellent quantitative explanation of the lifetimes of radioactive isotopes [14]. More "modern" examples can be found, e.g., in the field of laser ionization of atoms where tunneling manifests in various ways. A particularly complex situation arises in the *nonsequential double ionization* of two-electron atoms that are exposed to an intense laser field [15, 16]. As was worked out in a number of experimental and theoretical investigations [17–20], this process takes place via a combination of both classically forbidden and classically allowed components, namely the field-induced emission of the outer electron (due to tunneling) and the ejection of the inner electron due to a recollision process (induced by the

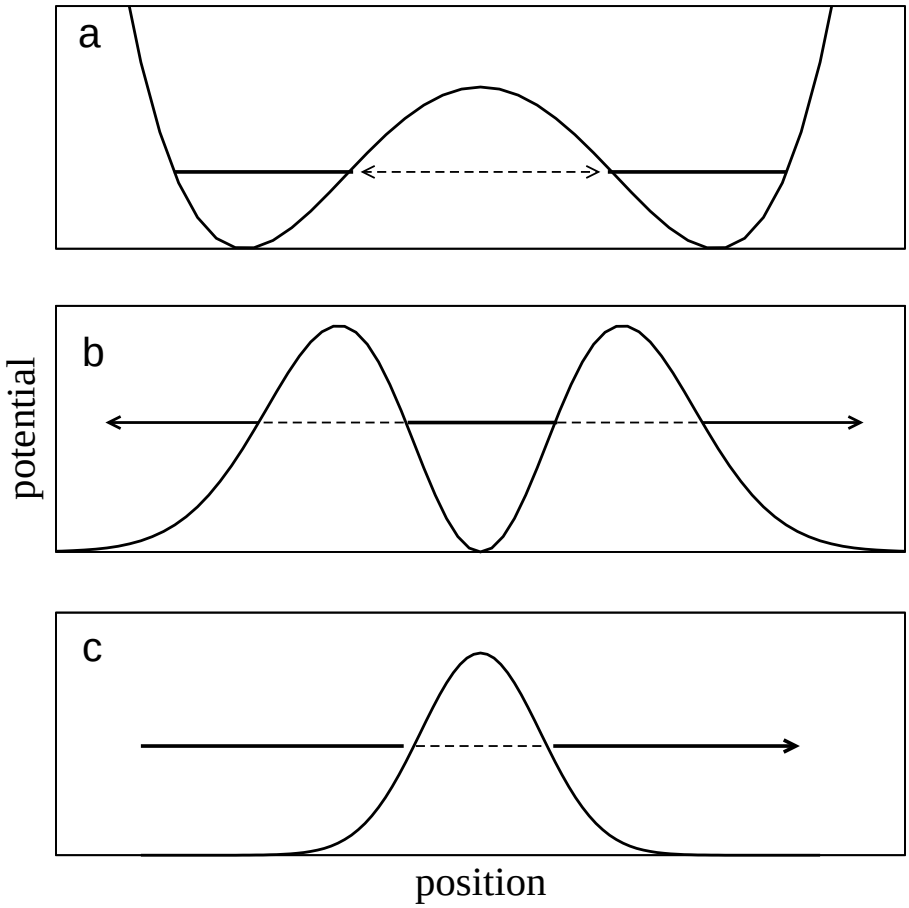

Figure 1.1: Three elementary scenarios for the manifestation of tunneling: (a) Rabi oscillations in a symmetric double well potential. The spectral manifestation of tunneling consists of a small level splitting between the symmetric and the antisymmetric eigenstate. (b) Decay from a metastable trapping potential. The quasibound state in the potential well is embedded into the continuum of unbound states, and its decay rate is given by the width of the associated spectral resonance. (c) Transmission through a potential barrier. In case of more complex barriers (such as the potential shown in panel (b)), perfect transmission may arise at energies that correspond to the internal quasibound states of the barrier potential.

classical back-scattering of the outer electron). This example illustrates that the simple picture sketched in Figure 1.1(b) may represent a rather complicated process in realistic systems.

A third scenario, which is particularly relevant in the electronic transport physics on the mesoscopic scale [21], is the classically forbidden transmission of quantum par-

ticles through potential barriers (see Figure 1.1(c)). Examples include the scanning tunneling microscope as well as the conduction of electrons through point contacts, quantum wells, and quantum dots in semiconductor heterostructures. In the latter two cases, the electrons effectively traverse a sequence of *two* barriers, which means that nearly perfect transmission can be achieved at energies that match the levels of internal quasi-bound states (cf. Figure 1.1(b)). This effect also manifests in transport processes on the nanometer scale, which was nicely demonstrated in an experiment on the electronic conduction through a carbon nanotube [22].

The examples mentioned so far are dealing with situations where a quantum particle is initially confined to one particular region in configuration space (which could be a potential well, for instance), and escapes from there into another spatial region via classically forbidden penetration through static potential barriers. Obviously, the invariance of classical mechanics under canonical transformations suggests that the concept of tunneling can be generalized to describe all kinds of classically forbidden transitions that can take place in phase space. Indeed, Rabi oscillations between two symmetry-related modes that do overlap in configuration space, but are disconnected from each other by invariant manifolds of the classical dynamics, are very similar, from the qualitative and quantitative point of view, to the above-mentioned double-well scenario. A straightforward example is the transition between clockwise and counterclockwise rotation in a quantum pendulum, which is classically forbidden and takes place via tunneling through dynamical barriers in momentum space.

This concept of "dynamical tunneling" was first introduced by Davis and Heller [23] who considered the quantum coupling between two spatially overlapping but classically distinct modes in a two-dimensional potential with near-integrable dynamics. The choice of this system was inspired from the vibrational dynamics within complex molecules [24], where such dynamical tunneling processes can arise in various ways. An explicit demonstration of dynamical tunneling was recently achieved in two simultaneous experiments on ultracold atoms that were stored in optical lattices with temporally modulated amplitudes [25, 26]. In this setup, the atoms are effectively subject to a one-dimensional periodic potential with a periodically time-dependent amplitude. For a suitable choice of parameters, this potential supports two classically stable eigenmodes that correspond to unbound motion into opposite directions (in close analogy to the rotational modes in the above case of the pendulum). Preparing the atoms in one of those stable modes, and performing absorption images that map the momentum distributions of the atoms after variable propagation times, clearly reveals periodic oscillations between "forward" and "backward" motion of the atoms (see Refs. [27, 28] for a theoretical account on this system).

Examples for dynamical tunneling can also be found in the *electromagnetic* context, e.g. in the dynamics of radiation in quasi two-dimensional microwave resonators [29] or optical microcavities [30]. In those systems, the "quantum theory"

is provided by the Helmholtz equation for the stationary distribution of the electric and magnetic field, and the analog of "classical motion" is given by ray optics involving straight-line trajectories with specular reflecions at the boundary of the resonator [31]. A straightforward scenario for tunneling in electromagnetic resonators is the transition between left-moving and right-moving "whispering-gallery" modes along the boundary of the resonator, which is forbidden within the ray dynamics of the system, but can take place in the actual wave description of the electromagnetic field. An advantage of microwave resonators in this context is that both the eigenfrequency splitting between those modes as well as the associated field distributions can be measured with rather high precision [29].

While the basic principle of tunneling is qualitatively well understood, the quantitative evaluation of the rates that characterize a specific tunneling process can be rather difficult, especially in multidimensional systems. Numerical *ab initio* calculations of such tunneling rates generally require a good representation of the wavefunction not only in the classically allowed region, but also in the forbidden domain, and are typically associated with a comparatively high effort. Semiclassical techniques might, in principle, provide feasible alternatives to evaluate such rates. From the semiclassical point of view, however, tunneling is well understood only in integrable systems. Small deviations from integrability — i.e., where the classical motion is still "regular" and dominantly evolves along invariant tori due to the Kolmogorov-Arnold-Moser (KAM) theorem — already introduce nontrivial modifications to the semiclassical description as compared to the integrable limit (see Section 2.3).

Further complications arise as soon as layers of chaotic motion are appreciably developed in phase space. In such a case of mixed regular-chaotic dynamics, the quantum eigenstates of the system can still be classified in "regular" and "chaotic" states [32], which are, in phase space, anchored on "islands" of regular motion and on the surrounding "chaotic sea", respectively, and dynamical tunneling processes might take place, e.g., between two symmetry-related quasi-modes that are associated with a pair of such regular islands. However, a general semiclassical theory of such tunneling processes, which is both accurate and permits a feasible evaluation of the associated rates and time scales, still represents an open problem.

Complications of different nature arise in the presence of *interaction*, i.e. in systems where the classically forbidden transition is not undertaken by a single quantum particle, but by an ensemble of many particles that weakly interact with each other. A particularly interesting case in this context are decay and transport processes of interacting *Bose-Einstein condensates* the dynamics of which is, on the lowest-order mean-field level, described by a nonlinear Schrödinger equation. Nontrivial conceptual problems arise in such intrinsically nonlinear systems, pertaining, e.g., to the notion of a "decaying state" of the condensate in a metastable potential well (cf. Figure 1.1(b)), as well as to the definition of the "transmission coefficient" of the condensate in a scattering process (cf. Figure 1.1(c)). The nonlineartiy furthermore

induces new phenomena, such as nonlinear self-trapping in the double-well scenario, as well as the appearance of multistable behaviour in resonant transport processes.

This thesis is specifically devoted to improve our understanding of such "complex" tunneling phenomena. We shall put particular emphasis on two topics: the semiclassical description of tunneling in presence of classical chaos, as well as classically forbidden transport and decay processes of Bose-Einstein condensates. To provide a solid introduction into the subject, we start in Chapter 2 with a general overview of the current status of the semiclassical theory of tunneling. In Chapter 3, we discuss the phenomenon of "chaos-assisted tunneling" and present its quantitative description in terms of nonlinear resonances of the classical dynamics. Chapter 4 is devoted to tunneling phenomena with interacting matter waves. We discuss, on one hand, macroscopic quantum self-trapping of a Bose-Einstein condensate in a double well potential and, on the other hand, resonant transport of a condensate through a double barrier geometry, which is also investigated from the point of view of decaying quasi-bound states. We conclude this thesis in Chapter 5 by pointing out possible future research directions that result from these investigations.

Semiclassical theory of tunneling

2.1 A simple example

Since the early days of tunneling [14], semiclassical techniques were employed to describe classically forbidden processes and to calculate the associated transition or decay rates. The underlying motivation is essentially twofold: On one hand, a semiclassical theory might provide a convenient description of the tunneling process in terms of the (pseudo) motion of a point particle through static and dynamical barriers. Such a description is particularly helpful for visualizing complex tunneling processes, as in the case of nonsequential double ionization [16]. Furthermore, useful insight into the essential *mechanism* that underlies such a process (such as nonlinear resonances, as we shall discuss in Chapter 3) might be obtained in this way. This would open the possibility to control tunneling, by applying external perturbations that enhance or suppress the effect of this mechanism.

On the other hand, a *quantitative* prediction of the relevant rates and time scales can be obtained by a semiclassical description of the tunneling process. This aspect has become less relevant in our time, due to the availability of high-power computers that permit quantum *ab initio* calculations for rather complicated systems, but it still not completely meaningless: We mention as an example the decay of highly correlated nondispersive wave packet states in the doubly excited helium atom [33]. Those wave packets are classically stabilized by a resonant (laser or microwave) driving [34, 35], and decay via a dynamical tunneling process that involves many degrees of freedom of the two-electron atom [36, 37]. A full-blown three-dimensional *ab initio* calculation of their lifetimes is beyond the capabilities of present-day computer technology [38], what makes a semiclassical theory of such multidimensional tunneling processes (which is not yet available) highly desirable.

To illustrate how semiclassical techniques can be used in the context of tunneling, we consider the simple case of the one-dimensional dynamics of a point particle with

mass m in a symmetric double-well potential. The Hamiltonian of this system reads

$$H = -\frac{\hbar^2}{2m}\frac{\partial^2}{\partial x^2} + V(x) \tag{2.1}$$

where the potential is, for instance, given by

$$V(x) = V_0(x^2 - a^2)^2 \tag{2.2}$$

for $V_0, a > 0$. Solutions of the stationary Schrödinger equation

$$H\psi(x) = E\psi(x) \tag{2.3}$$

can be obtained with the Wentzel-Kramers-Brillouin (WKB) method [39]. To this end, we make the ansatz

$$\psi(x) = \exp\left(\frac{\mathrm{i}}{\hbar}s(x)\right) \tag{2.4}$$

with complex $s(x)$. Inserting this ansatz into the stationary Schrödinger equation (2.3) yields

$$[s'(x)]^2 = p^2(x) + \mathrm{i}\hbar s''(x) \tag{2.5}$$

where

$$p(x) := \sqrt{2m(E - V(x))} \tag{2.6}$$

denotes the classical momentum of the particle at energy E.

In the formal limit $\hbar \to 0$, solutions of Equation (2.5) can be obtained by iteratively inserting approximate expressions for $s(x)$ in the $\hbar$-dependent term on the right-hand side, starting with the zero-order expression $s'(x) = \pm p(x)$ that would result for $\hbar = 0$. This yields in first order in $\hbar$

$$s'(x) = \pm p(x) + \mathrm{i}\hbar\frac{p'(x)}{2p(x)} + \mathcal{O}(\hbar^2)\,. \tag{2.7}$$

After integration and exponentiation of this first-order expression, we obtain the two linearly independent solutions

$$\psi_\pm(x) = \frac{a_\pm}{\sqrt{p(x)}}\exp\left(\pm\frac{\mathrm{i}}{\hbar}\int_{x_0}^{x} p(x')dx'\right) \tag{2.8}$$

of the stationary Schrödinger equation in the WKB approximation.

In the above derivation, we implicitly assumed $V(x') < E$ for $x_0 < x' < x$, i.e. the particle is moving in the classically allowed region. A very similar expression for the two WKB solutions is obtained in the *forbidden* domain $V(x') > E$, namely

$$\tilde{\psi}_\pm(x) = \frac{\alpha_\pm}{\sqrt{\tilde{p}(x)}}\exp\left(\pm\frac{1}{\hbar}\int_{x_0}^{x} \tilde{p}(x')dx'\right) \tag{2.9}$$

where

$$\tilde{p}(x) := \sqrt{2m(V(x) - E)} \tag{2.10}$$

can be denoted as the "imaginary momentum" of the particle. Linear combinations of ψ_+ and ψ_- as well as of $\tilde{\psi}_+$ and $\tilde{\psi}_-$ give then rise, respectively, to oscillatory behaviour in the allowed domain, as well as to a rapid increase or decrease of the wavefunction in the forbidden domain.

In order to determine the actual eigenfunctions of the system, it is necessary to solve the "connection problem", i.e. to evaluate how a specific linear combination of ψ_+ and ψ_- is continued across a classical turning point x_1 (with $V(x_1) = E$) into the forbidden domain. For our case of a one-dimensional potential, this task is most conveniently accomplished by comparing this linear combination with the asymptotic behaviour of the eigenfunctions in the linearized potential $\tilde{V}(x) := E + V'(x_1)(x - x_1)$, which are given in terms of Airy functions [40]. This *uniform approximation* yields e.g. for the inner turning point $x_1 = -b$ in the left well of the potential (2.2) (see Figure 2.1) that the linear combination

$$\psi(x) = \frac{2\alpha_-}{\sqrt{p(x)}} \cos\left(\frac{1}{\hbar}\int_x^{-b} p(x')dx' - \frac{\pi}{4}\right) \tag{2.11}$$

is continued into the wavefunction $\tilde{\psi}_-(x)$, defined by Equation (2.9) with $x_0 = -b$. A very similar expression (with as sine instead of a cosine, and with the prefactor $2\alpha_-$ being replaced by $-\alpha_+$) is obtained for the linear combination of ψ_+ and ψ_- that is continued into $\tilde{\psi}_+(x)$.

Applying those connection formulas and imposing that the eigenfunction is normalized, we finally obtain the semiclassical expressions $\psi_n^{(\pm)}$ for the symmetric and antisymmetric eigenstates in the double well potential, together with their energies $E_n^{(\pm)} = E_n \pm \frac{1}{2}\Delta E_n$. Here, E_n denotes the semiclassical energy of the nth excited quasi-mode in the left or right well (we only consider eigenenergies below the barrier height, i.e. $E_n^{(\pm)} < V_0 a^4$), which satisfies the condition

$$\int_b^c \sqrt{2m(E_n - V(x))}dx = \pi\hbar(n + 1/2) \tag{2.12}$$

where b and c are the inner and outer turning point, respectively, of the right well (see Figure 2.1). In the limit of comparatively small $\hbar$, the splitting between the symmetric and the antisymmetric eigenenergy is obtained as

$$\Delta E_n = \frac{\hbar\omega_n}{\pi} \exp\left(-\frac{1}{\hbar}\int_{-b}^{b} \sqrt{2m(V(x) - E_n)}dx\right) \tag{2.13}$$

where ω_n is the frequency of classical oscillations along the quantized orbit with energy E_n. Rabi oscillations between the wells therefore take place with the frequency $\Delta E_n/(2\hbar)$ which decreases exponentially with $1/\hbar$.

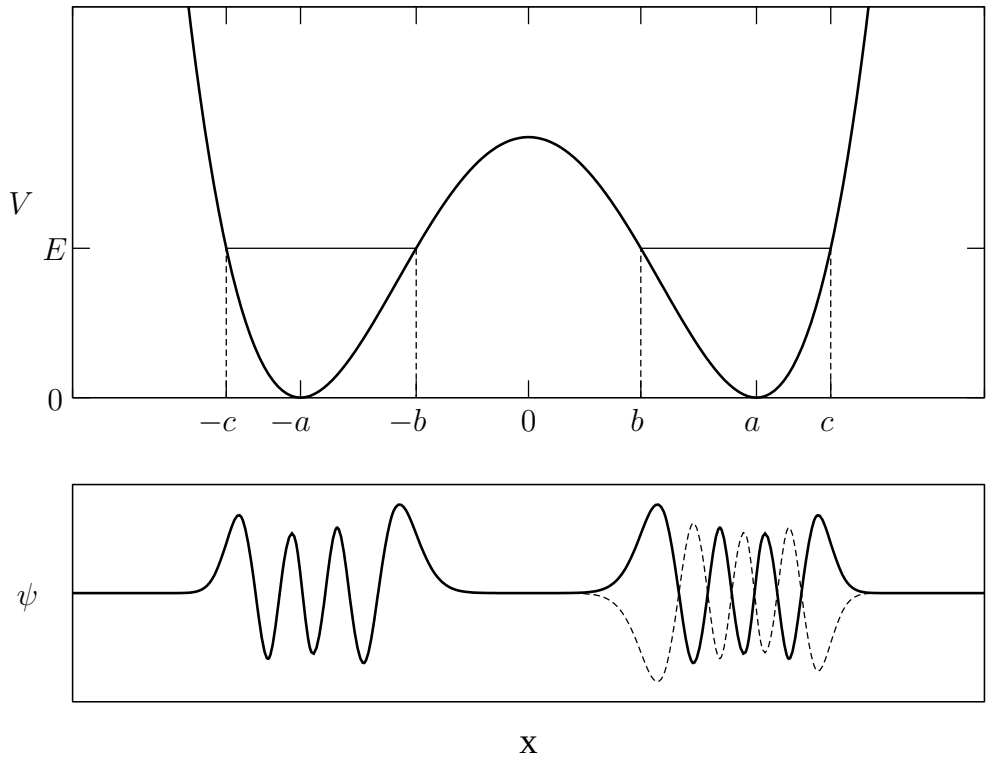

Figure 2.1: Tunneling in the double well potential. The upper panel displays the potential (2.2) together with an energy level E that corresponds to a locally quantized eigenmode in the left and right well, respectively. The lower panel shows the wavefunctions of the 5th excited symmetric and antisymmetric eigenstates (solid and dashed lines, respectively).

2.2 Tunneling in terms of complex orbits

The above derivation is, of course, not restricted to the specific functional form (2.2), but applies to other double-well potentials as well. It explicitly relies, however, on the kinetic-plus-potential form (2.1) of the Hamiltonian and cannot be generalized in a straightforward way to describe more general types of tunneling processes, such as dynamical tunneling in momentum space for the pendulum Hamiltonian. It is therefore convenient to adopt a more *geometric* point of view, which consists in constructing the WKB wavefunction along the Lagrangian manifolds of the classical dynamics [10]. Those Lagrangian manifolds correspond in Figure 2.1 to the invariant elliptic curves describing the bounded motion within the wells, and are, in integrable systems with more than one degree of freedom, topological equivalent to tori in the

phase space. By taking into account the appropriate phase change of the wavefunction at caustics [10], and by requiring self-consistency along the whole manifold, one obtains the Einstein-Brillouin-Keller (EBK) condition for the quantized invariant tori — namely

$$\oint_{\mathcal{C}} \mathbf{p}\, d\mathbf{q} = 2\pi\hbar \left(n + \frac{\mu}{4}\right) \tag{2.14}$$

for any closed curve $\mathcal{C}$ along the surface of the torus, where n is an integer and μ is the *Maslov index* [10] counting the number of turning points along the curve.

Tunneling can be incorporated into this framework by taking into account the *analytic continuation* of the invariant tori into complex domain. This analytic continuation can be explicitly constructed by *complex-time* propagation of the classical dynamics, i.e. by integrating Hamilton's equations of motion $\dot{\mathbf{p}} = -\frac{\partial H}{\partial \mathbf{q}}$ and $\dot{\mathbf{q}} = \frac{\partial H}{\partial \mathbf{p}}$ along paths in complex time domain [41]. During such a complex-time propagation, the action variables of the invariant torus remain constant, while the angle variables assume complex values, thereby tracing the extension of the torus in the complexified phase space. Due to the analyticity of the equations of motion, the phase space point that results from this propagation does not change under continuous deformations of the integration path, as long as the initial and the final time of the path are kept fixed, and as long as singularities (i.e., complex propagation times where the position and momentum variables assume infinite values) are not touched by such deformations.

In general, symmetry-related invariant tori that are confined to separate regions in the phase space of an integrable system are connected to each other in the complexified phase space. This is illustrated in Figure 2.2 for the case of the double well potential (2.2), which shows a part of the analytic continuation of two mirror-symmetric invariant curves within the wells. Requiring self-consistency of the semiclassical wavefunction along all possible loops within this complex manifold, the EBK quantiziation condition (2.14) becomes modified and gives rise to the splitting (2.13) between the levels of the symmetric and the antisymmetric eigenstate. The exponential suppression of the splitting now arises from the action integral along the manifold, which, being evaluated on the complex path that crosses the barrier along the $\mathrm{Re}(p) = 0$ axis, acquires an imaginary part of the form $\int_{-b}^{b} \mathrm{Im}(p(x))dx$.

The application of this semiclassical quantization procedure to more general tunneling processes between symmetry-related regions in phase space requires to formulate a representation-independent prescription how the wavefunction is to be continued across a turning point of the classical dynamics. In principle, this connection problem can be solved in a geometric way by encircling the turning point in the complex phase space [42]. For the one-dimensional potential (2.2), this means that the WKB wavefunction (2.8) is continued into the classically forbidden domain by performing the integration of Equation (2.7) along a path that moves around the

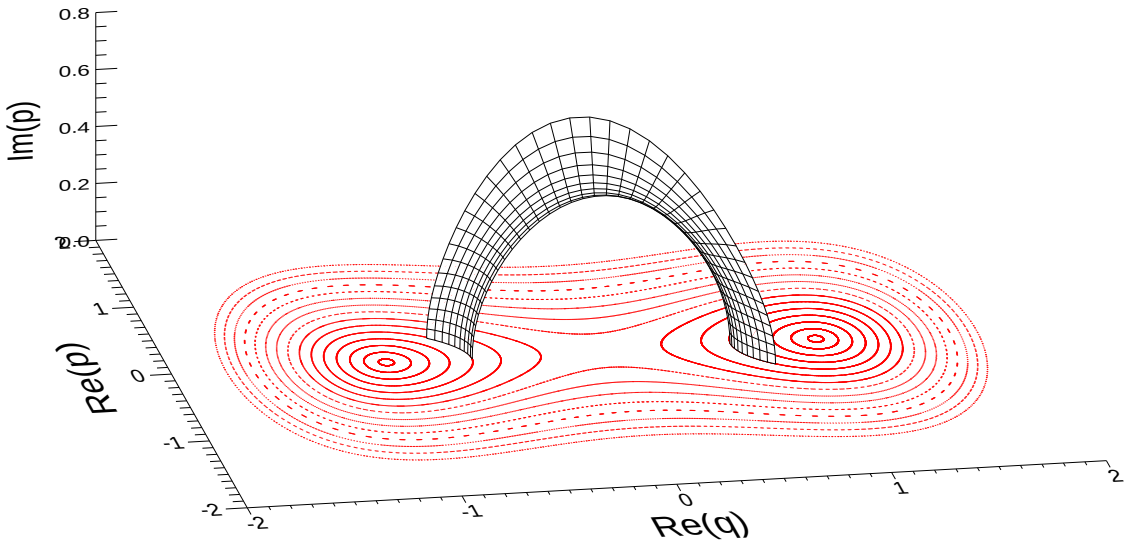

Figure 2.2: Analytic continuation of the invariant tori in the double well potential. The horizontal plane, spanned by $\mathrm{Re}(q)$ and $\mathrm{Re}(p)$, shows the phase space of the classical motion of a particle (with mass $m = 1$) within the potential (2.2) (with $a = 1$ and $V_0 = 0.25$). The manifold that connects the symmetry-related tori in the wells is calculated by imaginary-time integration of Hamilton's equations of motion, starting in the right well at $\mathrm{Im}(t) = 0$ and ending in the left well at $\mathrm{Im}(t) \simeq 3.8$. For the sake of clarity, the $\mathrm{Im}(q)$-component of the manifold is not plotted.

turning point in complex position space. Care needs to be taken here, however, insofar as the coefficients $a_\pm$ of the linear combination of ψ_+ and ψ_- would, for the "true" quantum wavefunction, *not* remain constant along such a path: Substantial variations do indeed occur at the so-called "Stokes lines" where the exponent in Equation (2.8) becomes purely real. At those Stokes lines, the prefactor of the *subdominant* component of the wavefunction, i.e. for which the exponent is negative, undegoes a drastic change, which can be evaluated to be of the form $a_+ \mapsto a_+ - \mathrm{i}a_-$ for the case that ψ_+ is subdominant [42]. Taking into account this Stokes phenomenon, general rules can be derived how to connect the amplitudes $a_\pm$ and $\alpha_\pm$ of the semiclassical wavefunctions on the allowed and forbidden side of a caustic in phase space [43]. Those rules allow one to semiclassically calculate the level splittings for general dynamical tunneling processes that take place in phase space [43].

2.3 Nonintegrable systems

The above approach can be applied to multidimensional systems as well, even if they are nonseparable [43]. It breaks down, however, as soon as a nonintegrable perturbation is added to the system. In that case, invariant tori of the classical dynamics may still exist due to the Kolmogorov-Arnold-Moser (KAM) theorem [44], but they are no longer given by analytic functions of the phase space variables.

For a system with two degrees of freedom, this fact can be best illustrated by a *Poincaré section* of the phase space, where the intersections of the trajectories with a surface defined by constant energy and by an additional condition, say $q_2 = 0$, are monitored. Plotting p_1 versus q_1 in this Poincaré surface of section yields, in the case of nearly integrable dynamics, a very similar picture as for a one-dimensional system, showing a phase space that is structured by invariant elliptic curves. In between those invariant curves, however, substructures consisting of small regular islands and tiny chaotic layers appear at *nonlinear resonances*, where the two frequencies characterizing the near-integrable dynamics are rationally related. Exactly the same behaviour is found for one-degree-of-freedom systems that are subject to a perturbative periodic driving, where a *stroboscopic* Poincaré section is defined by plotting p versus q at fixed phase of the driving.

The resonance-induced substructures give rise to tiny modulations of the invariant KAM tori, which are hardly visible in the "real" Poincaré surface of section, but appreciably manifest themselves in the complexified phase space. Indeed, any attempt to analytically continue a KAM torus of a nonintegrable system to the complex domain (e.g. by making a Fourier series expansion in the angle variables) will fail beyond critical values of the imaginary angle variables [45]. The KAM torus therefore has a *natural boundary* in the complex phase space beyond which it is no longer defined. In the complexified version of the Poincaré surface of section (which would be spanned by the complex variables p_1 and q_1 at $q_2 = 0$ and at fixed total energy), this natural boundary would correspond to a line of weak singularities which is manifested by a self-similar structure of the complex torus [45].

Despite this complication, it is still possible to devise approximate semiclassical methods that permit to reproduce tunneling rates in the limit of weak perturbations from integrability. Most influential in this context was the approach suggested by Wilkinson [46], which assumes that the two manifolds that emanate from the analytic continuation of two symmetry-related invariant tori do not coincide (this would imply the existence of an additional constant of motion), but intersect at some finite angle in the complex phase space. Under this assumption, a Bardeen-type formula [47] can be used where the energy splitting between the symmetric and the antisymmetric state is given by an integral over the tunneling tails of the quasimode wavefunctions along a line (or hyperplane, in higher dimensional systems) that separates the two wells. This integral can be performed by the stationary-phase ap-

proximation, using semiclassical expressions for the wavefunctions constructed along the above complex manifolds. For a system with n degrees of freedom, this yields, in lowest order in $\hbar$, a splitting of the form $\Delta E \simeq \hbar^{(n+1)/2} A \exp(-\sigma/\hbar)$ where the tunneling action σ as well as the prefactor A are purely classical quantities, i.e., independent of $\hbar$. This approach was applied to a number of near-integrable tunneling problems [48–51] where various methods were used to construct approximate continuations of the generating functions that determine the invariant tori (see also Ref. [52]).

A completely different ansatz is required for strongly perturbed systems, where the dynamics within the wells is dominantly characterized by chaotic motion. In that case, torus quantization methods for the construction of quasimodes can no longer be employed, and the semiclassical theory of tunneling between the wells rather needs to be based on Gutzwiller-like trace formula approaches [53] involving summations over periodic orbits that cross the barrier in complex propagation time. Creagh and Whelan [54] used for this purpose the splitting-weighted density of states $f(E) = \sum_n \Delta E_n \delta(E - E_n)$, where E_n denotes the energy of the nth local eigenstate within the left and right chaotic well, respectively, and ΔE_n is the corresponding level splitting induced by tunneling. This quantity can be written as the difference of the two staircase functions corresponding to the integrated densities of symmetric and antisymmetric states, respectively, and those densities of states allow for a straightforward periodic-orbit expansion. A careful analysis of the tunneling process between two disconnected wells with chaotic dynamics shows that the splittings ΔE_n are mainly induced by orbits that involve a single, instanton-like complex path across the barrier, which is distinguished by a minimal value for the imaginary action integral [54]. This result is also obtained with more sophisticated approaches [55,56] based on a Bardeen-type evaluation of matrix elements that are defined on a suitable Poincaré surface of section.

In the above discussion, we implicitly assumed the presence of a *static* tunneling scenario, where the two wells are separated from each other by an energetic barrier. In the multidimensional context, this scenario could be realized by coupling the one-dimensional double well potential (2.2) to a harmonic oscillator in the perpendicular spatial direction, yielding, e.g., the two-dimensional potential

$$V(x, y) = V_0(x^2 - a^2)^2 + \frac{1}{2}\omega^2 y^2 + \gamma x^2 y^2 \,. \tag{2.15}$$

For energies below the barrier height (i.e., $E < V_0 a^4$), a Poincaré section defined by $y = 0$ yields two disconnected regions in phase space which exhibit regular, near-integrable dynamics.

As can be seen in Figure 2.3, the situation is qualitatively different for energies *above* the barrier height ($E > V_0 a^4$). In this regime, the Poincaré surface of section will, for not too large γ, again display two different regular regions, corresponding to

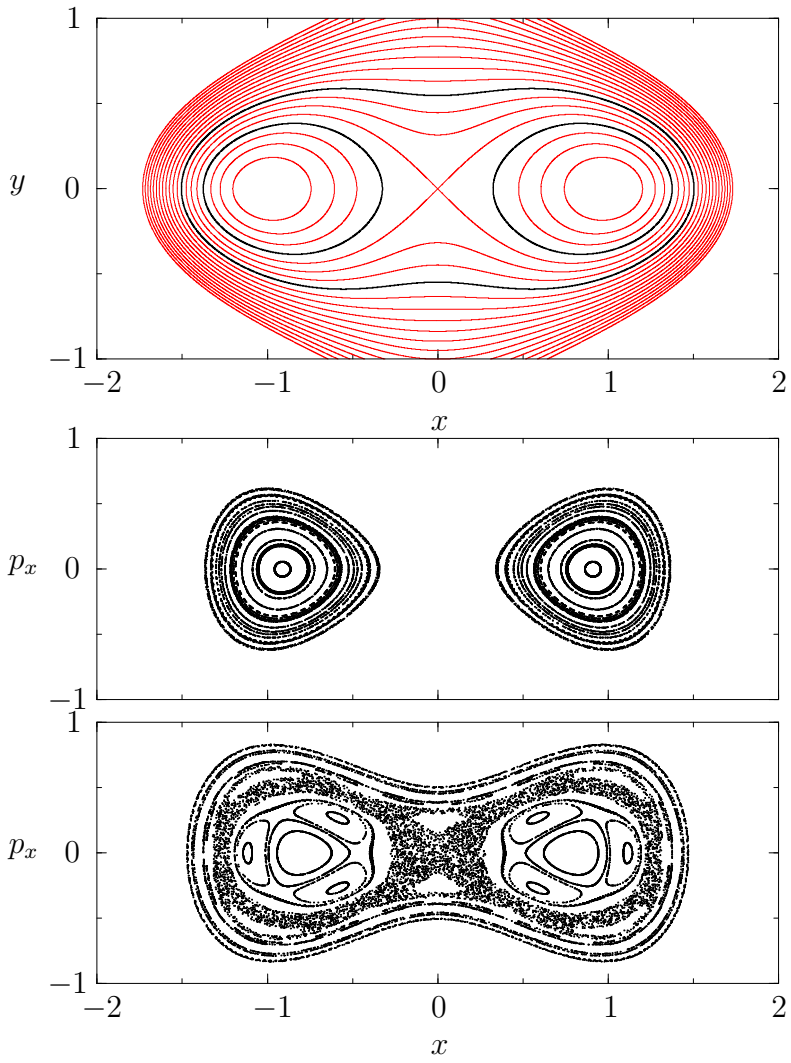

Figure 2.3: Static and dynamical tunneling in a two-dimensional double well potential. The upper panel displays the equipotential lines for the potential (2.15) at $V_0 = 0.25$, $a = 1$, $\omega = 1$, and $\gamma = 1$. The middle and lower panels show Poincaré surfaces of section of the dynamics in this two-dimensional potential at the energies $E = 0.2$ (below the barrier) and $E = 0.4$ (above the barrier), respectively, which are marked by thick solid lines in the upper panel. At $E = 0.2$, the stable modes in the left and right well are separated from each other by energetic barriers, what leads to disconnected regular regions in the Poincaré surface of section. At $E = 0.4$, on the other hand, such energetic barriers do no longer exist, and the motion around the center of the wells remains stable only due to the presence of invariant KAM tori.

the motion in the left and right well, respectively (where the energy is mainly stored in the perpendicular degree of freedom). These two regions, however, are now part of the *same*, singly connected hypersurface of constant energy, which means that the associated stable modes are classically separated from each other only by *dynamical* barriers. In such a situation, the semiclassical tunneling process between the wells is generally expected to proceed via a multitude of complex paths, which may involve both classically forbidden and classically allowed components (see also the discussion in Chapter 3). This is especially true for finite values of the coupling strength γ, where an appreciable layer of chaotic motion, formed around the separatrix structure of the one-dimensional double well potential, is manifested in the Poincaré surface of section (see the lowest panel in Figure 2.3).

The complications that arise for dynamical tunneling processes in mixed regular-chaotic systems were impressively demonstrated by Shudo and Ikeda [57–59]. In this work, the authors studied the propagation of a wave packet in a periodically driven one-degree-of-freedom system, where the initial state was assumed to be localized on an "island" of regular motion in a dominantly chaotic phase space. The escape of the wave packet from the island into the surrounding "chaotic sea" was semiclassically reproduced by expanding the time evolution operator of the system in terms of complex orbits that evolve in real time and exhibit real initial and final momenta (the wavefunction was calculated in momentum space) [57]. Shudo and Ikeda showed that the set of complex initial positions that satisfy those boundary conditions exhibits a complicated, self-similar structure which is reminiscent of Julia sets [60]. The selection of paths that contribute to the time evolution of the wave packet requires a careful evaluation of the Stokes phenomenon in the complex domain, in order to avoid "forbidden" trajectories that would lead to an exponential increase (instead of decrease) of the tunneling amplitude [58].

The above studies [57–60] are successful from the quantitative point of view, insofar as they yield an almost perfect agreement between the semiclassically calculated wavefunction and the exact quantum result. It is not obvious, however, to which extent the underlying semiclassical approach can be applied in a feasible way to more complicated tunneling processes (e.g., in systems with more than two degrees of freedom), where the identification of contributing complex trajectories might turn into a formidable computational task. For such applications, more insight into dominant *mechanisms* that govern the classically forbidden transition would be rather helpful. Progress into this direction was recently obtained by analogous studies on the scattering process through a potential barrier the height of which is periodically modulated in time [61–64]. This latter scenario can be studied in terms of the energy-dependent scattering matrix, which allows for a semiclassical expansion in terms of trajectories that traverse the barrier in complex time domain [61]. A careful analysis of this process reveals that dominant contributions to the scattering state arise from those trajectories that are part of the complexified stable manifold

associated with the saddle point of the barrier [63, 64]. To which extent this mechanism manifests itself also in escape processes or in the dynamical tunneling between symmetry-related regular regions in phase space remains an open question.

Resonance- and chaos-assisted tunneling

3.1 Chaos-assisted tunneling

In the early nineties, it became evident that the presence of an appreciable chaotic layer can have a dramatic effect on the dynamical tunneling process between two symmetry-related regular regions in the phase space: The level splittings between symmetric and antisymmetric linear combinations of quasi-modes that are localized on such regular islands are drastically enhanced (typically by many orders of magnitude) as compared to the integrable case. This effect even arises if the quantized torus with which the quasi-modes are associated is located *far away* from the "chaos border" (which is defined by the outermost invariant KAM torus of the island) and becomes more pronounced the more one proceeds towards the semiclassical limit $\hbar \to 0$. In addition, the splittings do, in systems with mixed regular-chaotic dynamics, no longer display a smooth behaviour as a function of $\hbar$, as would be suggested by an expression of the form (2.13), but may exhibit rather large fluctuations at small variations of Planck's constant or of any other parameter of the system.

The enhancement of dynamical tunneling due to chaos was first verified in periodically driven double-well systems [65–68], which are typically described by the Hamiltonian $H = p^2/2 + V(x) + Fx\cos(\omega t)$ where $V(x)$ represents a double well potential of the form (2.2). Related studies, which also revealed the high sensitivity of the splittings with respect to variations of parameters, were performed with the quartic oscillator [69–71], with quantum maps [72], as well as with the "annular billiard" [73]. The latter dynamical system is characterized by free motion within the space that is confined in between two non-concentric circles with different radii, which is combined with specular reflection at the outer and inner circular boundaries. Dynamical tunneling takes place between quasimodes that are located on clockwise and counterclockwise whispering-gallery modes in this system. The an-

nular billiard is particularly suited for a semiclassical analysis of the chaos-induced enhancement of tunneling [74,75]. It can, furthermore, be realized with metallic microwave resonators, which allowed for the first experimental demonstration of this effect [29].

The basic principle behind "chaos-assisted tunneling" can be illustrated with a simple three-state model which was introduced by Tomsovic and Ullmo [70]: We consider a doublet of levels, with the energies $E_\pm = E_0 \pm \delta$, which correspond to the symmetric and antisymmetric linear combination $|v_\pm\rangle$ of the quasi-modes that are located on a given quantized KAM torus in a pair of symmetry-related regular islands. In contrast to integrable systems, this doublet is not isolated in the spectrum, but may resonantly interact with states that are supported by the chaotic sea. Let us suppose that the level E_c of one of those chaotic states $|v_c\rangle$ crosses the doublet at the variation of a system parameter λ. In the basis spanned by the above states ($|v_-\rangle$, $|v_+\rangle$, $|v_c\rangle$), the effective Hamiltonian describing this system takes on the form

$$H_{\text{eff}} = \begin{pmatrix} E_0 - \delta & 0 & 0 \\ 0 & E_0 + \delta & V \\ 0 & V & E_c(\lambda) \end{pmatrix} . \tag{3.1}$$

Here we assume, without loss of generality, that the chaotic state is, in the same way as $|v_+\rangle$, symmetric with respect to the parity operator that characterizes the system. A finite matrix element V arises therefore between $|v_+\rangle$ and $|v_c\rangle$, while $|v_-\rangle$ and $|v_c\rangle$ remain uncoupled [76,77].

Figure 3.1 displays the eigenvalue spectrum that results from the diagonalization of (3.1) for $E_c(\lambda) = E_0 + \lambda E_1$ and $\delta/V = 0.1$. Clearly, we recognize a large avoided crossing between the symmetric regular state $|v_+\rangle$ and the chaotic state $|v_c\rangle$ at $\lambda = 0$, while the eigenvalue of $|v_-\rangle$ remains unaffected. The splitting between the two "regular" states is most conveniently defined by the difference $|\tilde{E}_+(\lambda) - E_-|$ where $\tilde{E}_+$ denotes the energy of the eigenstate of H_{eff} that exhibits the largest overlap with $|v_+\rangle$. Quite obviously, a maximal value of the splitting, which is considerably enhanced with respect to the uncoupled case, thereby occurs at $\lambda = 0$, where $\tilde{E}_+$ suddenly switches from the energetically upper to the lower branch of the avoided crossing.

In addition to this maximum, there is also a value for λ at which an *exact* crossing between $\tilde{E}_+(\lambda)$ and E_- arises. At this particular point, the tunneling rate between the regular islands *vanishes*, which means that a wave packet that is prepared on the quasi-mode in one of the islands will remain there forever [66]. This phenomenon, which was named "coherent destruction of tunneling" by Grossmann et al. [66] (as opposed to the interruption of the tunneling process due to incoherent effects, such as the coupling to a measurement device or a thermal bath), represents a generic feature in mixed regular-chaotic systems. Its experimental observation is, however, rather difficult due to the fact that system parameters need to be tuned in a very

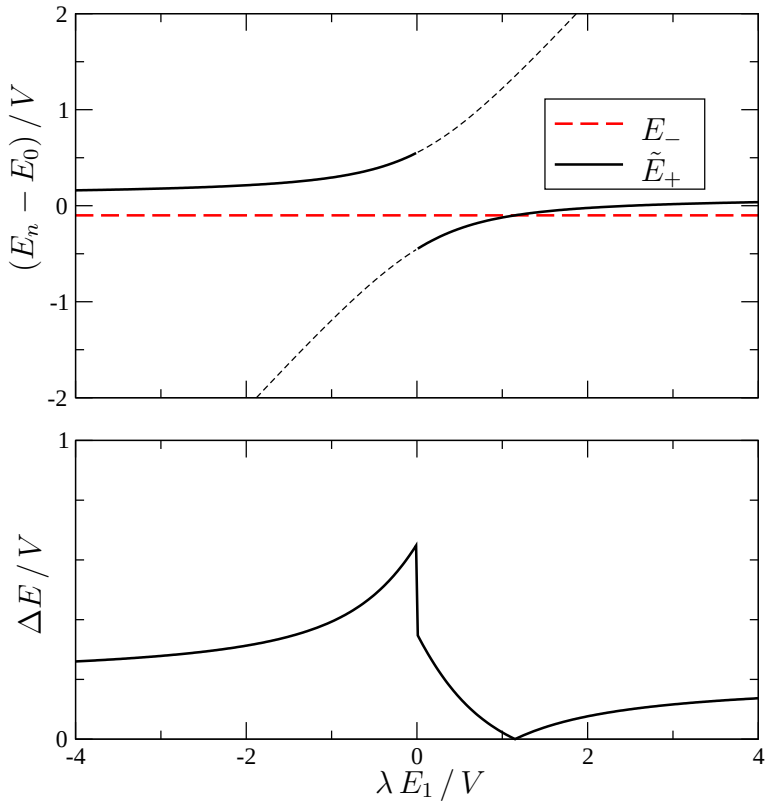

Figure 3.1: Three-level model for chaos-assisted tunneling. The upper panel shows the eigenvalues of the Hamiltonian (3.1) as a function of λ for $E_c(\lambda) = E_0 + \lambda E_1$ and $\delta/V = 0.1$. Boldly marked are the energy E_- of the antisymmetric state (thick dashed line) and the energy $\tilde{E}_+$ of the symmetric eigenstate that has the largest overlap with the unperturbed state $|v_+\rangle$. The lower panel shows the eigenvalue splitting $\Delta E = |\tilde{E}_+ - E_-|$. In addition to the pronounced maximum at $\lambda = 0$, an exact crossing of the levels occurs at $\lambda E_1/V = 1.15$. At this particluar value of the control parameter λ, the tunneling rate diverges, which means that a quantum state prepared on one of the quasi-modes will remain there forever.

precise manner to values where such a crossing occurs. It was recently argued [78] that the experiments on dynamical tunneling of cold atoms in periodically modulated optical lattices [25,26] might provide a convenient setup to observe the phenomenon of coherent destruction of tunneling.

In general, the level splittings between quasi-modes on symmetry-related regular islands are not only influenced by single avoided crossings with the energetically

nearest chaotic states, but undergo an enhancement also due to the (non-resonant) interaction with all other states that are supported by the chaotic sea. The combined effect of the chaotic states onto the dynamical tunneling process can be described by a straightforward generalization of the above three-state model [70, 71]. To this end, we formally assume the existence of a globally integrable Hamiltonian (to be derived, e.g., by classical perturbation theory [44]) that reproduces quite well the dynamics within the regular islands. Expanding the "true", nonintegrable Hamiltonian in the eigenbasis of this integrable approximation yields a nearly diagonal matrix for states that are located on invariant tori within the regular islands, whereas strong off-diagonal coupling matrix elements occur within the chaotic sea. Restricted to the symmetric or antisymmetric linear combination of the quasi-modes that are associated with one particular doublet, and to those chaotic states that exhibit the same discrete symmetry as this regular state, the Hamiltonian matrix effectively reads

$$H_{\text{eff}}^{\pm} = \begin{pmatrix} E_0 & v_1 & \cdots & v_N \\ v_1 & H_{11}^{\pm} & \cdots & H_{1N}^{\pm} \\ \vdots & \vdots & & \vdots \\ v_N & H_{N1}^{\pm} & \cdots & H_{NN}^{\pm} \end{pmatrix} . \tag{3.2}$$

Here, E_0 represents the unperturbed energy of the doublet, $H_{11}^{\pm}, \ldots, H_{NN}^{\pm}$ are the matrix elements within the symmetric or antisymmetric subspace of chaotic states, and $v_1, \ldots, v_N$ describe small couplings between the regular state and the chaos. For the sake of simplicity, we neglect the "direct" splitting δ that arises from the diagonalization of the approximate integrable Hamiltonian, and assume that the coupling matrix elements v_j do not depend on the symmetry class. However, the matrix elements $H_{ij}^{\pm}$ are, in general, different for symmetric and antisymmetric states. As a consequence, different shifts $\delta E^{\pm}$ of the regular level E_0 result from the coupling to the chaos, what leads to a finite level splitting $\Delta E = |\delta E^{+} - \delta E^{-}|$.

The average behaviour of the splitting ΔE as well as its fluctuations at variations of system parameters can be quantitatively evaluated by making a *random matrix* ansatz for the sub-block $(H_{ij}^{\pm})_{N\times N}$, i.e., by modelling this "chaos block" with an element from the Gaussian Orthogonal Ensemble (GOE) [79]. This random matrix ansatz is applied to the perturbative expression for the level shift $\delta E^{\pm}$, which results from the elminination of the weak coupling to the chaotic eigenstates [70, 71]: we obtain

$$\delta E^{\pm} = \sum_{j=1}^{N} \frac{(\mathcal{V}_j^{\pm})^2}{E_0 - \mathcal{E}_j^{\pm}} \tag{3.3}$$

with

$$\mathcal{V}_j^{\pm} = \sum_{i=1}^{N} C_{ij}^{\pm} v_i \tag{3.4}$$

where $\mathcal{E}_j^{\pm}$ are the eigenvalues of $(H_{ij}^{\pm})$, and $(C_{ij}^{\pm})_{N\times N}$ denotes the matrix of the corresponding orthogonal eigenvectors. The random matrix average over the latter yields

$$\langle(\mathcal{V}_j^{\pm})^2\rangle = \frac{1}{N}\sum_{i=1}^{N} v_i^2 \tag{3.5}$$

for all $j = 1 \ldots N$, which simply expresses the fact that none of the basis states is distinguished within the chaos block.

Leyvraz and Ullmo showed [71] that the average over the eigenvalues $\mathcal{E}_j^{\pm}$ leads to a *Cauchy distribution* for the probability $P(\Delta E)$ to find the level splitting ΔE, namely

$$P(\Delta E) = \frac{2}{\pi}\frac{\overline{\Delta E}}{(\Delta E)^2 + (\overline{\Delta E})^2}\,. \tag{3.6}$$

with

$$\overline{\Delta E} = \frac{2\pi}{N\Delta_c}\sum_{j=1}^{N} v_j^2 \tag{3.7}$$

where Δ_c denotes the mean spacing between the eigenenergies of the chaos block. This Cauchy distribution is valid for splittings ΔE that are much smaller than the average coupling strength $\bar{v} = \sqrt{v_1^2 + \ldots + v_N^2}$, and exhibits a cutoff at $\Delta E \sim 2\bar{v}$. This cutoff effectively ensures that the statistical expectation value for the splitting does not diverge.

The above random matrix ansatz, which can in principle also be applied to describe the decay of a regular state into the surrounding chaotic sea (as was considered in Ref. [80]), assumes that the states within the chaotic domain are, on average, equally strongly coupled to each other. This assumption should be valid for strongly perturbed systems where the chaotic sea is essentially "structureless", but might represent a crude approximation in presence of relevant *partial barriers* in the chaotic part of the phase space. Such partial barriers arise due to the manifestation of "Cantori", i.e. broken invariant tori which form a Cantor set in the Poincaré surface of section [81], as well as due to the intersections of the stable and unstable manifolds that are associated with unstable periodic orbits [69]. In the quantum system, they effectively lead to a subdivision of the chaotic part $(H_{ij}^{\pm})$ of the Hamiltonian into several sub-blocks that are weakly coupled to each other. Tomsovic and Ullmo proposed for this case a generalized random-matrix ansatz which explicitly takes into account this subdivision [70]. For the special case that a prominent partial barrier is located at the symmetry line that separates the two regular islands, a modification of the above probability distribution (3.6) for the splittings can be derived, which is found to be in good agreement with numerical results obtained for the quartic oscillator model [71].

3.2 Resonance-assisted tunneling in near-integrable systems

The investigations of Tomsovic, Ullmo, and Leyvraz focused on the comparison of the functional form of the probability distribution (3.6) with numerical data, where the intrinsic energy scale (3.7) was treated as an unknown parameter [70, 71]. Indeed, no semiclassical theory existed, at that time, for the effective coupling strength $\bar{v}$ between the regular state and the chaotic domain. Hence, further quantitative information such as the prediction of the *average* value for the level splittings, which obviously depends on $\bar{v}$ via the energy scale $\overline{\Delta E}$ and which is a most relevant information from the practical point of view, could not be extracted from the Cauchy distribution (3.6).

Progress into this direction was obtained within the conceptually simpler case of *near-integrable* dynamics, where the deviation from integrability is not strong enough for the development of appreciable chaotic layers in the phase space. Even in this seemingly "regular" case, the tunneling rates may display surprisingly complicated variations as a function of $\hbar$ [72, 82], which in general cannot be described by a smooth monotonic function of the form (2.13). It is established by now that such variations are mainly induced due to the manifestation of *nonlinear resonances* in the classical phase space. These resonances basically correspond to invariant tori with rational winding numbers, which break up in presence of the perturbation from integrability and form substructures around a set of alternatingly stable and unstable periodic orbits according to the Poincaré-Birkhoff theorem [44].

The relevance of nonlinear resonances for dynamical tunneling was already recognized in the eighties, what is documented by various semiclassical and perturbative studies on the quantum coupling process across such a resonance [83–85]. A particularly convenient approach for the description of this coupling process was proposed by Ozorio de Almeida [84], which is based on the semiclassical quantization of the effective pendulum Hamiltonian that describes the dynamics in the vicinity of the resonance (see Equation (3.10) below). Bonci et al. argued, in a quantitative study on the periodically driven pendulum Hamiltonian [82], that the presence of such nonlinear resonances can induce similar fluctuations of level splittings as in the mixed regular-chaotic case, due to the appearance of near-degeneracies between lowly and highly excited states within a phase space domain of bounded motion [82].

The pieces of information were put together and transformed into a quantitative theory in our work on resonance-assisted tunneling [86, 87]. This theory was formulated for the case of one-dimensional systems that are subject to a periodically time-dependent perturbation and that exhibit, in the limit of unperturbed dynamics, two symmetry-related wells of bounded motion. Expressed in terms of the "action-angle variables" (I, θ) describing the dynamics within one of the wells,

the Hamiltonian of this system is written as

$$H(I,\theta,t) = H_0(I) + V(I,\theta,t) \tag{3.8}$$

where $V(I,\theta,t) = V(I,\theta,t+2\pi/\omega)$ represents the time-dependent perturbation.

As in the work of Ozorio de Almeida [84], secular classical perturbation theory [44] was applied to obtain an effective integrable Hamiltonian in the vicinity of an "r:s resonance", i.e. where the unperturbed system performs s oscillations in the well within r periods of the external perturbation. To this end, a canonical transformation to the co-rotating frame is defined by introducing the slowly varying angle variable

$$\vartheta = \theta - \frac{s}{r}\omega t\,. \tag{3.9}$$

By means of an additional canonical transformation $(I,\vartheta) \mapsto (\tilde{I},\tilde{\vartheta})$ of infinitesimal nature, it is possible to eliminate the remaining time-dependence of the Hamiltonian in lowest order of the perturbation. This yields, for action variables I in the immediate vicinity of the resonance, the effective pendulum Hamiltonian

$$H_{\text{eff}} = \frac{(\tilde{I}-I_{r:s})^2}{2m_{r:s}} + 2V_{r:s}\cos(r\tilde{\vartheta}+\varphi)\,. \tag{3.10}$$

Here, $I_{r:s}$ represents the action variable at which the r:s resonance occurs, the effective mass parameter $m_{r:s}$ is given by

$$\frac{1}{m_{r:s}} = \frac{d^2H_0}{dI^2}(I_{r:s})\,, \tag{3.11}$$

and the coupling strength $V_{r:s}$ is approximately evaluated as [44]

$$V_{r:s}e^{\mathrm{i}\varphi} = \int_0^{2\pi}\frac{d\theta}{2\pi}\int_0^{2\pi/\omega}\frac{dt}{2\pi/\omega}V(I_{r:s},\theta,t)e^{-\mathrm{i}(r\theta-s\omega t)}\,. \tag{3.12}$$

Following the lines of Ref. [84], we investigate the quantum implications of this r:s resonance within the direct semiclassical quantization of the effective Hamiltonian (3.10). This quantization is obtained through the replacement $(\tilde{I},\tilde{\vartheta}) \mapsto (\hat{I},\hat{\vartheta})$ where the "action operator" is defined via

$$\hat{I} \equiv \frac{\hbar}{\mathrm{i}}\frac{\partial}{\partial\tilde{\vartheta}}\,. \tag{3.13}$$

In this representation, the eigenfunctions of the unperturbed Hamiltonian H_0 are given by the plane waves $\langle\tilde{\vartheta}|n\rangle \sim \exp(\mathrm{i}n\tilde{\vartheta})$, and their unperturbed semiclassical energies read $E_n = H_0(I_n)$ with the quantized actions

$$I_n = \hbar(n+1/2)\,. \tag{3.14}$$

Here we take into account the generic Maslov index $\mu = 2$ for domains of bounded motion.

Applying quantum perturbation theory to the quantized version of the effective pendulum Hamiltonian (3.10), we find that *couplings* are introduced between states $|n\rangle$, $|n'\rangle$ the quantum numbers of which differ by integer multiples of the order r of the resonance — i.e.,

$$n - n' = kr \quad \text{with} \quad k \in \mathbb{Z}\,. \tag{3.15}$$

The true eigenfunctions of H_{eff} can be written as

$$|\tilde{n}\rangle = |n\rangle + \sum_{k\neq 0} \mathcal{A}^{r:s}_{n,k} |n + kr\rangle \tag{3.16}$$

where the coupling amplitudes are, in lowest nonvanishing order in the perturbation, given by

$$\mathcal{A}^{r:s}_{n,k} = \prod_{\ell=1}^{|k|} \frac{V_{r:s} e^{\mathrm{i}\varphi\,\mathrm{sgn}(k)}}{\tilde{E}_n - \tilde{E}_{n+\ell r}} \tag{3.17}$$

with

$$\tilde{E}_n = \frac{(I_n - I_{r:s})^2}{2m_{r:s}}\,. \tag{3.18}$$

These resonance-induced couplings can provide *efficient shortcuts* for the classically forbidden transition between the two symmetry-related wells. Instead of the "direct" tunneling process which is characterized by a semiclassical level splitting $\Delta E^{(0)}_n$ of the form (2.13), the system can undergo perturbative transitions to highly excited states whose unperturbed tunneling rates $\Delta E^{(0)}_{n+kr}$ are much larger due to the reduced action integral in the exponent of Equation (2.13). Neglecting interference effects, we obtain the perturbative expression

$$\Delta E_n = \Delta E^{(0)}_n + \sum_{k\neq 0} \left|\mathcal{A}^{r:s}_{n,k}\right|^2 \Delta E^{(0)}_{n+kr} \tag{3.19}$$

for the modified level splitting of the nth excited doublet.

As was worked out in Refs. [86,87], the sum in Equation (3.19) is typically dominated by a single contribution, namely the one that corresponds to the admixture of the state $|n' \equiv n + kr\rangle$ which in phase space is most closely located on the *opposite side* of the resonance, as "seen" from the state $|n\rangle$ (see Figure 3.2). This condition can be written as $\frac{1}{2}(I_n + I_{n'}) \simeq I_{r:s}$ and implies that the denominator $E_n - E_{n'}$ becomes rather small. As a consequence, resonance-assisted tunneling becomes effective only if the r:s resonance is located "above" the quantized torus of the nth excited state (i.e., $I_{r:s} > I_n$) and if at least $n + r$ states are supported within the domain of bounded motion. Otherwise, the direct transition characterized by $\Delta E^{(0)}_n$ will dominate the tunneling process.

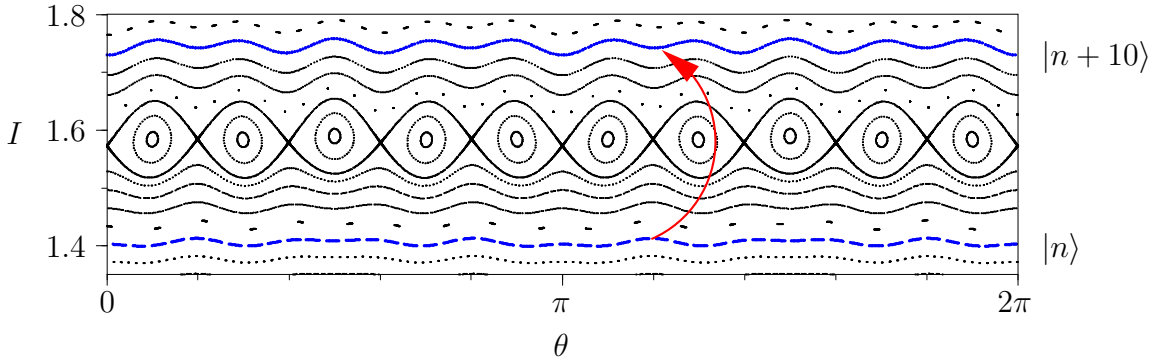

Figure 3.2: Visualization of the coupling process between the states $|n\rangle$ and $|n+10\rangle$ across a 10:1 resonance. The phase space, which is plotted as a function of the action-angle variables I and θ, is taken from the kicked Harper model at $\tau = 1$. The resonance-induced coupling matrix element becomes particularly strong if in action-angle space the nonlinear resonance is symmetrically located in between the two quantized tori on which the states are localized (thick solid and dashed lines, respectively). In the semiclassical limit, this coupling across the 10:1 resonance represents a dynamical tunneling process, which can, consequently, be enhanced due to the presence of high-order resonances that manifest in between the states $|n\rangle$ and $|n+10\rangle$.

It is instructive to realize that the perturbative transition across the r:s resonance represents again a dynamical tunneling process. Hence, according to the above reasoning, it can also be assisted by the appearance of nonlinear r':s' resonances of higher order that manifest in between the quantized torus and the r:s resonance. In the deep semiclassical limit, the modified level splitting will therefore be given by a multiple sum over products of admixtures $|\mathcal{A}_{n,k}^{r_j:s_j}|^2$. It was worked out in Refs. [86,87] that this sum will again be dominated by few major combinations involving transitions between states that are near-degenerate within the corresponding co-rotating frames of the $r_j : s_j$ resonances.

The validity of the resonance-assisted coupling scheme is demonstrated within the "kicked Harper" model, which was first introduced in Ref. [88]. In its symmetric formulation, this model is described by the one-dimensional time-dependent Hamiltonian

$$H(p,q,t) = \cos p + \sum_{n=-\infty}^{\infty} \tau\delta(t-n\tau)\cos q \tag{3.20}$$

that is characterized by the parameter $\tau > 0$, representing both the period of the driving as well as the strength of the perturbation from integrability. The classical

dynamics of this system is integrated through the map $(p,q) \mapsto (p',q')$ with

$$p' = p + \tau \sin q \tag{3.21}$$
$$q' = q - \tau \sin p' \tag{3.22}$$

which generates the stroboscopic Poincaré section at times immediately before the kick. The quantum counterpart of the kicked Harper model is given by the unitary time evolution operator

$$U = \exp\left(-\frac{\mathrm{i}\tau}{\hbar}\cos\hat{p}\right)\exp\left(-\frac{\mathrm{i}\tau}{\hbar}\cos\hat{q}\right) \tag{3.23}$$

where $\hat{p}$ and $\hat{q}$ denote the position and momentum operator, respectively.

The quantum eigenvalue problem of the kicked Harper is drastically simplified for $\hbar = 2\pi/N$ with integer $N > 0$. In that case, the eigenfunctions of U can, due to the periodicity in p and q, be written as simultaneous Bloch functions in position and momentum, with the properties

$$\psi(q+2\pi) = \psi(q)\exp(i\xi_q) \tag{3.24}$$
$$\tilde{\psi}(p+2\pi) = \tilde{\psi}(p)\exp(i\xi_p) \tag{3.25}$$

where $\tilde{\psi}$ denotes the Fourier transform of ψ (see Refs. [88, 89]). Since the subspace of wave functions satisfying (3.24,3.25) at fixed Bloch phases ξ_q and ξ_p is N dimensional, finite matrices need to be diagonalized to obtain the eigenstates of U.

We shall, in the following, focus on eigenfunctions that are periodic in momentum (i.e., $\xi_p = 0$) and may exhibit either periodic or antiperiodic boundary conditions in position (i.e., $\xi_q = 0$ or $\xi_q = \pi$). In this way, the relevant part of the phase space is effectively reduced to two fundamental cells, given e.g. by the region within $-\pi \le q \le 3\pi$ and $-\pi \le p \le \pi$ as shown in Figure 3.3, and the tunneling problem is mapped onto a double well configuration, with the two symmetric wells given e.g. by the regions around $(p,q) = (0,0)$ and $(0,2\pi)$. The rates for dynamical tunneling between these two wells is described by the eigenphase differences

$$\Delta\varphi_n = |\varphi_n^{(\xi_q=0)} - \varphi_n^{(\xi_q=\pi)}|\,, \tag{3.26}$$

where $\varphi_n^{(\xi_q)}$ denotes the eigenphase of the nth excited eigenstate of U, as counted from the center of the regular region, at the Bloch phase ξ_q. These eigenphases are computed by a numerical diagonalization of U (using multiple precision arithmetics) and by comparing its eigenstates with the nth excited state (as counted from the center of the region) of the time-independent Hamiltonian

$$\begin{aligned} H_0(p,q) = {} & \cos p + \cos q - \frac{\tau}{2}\sin p \sin q \\ & -\frac{\tau^2}{12}\left(\cos p \sin^2 q + \cos q \sin^2 p\right) - \frac{\tau^3}{48}\sin(2p)\sin(2q)\,, \end{aligned} \tag{3.27}$$

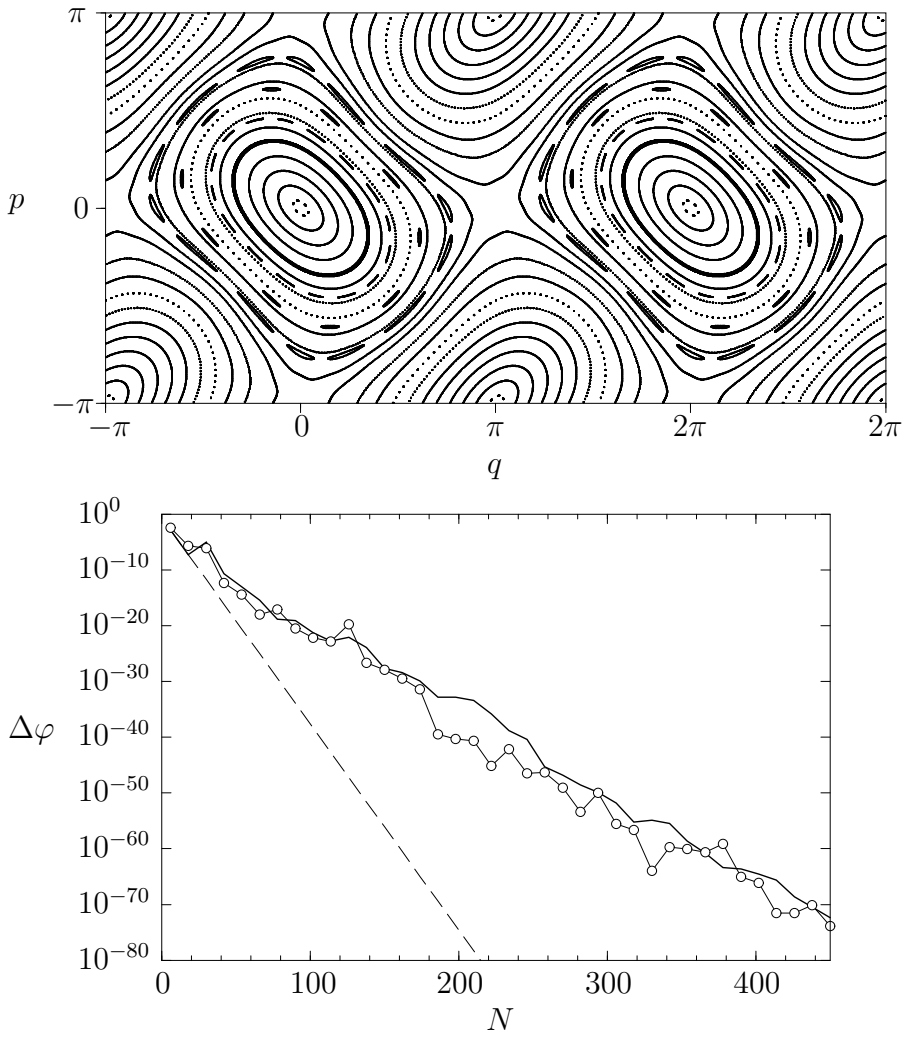

Figure 3.3: Resonance-assisted tunneling in the kicked Harper model. The upper panel shows the stroboscopic Poincaré section of the classical phase space at $\tau = 1$. The lower panel displays the eigenphase splittings of the nth excited states at $N \equiv 2\pi/\hbar = 6(2n+1)$, i.e. of all states that are semiclassically localized on the torus with the action variable $\pi/6$ (boldly marked in the upper panel). The decay of the exact quantum splittings (circles) is quite well reproduced by the semiclassical prediction (thick solid line) which is obtained through a multistep process involving subsequent transitions across the 16:2, the 10:1, and the 14:1 resonance. The dashed line represents the prediction that would be obtained from the integrable approximation $H_0(I)$ without taking into account the effect of the resonances.

which represents a very good integrable approximation of H at small τ [87].

Figure 3.3 shows the eigenphase splittings of the kicked Harper model in the near-integrable regime at $\tau = 1$. The splittings were calculated for the nth excited states at $N = 6(2n+1)$, i.e. for all possible states that are, in phase space, localized on the same classical torus with action variable $\pi/6$. The thick solid line shows the semiclassical prediction of the eigenphase splittings, which is based on three prominent nonlinear resonances that are located between this torus and the separatrix: the 16:2 resonance (with the oscillation period $T = 8\tau$, where the number of islands is doubled for symmetry reasons), the 10:1 resonance, and the 14:1 resonance. Below $N \simeq 100$, we find that the semiclassical tunneling process is entirely induced by the 10:1 resonance, which has the largest coupling matrix element $V_{r:s}$ and which is the most dominant one according to the criterion that r and s be minimal. The other two resonances come into play above $N \simeq 100$, where they "assist" at the transition across the 10:1 resonance.

The overall agreement between the semiclassical prediction and the exact quantum splittings is quite good below $N \simeq 200$, while a systematic overestimation of the quantum splittings occurs deeper in the semiclassical regime. These deviations might arise due to incorrect energy denominators and coupling matrix elements that result from the simplified form (3.10) of the effective pendulum Hamiltonian. We remark, however, that the average exponential decay of the quantum splittings is well reproduced by the semiclassical theory. A comparison with the "unperturbed" splittings $\Delta\varphi_n^{(0)}$ (dashed line in Figure 3.3), which are directly calculated from the integrable approximation (3.27) and which strongly underestimate the exact quantum splittings by many orders of magnitude, clearly demonstrates the validity of the resonance-assisted tunneling mechanism.

We note that at the values for N that are considered in Figure 3.3, the individual islands of the relevant r:s resonances are still "invisible" for the quantum system: The area of one of the islands belonging to the 16:2 resonance, for instance, is calculated to be of the order of $A \simeq 6.2 \cdot 10^{-4}$, which would, according to the EBK criterion (see Equation (2.14) in Chapter 2), imply the condition $N \equiv 2\pi/\hbar \gtrsim 2\pi^2/A \simeq 3 \cdot 10^5$ for the manifestation of localized quantum states on that island. This clearly underlines that the relevance of nonlinear resonances is *not* related to the size of their islands, but rather to the possibility of inducing couplings according to the selection rule (3.15) within the phase space domain of bounded regular motion. As was also verified in mixed regular-chaotic systems, which are discussed in the following section, we generally find that more than $r/2$ states need to be localized in between the quasimode under consideration and the relevant separatrix structure, in order for an r:s resonance to participate at the tunneling process.

3.3 The role of resonances in mixed systems

The significant influence of nonlinear resonances in near-integrable tunneling processes was verified not only in the kicked Harper model [86, 87], but also, from the qualitative point of view, in the periodically driven pendulum [82] as well as, in a more recent study, in the decay rates of quantum accelerator modes in the kicked rotor [90]. Moreover, Keshavamurthy demonstrated that the presence of nonlinear resonances enhances tunneling also in autonomous systems with two and even three degrees of freedom [91–93]. In this latter case [93], transitions between near-degenerate states were clearly traced back to the manifestation of dominant resonance channels in the Arnol'd web, what indicates that the principle of resonance-assisted tunneling prevails in high-dimensional systems and could possibly be used to control classically forbidden processes in complex environments.

In the above-mentioned examples, chaos did not play a significant role, since the relevant chaotic layers were too small to be resolved by quantum mechanics. This is also true for the kicked Harper model at $\tau = 1$, but would change if the perturbation parameter was enhanced. At $\tau = 2$ for instance, the system exhibits a mixed phase space, containing regular islands centred around the elliptic fixed points at $(p, q) = (0, 0)$ and $(0, 2\pi)$ as well as a finite chaotic layer formed around the separatrix structure. In that case, the effective Hamiltonian (3.10) would provide a reliable description of the system's dynamics only within the regular islands. Outside the outermost invariant torus of the island, the presence of other nonlinear resonances with comparably strong influence (the overlapping of which represents a sufficient criterion for the manifestation of chaos in phase space [94]) would give rise to a number of additional coupling matrix elements between various quasi-modes of H_0, even if they are located on different sides of the separatrix structure of the integrable approximation.

The effective Hamiltonian matrix that would result from this consideration is sketched in Figure 3.4. For the sake of clarity, the representation of the matrix is restricted to one particular symmetry class (e.g. to even states with respect to the discrete symmetry of the system) and describes only couplings between the basis states of H_0 that are connected to the ground state of the island via the r:s resonance (taking into account the selection rule $n \mapsto n + kr$ with $k \in \mathbb{Z}$, see Equation (3.16)). The Hamiltonian matrix is effectively tridiagonal within the sub-block of states that are still located within the regular islands, and exhibits additional off-diagonal matrix elements in the chaotic domain. The borderline between those two subspaces is approximately given by the boundary of the regular island, what defines the integer k_c according to

$$I_{(k_c-1)r} < I_c < I_{k_c r} \tag{3.28}$$

where I_c denotes the action variable of the outermost invariant torus of the island.

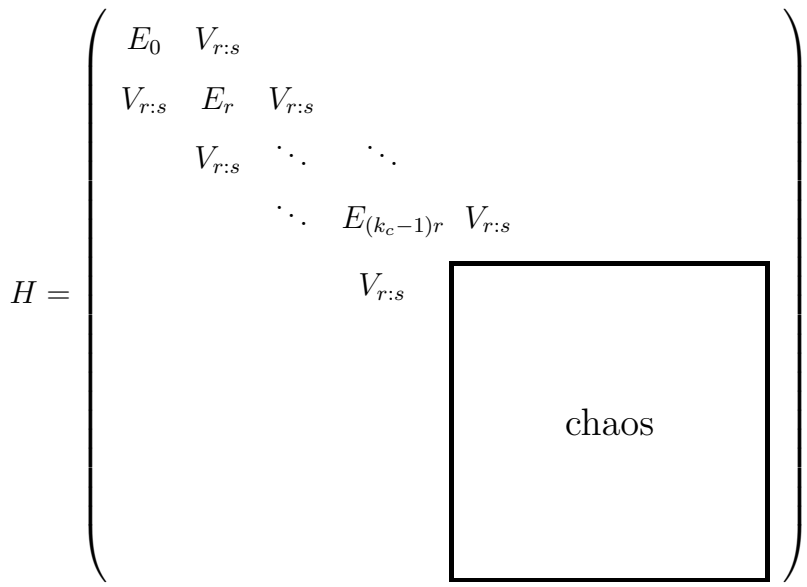

Figure 3.4: Sketch of the effective Hamiltonian matrix that describes the coupling between the regular island and the chaotic domain for one particular symmetry class (i.e., for "even" or "odd" states with respect to the discrete symmetry of the system). The regular part (upper left band) includes only components that are coupled to the island's central state by the r:s resonance. In the simplest possible approximation, the chaotic part consists of a full sub-block with equally strong couplings between all basis states with actions beyond the outermost invariant torus of the island.

The connection to the phenomenological matrix model (3.2) that was introduced in the context of chaos-assisted tunneling [70, 71] is ultimately established by a perturbative elimination of all intermediate regular states $|r\rangle$, $|2r\rangle$, ..., $|(k_c-1)r\rangle$ via which the ground state of the island is coupled to the chaotic domain. According to Equation (3.16) (with $\varphi \equiv 0$ without loss of generality), the pre-diagonalization of the upper left "regular" block of the Hamiltonian matrix yields the modified ground state as

$$|\tilde{0}\rangle = |0\rangle + \sum_{k=1}^{k_c-1} \left(\prod_{\ell=1}^{k} \frac{V_{r:s}}{\tilde{E}_0 - \tilde{E}_{\ell r}} \right) |kr\rangle \tag{3.29}$$

in lowest nonvanishing order in the coupling strength $V_{r:s}$. Recalling that only the basis state $|(k_c-1)r\rangle$ is connected to the chaos block via the matrix element $V_{r:s}$ (see Figure 3.4), we therefore obtain

$$\langle k_c r|H|\tilde{0}\rangle = \left(\prod_{k=1}^{k_c-1} \frac{V_{r:s}}{\tilde{E}_0 - \tilde{E}_{kr}} \right) \langle k_c r|H|(k_c-1)r\rangle = V_{\text{eff}} \tag{3.30}$$

with the effective coupling matrix element

$$V_{\text{eff}} = V_{r:s} \prod_{k=1}^{k_c-1} \frac{V_{r:s}}{\tilde{E}_0 - \tilde{E}_{kr}} \,. \tag{3.31}$$

Using $|\tilde{0}\rangle$ as new basis state, the relevant part of the effective Hamiltonian matrix now reads

$$H = \begin{pmatrix} E_0 & V_{\text{eff}} & 0 & \cdots & 0 \\ V_{\text{eff}} & H_{11} & \cdots & \cdots & H_{1N} \\ 0 & \vdots & & & \vdots \\ \vdots & \vdots & & & \vdots \\ 0 & H_{N1} & \cdots & \cdots & H_{NN} \end{pmatrix} \tag{3.32}$$

where H_{ij} (with $i, j = 1, \ldots, N$) represent the matrix elements of the chaotic sub-block.

Making again a random matrix ansatz for the chaos block (H_{ij}), we are now in a position to determine the energy scale $\overline{\Delta E}$ in the Cauchy distribution (3.6) for the level splitting between the symmetric and the antisymmetric regular state; we obtain

$$\overline{\Delta E} = \frac{2\pi V_{\text{eff}}^2}{N\Delta_c} \tag{3.33}$$

where Δ_c denotes, as in Equation (3.7), the mean spacing between the eigenenergies of the chaos block. This enables us to make *quantitative predictions* of the average level splittings, which are *free of any adjustable parameters*.

Since tunneling rates and their parametric variations are most often studied on a logarithmic scale (i.e., $\log(\Delta E)$ rather than ΔE is typically plotted vs. $1/\hbar$), the relevant quantity to be calculated in this context is the *geometric mean* of the level splittings, i.e.

$$\langle \Delta E \rangle_g \equiv \exp\left[\langle \ln(\Delta E) \rangle\right] \,, \tag{3.34}$$

which involves the average of the *logarithm* of ΔE,

$$\langle \ln(\Delta E) \rangle = \int_0^\infty \ln(\Delta E) P(\Delta E) d(\Delta E) \,, \tag{3.35}$$

rather than the average of ΔE itself [95]. Using the Cauchy distribution (3.6), we obtain as a result the above energy scale (3.33):

$$\langle \Delta E \rangle_g = \overline{\Delta E} = \frac{2\pi V_{\text{eff}}^2}{N\Delta_c} \,. \tag{3.36}$$

This expression simplifies even more for our specific case of periodically driven systems, where the time evolution operator U is modeled by the dynamics under

the effective Hamiltonian (3.32) over one period $\tau \equiv 2\pi/\omega$. In this case, the chaotic eigenphases φ_j of U are randomly distributed in a uniform way within the interval $0 < \varphi_j < 2\pi$. We therefore obtain

$$\Delta_c = \frac{\hbar\omega}{N} \tag{3.37}$$

for the mean level spacing near E_0, what leads to

$$\langle \Delta\varphi \rangle_g \equiv \frac{\tau}{\hbar}\langle \Delta E \rangle_g = \left(\frac{\tau V_{\text{eff}}}{\hbar}\right)^2 \tag{3.38}$$

for the geometric mean of the ground state's eigenphase splitting. Note that this final result does not depend on how many of the chaotic states do actually participate in the sub-block $(H_{ij}^{\pm})$. As long as this number is sufficiently large to justify the validity of the Cauchy distribution (3.6) (see Ref. [71]), the geometric mean of the eigenphase splitting is, up to a trivial prefactor, entirely given by the square of the coupling V_{eff} between the ground state and the chaos.

The applicability of our theory is demonstrated within the "kicked rotor" model, which is described by the Hamiltonian

$$H(p,q,t) = \frac{p^2}{2} + K\sum_{n=-\infty}^{\infty}\delta(t-n)\cos q \tag{3.39}$$

for $K \in \mathbb{R}$. The classical dynamics of this model is integrated by the well-known "standard map" [94] $(p,q) \mapsto (p',q')$ with

$$p' = p + K\sin q \tag{3.40}$$
$$q' = q + p' \tag{3.41}$$

which generates the stroboscopic Poincaré section at times immediately before the kick. Its quantum counterpart is, correspondingly, represented by the unitary time evolution operator

$$U = \exp\left(-\frac{\mathrm{i}}{\hbar}\frac{\hat{p}^2}{2}\right)\exp\left(-\frac{\mathrm{i}}{\hbar}K\cos\hat{q}\right) \tag{3.42}$$

which describes the effect of the kick as well as the free motion in between two kicks.

Similarly to the case of the kicked Harper, the quantum eigenvalue problem considerably simplifies if we choose $\hbar = 2\pi/N$ with even $N > 0$ and restrict our study to eigenfunctions of U that are periodic in position. In that case, one can show that the eigenfunction $\psi(q)$ can be written as a Bloch function in momentum — i.e., $\tilde{\psi}(p+2\pi) = \tilde{\psi}(p)\exp(i\xi_p)$ where $\tilde{\psi}$ denotes the Fourier transform of ψ (see Equation (3.25)). This again implies that the numerical solution of the eigenvalue problem amounts to the diagonalization of finite $N \times N$ matrices.

We now focus on the value $K = 3$ for the kick strength, at which the classical phase space contains a prominent regular island that is embedded in the chaotic sea (see the upper panel of Figure 3.5). The tunneling-induced transition rate between the ground state of this island and its periodically shifted counterpart is, again, given by the eigenphase difference

$$\Delta\varphi_0 = |\varphi_0^{(\xi_p=0)} - \varphi_0^{(\xi_p=\pi)}|\,, \tag{3.43}$$

where $\varphi_0^{(\xi_p)}$ denotes the eigenphase of the island's ground state at the Bloch phase ξ_p. This eigenphase is identified in the spectrum of U by computing the overlap matrix elements of the eigenstates of U with a Husimi function that is centred around $(p, q) = (0, \pi)$.

The lower panel of Figure 3.5 shows the quantum splittings of the kicked rotor as a function of $N \equiv 2\pi/\hbar$, together with their semiclassical prediction based on theory of resonance-assisted tunneling. The latter was evaluated by means of a prominent 10:3 resonance that is manifested in phase space near the boundary of the regular island. The parameters $I_{r:s}$, $V_{r:s}$, and $m_{r:s}$ that characterize the effective pendulum Hamiltonian (3.10) describing the dynamics in the vicinity of the 10:3 resonance were directly calculated from the classical phase space, using only the traces of the stability matrices that are associated with the periodic points of the resonance, as well as the phase space areas that are enclosed by the corresponding separatrix structures (see Refs. [97,98] for more details). This allows us to compute the effective coupling matrix element V_{eff} between the ground state and the chaotic domain (3.31) (where the energy differences in the denominators are evaluated through the relation (3.18)), and to thereby evaluate the prediction for the mean level splittings according to Equation (3.38) with $\tau = 1$. The critical number k_c of perturbative steps by which the island's ground state is connected to the chaotic domain is determined by means of the numerically computed value $S_c = 2\pi I_c$ of the phase space area that is enclosed by the regular island.

The appearance of discontinuous steps in the semiclassical prediction for the splittings is a direct consequence of the artificially sharp separation between perfectly regular dynamics within and perfect structureless chaos outside the island. At $N \simeq 90$ for instance, exactly 10 semiclassically quantized eigenstates fit within the island, which means, due to the selection rule $n \mapsto n \pm 10$ of the 10:3 resonance, that the number of perturbative steps by which the ground state is connected to the chaos is discontinuously enhanced from $k_c = 1$ (for $N < 90$) to $k_c = 2$ (for $N > 90$), reducing thereby the effective matrix element (3.31). In reality, the presence of other, high-order nonlinear resonances near the boundary of the island as well as of partial barriers within the chaotic domain will lead to a rather smooth transition from regular to chaotic motion. Hence, we expect that the sharp steps should "wash out" in a more realistic theory where the effect of those structures is properly taken into account.

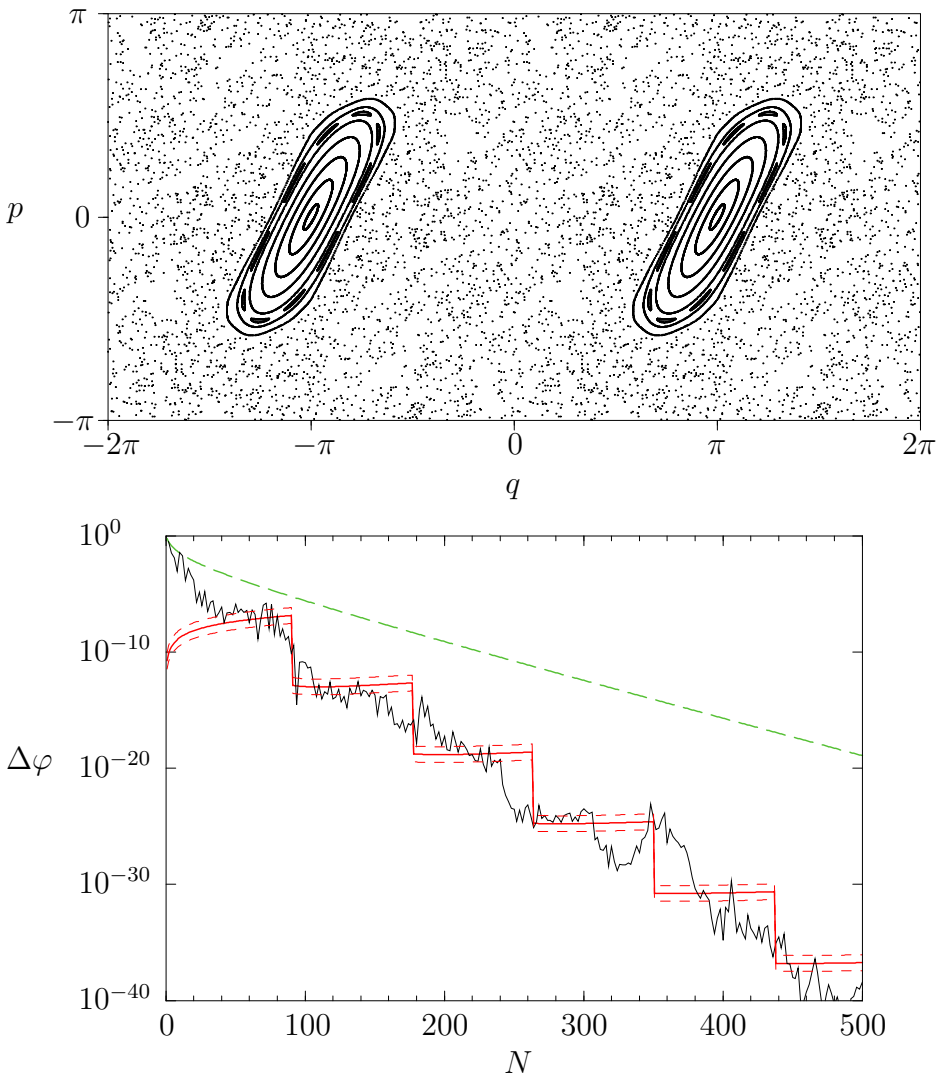

Figure 3.5: Resonance- and chaos-assisted tunneling in the kicked rotor model. The upper panel shows the stroboscopic Poincaré section of the classical phase space at $K = 3$. The lower panel displays the quantum eigenphase splittings of the island's ground state as a function of $N \equiv 2\pi/\hbar$, together with the semiclassical prediction (3.38) given by the step-like curve. The latter is based on the presence of a prominent 10:3 resonance within the regular island. The dashed lines below and above the semiclassical curve indicate the size of the logarithmic standard deviation according to Equation (3.44). The long-dashed curve represents the estimation (3.45) based on the proposal of Podolskiy and Narimanov [96].

It is nevertheless remarkable, however, that these step-like structures do leave their traces in the exact quantum splittings. We clearly recognize in Figure 3.5 the appearance of a sequence of four approximate plateaus in the quantum splittings, the positions and heights of which coincide relatively well with the semiclassical prediction. This strongly confirms that the tunneling process between the islands is indeed governed by the 10:3 resonance, and that the underlying semiclassical theory is well suited to describe the process from the quantitative point of view.

Apart from the geometric mean value $\langle \Delta\varphi \rangle_g$, also the logarithmic *variance* of the eigenphase splitting can be extracted from the Cauchy distribution (3.6): we obtain

$$\left\langle [\ln(\Delta\varphi_0) - \langle \ln(\Delta\varphi_0) \rangle]^2 \right\rangle = \frac{\pi^2}{4} \,. \tag{3.44}$$

This result, which is reminiscent of universal conductance fluctuations in mesoscopic physics [99, 100], predicts that the actual splittings may be enhanced or reduced compared to $\langle \Delta\varphi_0 \rangle_g$ by factors that are typically of the order of $\exp(\pi/2) \simeq 4.8$, independently of the values of $\hbar$ and external parameters. This is indeed the case for the level splittings of the kicked rotor at $K = 3$, where the size of the logarithmic standard deviation is indicated by the dashed lines immediately below and above the semiclassical prediction (which are explicitly defined by $\langle \Delta\varphi_0 \rangle_g \times \exp(\pm\pi/2)$). We clearly see that the size of fluctuations of the quantum splittings is well described by the "window" corresponding to Equation (3.44).

The appearance of plateau structures as well as the universal size of fluctuations in the logarithm of the splittings are *generic* phenomena, in the sense that they arise not only in the kicked rotor model at $K = 3$ but also in other mixed regular-chaotic systems [97, 98], including the driven pendulum Hamiltonian that describes dynamical tunneling of cold atoms in periodically modulated optical lattices [27, 28, 101]. In all cases studied so far, the plateau structures could be traced back to the manifestation of nonlinear r:s resonances within the involved regular islands, and a quantitative reproduction of the tunneling-induced level splittings could be achieved by means of simple classical phase space quantities that are associated with the resonances [102]. The agreement with the exact quantum splittings is not always as convincing as in Figure 3.5. This is partly attributed to the presence of a rich hierarchical substructure of "Cantori" and island chains in the vicinity of the regular island [81, 103], which can become rather relevant for chaotic layers that are not as large as the one shown in Figure 3.5. Such partial barriers are known to appreciably inhibit the quantum transport at finite values of $\hbar$ [104, 105], what enhances the effective size of the phase space region within which the quantum system "sees" localized states. More refined approaches, following the lines of Refs. [69, 70], would probably be required in order to obtain better predictions for such a case.

The theory of resonance-assisted tunneling consistently fails to reproduce the exact splittings in the regime of rather small values for $1/\hbar$, where less than $r/2$

states (in presence of an r:s resonance) are localized within the regular island. In this "deep quantum" regime, the effect of the nonlinear resonance is not manifested in the quantum system, and tunneling between the symmetry-related islands proceeds via a more "direct" mechanism the precise nature of which is still unknown. In this context, Podolskiy and Narimanov proposed a simple semiclassical expression for the level splittings [96], which is based on the effective overlap of the island's quasi-mode wavefunction with the chaotic domain, and which applies in the regime of rather large $\hbar$ where the effect of substructures within and outside the regular island can be neglected. Translated to our problem of estimating the eigenphase splittings between the periodic and antiperiodic ground state of the kicked rotor, this expression reads

$$\Delta\varphi \simeq \gamma\tau \frac{\Gamma(\nu, 2\nu)}{\Gamma(\nu+1, 0)} \overset{\nu\gg 1}{\simeq} \frac{\gamma\tau}{\sqrt{2\pi\nu^3}} \mathrm{e}^{-(1-\ln 2)\nu} \tag{3.45}$$

with $\nu = S_c/(\pi\hbar)$ where S_c represents the phase space area covered by the regular island. The prefactor γ represents an unknown, system-specific rate which, however, does not depend on $\hbar$ and is therefore a purely classical quantity. As the classical dynamics of the kicked rotor at $K = 3$ does not involve any scales that are very different from unity, we set $\gamma\tau \equiv 1$ to obtain a quantitative evaluation of Equation (3.45).

The result is displayed by the long dashed line in Figure 3.5. We see that the prediction of Equation (3.45) agrees reasonably well with the quantum splittings only in the limit of very small $N \lesssim 10$, and strongly overestimates the splittings deeper in the semiclassical regime. This discrepancy substantially limits the predictive power of the estimation (3.45), and underlines once more the importance of taking into account the effect of nonlinear resonances in nonintegrable tunneling problems.

3.4 Generalization to open systems

The discussion of the semiclassical theory of tunneling was, up to now, mainly restricted to closed systems, and focused on the level splittings between bound states that are localized on symmetry-related regular regions in phase space. It is quite obvious that most of the concepts and approaches presented in Chapter 2 can be straightforwardly generalized to *open* systems, in order to describe the decay of a quasi-bound state within a metastable potential well (see, e.g., Refs. [50, 55]). This is also true for the theory of resonance-assisted tunneling. Consider, for instance, a quasi-bound state that is confined in a potential well of the type shown in Figure 1.1(b). In presence of an external periodic driving of this system, the particle can escape not only via "direct" tunneling through the barriers of the well, but also by a resonance-induced coupling process to a highly excited state within the well, which would typically be characterized by a rather short lifetime.

The generalization of chaos-assisted tunneling to open systems was achieved by Zakrzewski, Delande, and Buchleitner [106]. The authors of Ref. [106] specifically focused on the ionization process of the highly excited hydrogen atom in a microwave field with linear or circular polarization. In this system, the nonlinear resonance between the external driving and the unperturbed Kepler motion of the electron may, for a suitable choice of the driving frequency and the field amplitude, induce a prominent regular island in the classical phase space of hydrogen, which is surrounded by a layer of chaotic and ionizing motion (see Figure 3.6) [107]. A Quantum (Floquet) eigenstate that is localized in the center of this island corresponds, in configuration space, to a minimum-uncertainty wave packet which follows the resonantly driven Kepler orbit of the classical electron *without spreading*, i.e., which is "kept in shape" due to the presence of field-induced dynamical phase space barriers [108–113]. Such nondispersive wave packets were indeed observed in recent experiments on singly excited lithium atoms (with the principal quantum number $n \simeq 70$), where the nonspreading wave packet motion was induced by a linearly polarized microwave field and detected by ionization with half-cycle pulses [114, 115].

With the ordinary spreading mechanism being suppressed, the wave packet can oscillate along the classical Kepler orbit over time scales of the order of one million Kepler cycles [110]. Indeed, the lifetime of such a nondispersive wave packet is ultimately limited by a *classically forbidden* process, namely dynamical tunneling through the phase space barriers of the regular island on which the wave packet is localized: once escaped from there into the surrounding chaotic sea, the electronic population can be rather efficiently transported to highly excited Rydberg states of the atom, from where it would undergo subsequent field-induced ionization. This chaos-assisted decay process can, in a similar way as for dynamical tunneling between a pair of symmetry-related regular islands, be represented by a Hamiltonian matrix of the form (3.2), involving the (Floquet) energy E_0 of the wave packet state on the island, the matrix elements H_{ij} between the states that are supported by the chaotic part of the phase space, as well as the couplings v_j between the regular state and the chaos block.

Ionization is now introduced by nonvanishing negative imaginary parts of the matrix elements H_{ij}, which would formally arise after a perturbative elimination of the coupling to the continuum of positive-energy states within the hydrogen atom. Assuming that only one single ionization channel significantly contributes to the decay of chaotic states (which would be the case, e.g., for a one-dimensional model of the atom) and making a random-matrix ansatz for the real parts of the matrix elements H_{ij}, Zakrzewski et al. derived the probability distribution

$$P(\Gamma) = \frac{1}{\pi} \frac{\sqrt{\Gamma_0/\Gamma}}{\Gamma + \Gamma_0} \tag{3.46}$$

for the decay rate Γ of the wave packet state [106]. As in the case of chaos-assisted

tunneling between symmetry-related regular islands (see Equation (3.6)), this distribution depends only on one single parameter, namely the intrinsic scale Γ_0 which contains the ionization rates of the states within the chaos block as well as their coupling rates $|v_j|^2$ to the regular island. Although level repulsion between eigenvalues of the chaotic matrix (H_{ij}) was explicitly neglected in the derivation of Equation (3.46), the functional form of this probability distribution turned out to agree very well with numerical data that were obtained from Floquet calculations within the periodically driven hydrogen atom [106].

Using the insight that *nonlinear resonances* govern the coupling process between the regular island and the chaotic domain in the semiclassical limit, we can now make quantitative predictions for the average decay rate of the nondispersive wave packets [116]. This is demonstrated for the special case of a hydrogen atom in a linearly polarized microwave field, where the electron is prepared on an extremal parabolic Rydberg state that is oriented along the polarization of the field. Using atomic units, this system is approximately described by the one-dimensional Hamiltonian

$$H = \frac{p^2}{2} - \frac{1}{z} + Fz\cos(\omega t) \tag{3.47}$$

where z and p denote the position and momentum, respectively, of the electron along the field polarization axis, and F and ω represent the field amplitude and frequency, respectively, of the microwave perturbation.

We shall, in the following, focus on the choice $\omega = \omega_0 n_0^{-3}$ and $F = F_0 n_0^{-4}$ of the field parameters, with $\omega_0 = 1$ and $F_0 = 0.041$. Scaling F and ω in such a way ensures that the classical dynamics of the driven hydrogen atom remains *invariant* under variation of n_0, with the position and momentum being rescaled according to $z \mapsto z n_0^2$ and $p \mapsto p n_0^{-1}$. Here n_0 corresponds to the principal quantum number of the Rydberg state that is most strongly affected by the resonant driving, and the variation of n_0 at fixed values for ω_0 and F_0 is strictly equivalent to the variation of $1/\hbar$ at fixed classical parameters in model systems such as the kicked rotor or the kicked Harper.

Figure 3.6 shows a stroboscopic Poincaré section of the classical phase space at the field phase $\omega t = 0 \pmod{2\pi}$. We clearly recognize the regular island at $z \simeq 2n_0^2$, which is induced by the resonant microwave perturbation and which supports, in the corresponding quantum system, the nondispersive wave packet state. This island contains a visible substructure which is induced by a nonlinear 5:1 sub-resonance between the driving and the free oscillation around the island's center. As in the case of the one-dimensional kicked systems discussed in Section 3.3, we can straightforwardly compute the parameters $I_{5:1}$, $m_{5:1}$, and $V_{5:1}$ that enter into the effective pendulum Hamiltonian (3.10) describing the dynamics in the vicinity of this resonance. Those parameters are, as explained in Red. [97], directly extracted from the classical phase space, together with the area covered by the island.

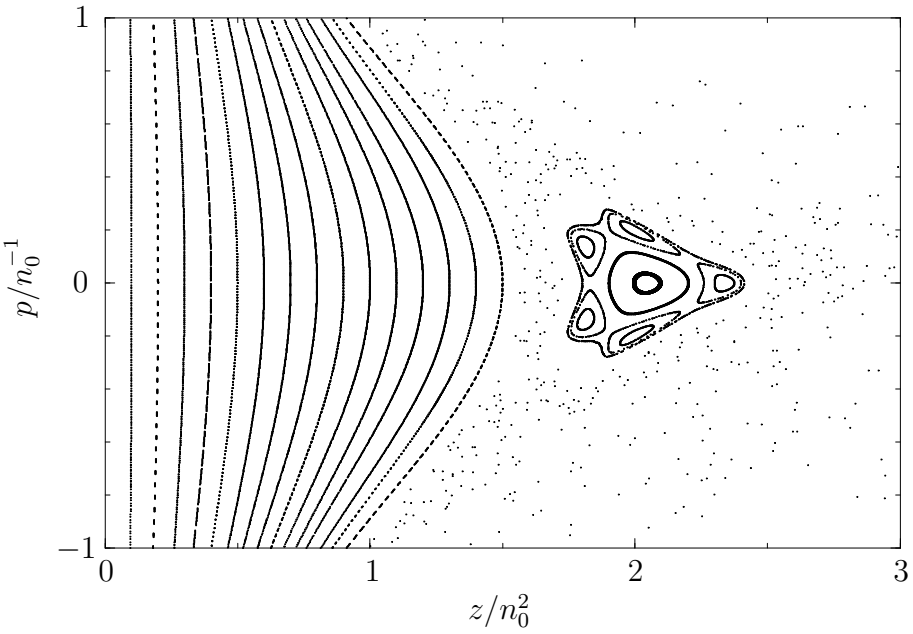

Figure 3.6: Classical phase space of the driven hydrogen atom at $\omega = n_0^{-3}$ and $F = 0.041 n_0^{-4}$. Shown is a stroboscopic Poincaré section of the electron's motion as a function of its position z and momentum p, at the driving field phase $\omega t = 0 \pmod{2\pi}$. The nondispersive wave packet is localized on the prominent regular island at $z/n_0^2 \simeq 2$, which periodically oscillates along the unperturbed Kepler orbit in the course of time evolution. The decay of the wave packet state is mainly induced by the nonlinear 5:1 sub-resonance that manifests itself within the regular island.

As was already mentioned above, ionization is formally introduced into the chaotic part of the Hamiltonian matrix by a perturbative elimination of single-photon transitions to the atomic continuum. This affects only Rydberg states with ionization potentials smaller than ω, i.e., with principal quantum numbers n above $n_c = n_0^{3/2}/\sqrt{2\omega_0}$, and only few of those are, in this high-frequency regime ($\omega \gg 1/n^3$), significantly coupled to the wave packet state. We therefore assume that only one state within the chaotic block of the Hamiltonian acquires a finite decay rate. The latter is very well estimated by the Golden Rule expression

$$\Gamma_c = 0.265 F^2 \omega^{-10/3} n_c^{-3} \tag{3.48}$$

for the single-photon ionization rate of a Rydberg state with quantum number n_c [117].

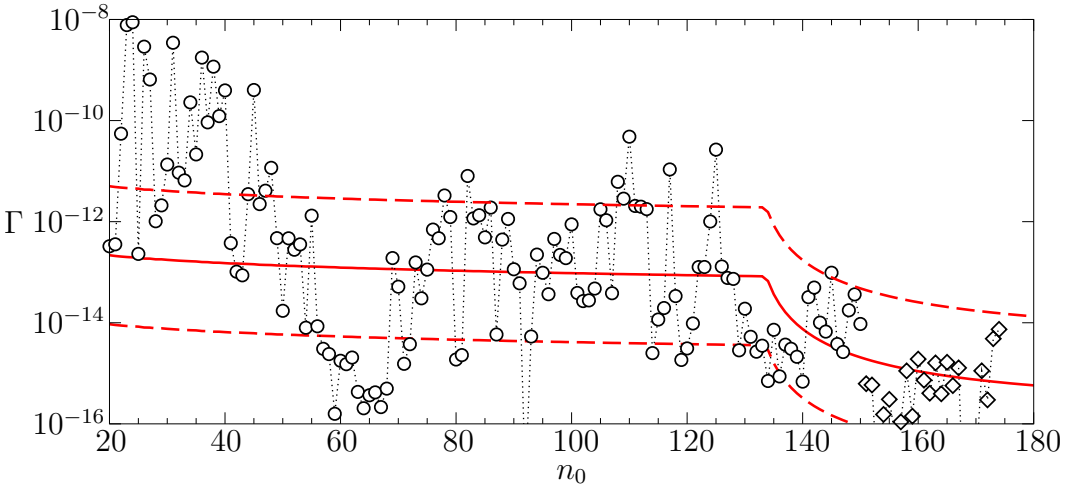

Figure 3.7: Decay rates of the nondispersive wave packet states at $\omega = n_0^{-3}$ and $F = 0.041 n_0^{-4}$, as a function of the principal quantum number n_0 at which this wave packet would most pronouncedly be encountered. The circles and diamonds (which are connected by dashed lines to guide the eye) represent the results of quantum Floquet calculations, which involve, respectively, all bound states with an ionization potential larger than the one-photon energy ω (circles) and, deeper in the semiclassical regime, only bound states below $2n_0$ (diamonds). The solid line shows the semiclassical prediction for the average decay rate (3.50), and the dashed lines indicate the size of the standard deviation according to Equation (3.51).

Altogether, we thereby obtain the effective Hamiltonian matrix

$$H = \begin{pmatrix} E_0 & V_{\text{eff}} & 0 & \cdots & 0 \\ V_{\text{eff}} & H_{11} & \cdots & \cdots & H_{1N} \\ 0 & \vdots & & & \vdots \\ \vdots & \vdots & & & \vdots \\ 0 & H_{N1} & \cdots & \cdots & H_{NN} - \frac{\mathrm{i}}{2}\Gamma_c \end{pmatrix} \tag{3.49}$$

for the decay of the wave packet state at energy E_0, where the resonance-induced coupling matrix element V_{eff} is again defined by Equation (3.31). Given this specific form of the Hamiltonian matrix, the intrinsic scale appearing in the probability distribution (3.46) is now evaluated as $\Gamma_0 = (\pi V_{\text{eff}}/\omega)^2 \Gamma_c$, which permits the calculation of average decay rates of the wave packet states. As in Section 3.3, we are most interested in a comparison with the exact decay rates on a *logarithmic* scale. We therefore compute again the *geometric* mean of Γ, which is given by the intrinsic

scale Γ_0:

$$\overline{\Gamma} \equiv \exp[\langle \ln(\Gamma) \rangle] = \Gamma_0 = \left(\frac{\pi V_{\text{eff}}}{\omega} \right)^2 \Gamma_c \,. \tag{3.50}$$

The corresponding logarithmic variance of the splittings is now evaluated as

$$\left\langle \left[\ln(\Gamma) - \ln(\overline{\Gamma}) \right]^2 \right\rangle = \pi^2 \,, \tag{3.51}$$

which again implies that the typical size of fluctuations on a logarithmic scale is independent of system-specific parameters.

Figure 3.7 shows the comparison between our semiclassical prediction based on the 5:1 resonance and the exact quantum splittings. The latter were numerically calculated by the diagonalization of the corresponding Floquet matrix, where the method of complex scaling was used to identify quasi-bound states in the continuous Floquet spectrum (see Refs. [108, 118] for technical details). We clearly see that the quantum decay rates develop a pronounced plateau structure in the range $70 \lesssim n_0 \lesssim 130$, followed by a cutoff near $n_0 \simeq 130$ where the decay rates fall below the limit $\sim 10^{-15}$ for the numerical precision of this calculation. Both the height of the plateau structure as well as the position of the cutoff (which arises at the value for n_0 where exactly 5 locally quantized states are supported by the regular island) are well predicted by the expression (3.50). Furthermore, the average size of fluctuations seems to be well characterized by the expression (3.51) for the logarithmic variance. This is indicated by the dashed lines which correspond to $\overline{\Gamma} \times \exp(\pm\pi)$ and which enclose to a large extent the rapidly fluctuating quantum splittings [116].

The present tunneling process is qualitatively different from the ones that were discussed in the previous section, insofar as it refers to a specific physical system that can be studied with state-of-the-art experiments [114, 115]. The experimental verification of resonance-assisted tunneling within microwave-driven Rydberg atoms is, in principle, in reach, but poses a number of technical challenges such as the preparation of highly excited states with $n_0 \simeq 100$ as well as the observation of lifetimes of the order of 10^{10} atomic units and more. It might seem more promising to consider *ultracold bosonic quantum gases* for this purpose [25, 26], where extraordinary experimental possibilities for the preparation, control, and detection of the dynamical tunneling process would be available. In such systems, however, *interaction effects* would have to be taken into account — what is the topic of the next chapter.

Tunneling and transport of Bose-Einstein condensates

4.1 Tunneling processes with interacting matter waves

The realization of *Bose-Einstein condensation* in atomic vapours, first achieved in 1995 [119–121], has lead to new possibilities to investigate condensed matter phenomena with an extraordinary degree of precision and control. The experimental research on Bose-Einstein condensates started with the exploration of the basic properties of the Bose-Einstein condensed state, such as the coherence and intereference properties (e.g. [122, 123]), the collective excitations of a condensate (e.g. [124, 125]) and the propagation of sound [126], as well as superfluidity properties (e.g. [127]) and the creation of vortices within rotating condensates (e.g. [128, 129]). In these experiments, the condensate was generally formed by a dilute gas of spin-polarized alkaline atoms (typically ^{87}Rb or ^{23}Na) that were prepared in a *magnetic trap*, where the Zeeman effect was used to confine atoms with antiparallel magnetic moment around a local minimum of the magnetic field strength. Laser cooling and evaporative cooling are typically applied to reduce the temperature of the gas down to $\sim 1\mu$K where the phase transition to the Bose-Einstein condensate takes place, and absorption images after a free expansion of the condensate in absence of the trapping potential are generally made in order to probe the momentum distribution of the atoms (see Ref. [130] for a review on experimental techniques).

Ultracold atomic gases can also be confined with *optical* techniques, using laser beams that are off-resonantly tuned with respect to the intra-atomic transition frequency $(E_p - E_s)/\hbar$ between the ground state $|s\rangle$ and the first excited state $|p\rangle$ of the atom. In presence of such a laser beam, the atom encounters the effective potential

$$V(\mathbf{r}) = -\frac{1}{2}\frac{|\langle p|\hat{\mathbf{d}}\cdot\hat{\epsilon}|s\rangle|^2}{E_p - E_s - \hbar\omega}\langle E^2(\mathbf{r},t)\rangle_t \tag{4.1}$$

where $\hat{\mathbf{d}}$ denotes the atomic dipole operator, $\hat{\epsilon}$ is the polarization unit vector of the laser field, ω is the laser frequency, and $\langle E^2 \rangle_t$ represents the temporal average of the square of the electric field amplitude, which corresponds to the laser intensity [131]. The optical potential $V(\mathbf{r})$ will be attractive if the laser is "red-detuned" with respect to the intra-atomic transition frequency, i.e. $\hbar\omega < E_p - E_s$, and repulsive in case of a "blue-detuned" laser, i.e. with $\hbar\omega > E_p - E_s$. With this principle, a *dipole trap* can, for instance, be realized in the center of a focused red-detuned laser beam, where the spatially dependent intensity acquires a local maximum.

A *spatially periodic* potential can, consequently, be induced by the standing-wave field of two counterpropagating laser beams. Such "optical lattices" introduce a new microscopic length scale, namely the period of the lattice which is given by the laser wavelength, and open the possibility to "simulate" condensed matter phenomena from solid-state physics with cold interacting atoms (see Refs. [132,133] for recent reviews). A most prominent example in this context is the realization of the quantum phase transition from a superfluid to a Mott insulator state [134], which was theoretically proposed by Jaksch et al. [135]. In this experiment, a Bose-Einstein condensate of repulsively interacting ^{87}Rb atoms was prepared in a three-dimensional optical lattice (i.e., with counterpropagating laser beams along all three spatial directions) the intensity of which was adiabatically tuned. Absorption images after free expansion clearly revealed the reversible transition from the superfluid phase at low laser intensities, where the atoms are coherently distributed over the whole lattice, to the Mott insulator phase at high intensities, where each atom is individually confined to a single site of the lattice [134].

Optical lattices also permit to investigate *tunneling processes* with interacting matter waves. This was first demonstrated by Anderson and Kasevich [136] who prepared a condensate in a vertically oriented one-dimensional optical lattice and observed a sequence of coherent matter-wave pulses that tunneled through the barriers of the lattice and propagated along the direction of gravity. This setup is clearly analogous to Bloch oscillations in semiconductor superlattices [137] and lead to further experimental and theoretical research with particular emphasis on the influence of the repulsive interaction between the atoms (e.g. [138–141]).

More recently, a double-well geometry was realized by Anker et al. [142] combining a dipole trap with an optical lattice. In close analogy to weak links between superconducting electrodes [143], this setup corresponds to a *Josephson junction* [2] for cold atoms. As was predicted by Smerzi et al. [144], a strong population imbalance between the two wells lead to the observation of *nonlinear self-trapping* [142]. This means that the atoms remain confined within the wells in which they were prepared, without tunneling back and forth across the barrier (what would occur if the wells were nearly equally populated with atoms). The self-trapping effect is a consequence of the repulsive interaction between the atoms and can be understood on the basis of a *mean field* description of the interacting condensate.

To explain this phenomenon, we start from the many-body Hamiltonian

$$\begin{aligned}\hat{H} &= \int d^3r \hat{\psi}^\dagger(\vec{r},t)\left(-\frac{\hbar^2}{2m}\Delta + V(\vec{r})\right)\hat{\psi}(\vec{r},t) \\ &\quad + \frac{1}{2}\int d^3r \int d^3r' \hat{\psi}^\dagger(\vec{r},t)\hat{\psi}^\dagger(\vec{r}',t)U(\vec{r}-\vec{r}')\hat{\psi}(\vec{r}',t)\hat{\psi}(\vec{r},t) \end{aligned} \tag{4.2}$$

for the condensate, where m is the mass of the atoms and $V(\vec{r})$ represents the external confinement potential. At temperatures of the order of $T \sim 1\mu$K, the possibility of electronic excitations within the atoms can be neglected (unless Feshbach resonances are involved), and the scattering process between two atoms is dominantly described by the contribution from s-wave scattering. This means that the interaction between two atoms of the condensate can be well approximated by the structureless contact potential

$$U(\vec{r}-\vec{r}') = U_0\delta(\vec{r}-\vec{r}') \tag{4.3}$$

with

$$U_0 = \frac{4\pi\hbar^2 a_s}{m} \tag{4.4}$$

where a_s is the s-wave scattering length of the atomic species (see, e.g., Ref. [145]). This choice of the interaction strength U_0 ensures that the asymptotic behaviour of the scattering process between two atoms is well reproduced by the model potential (4.3). In practice, a_s can, for a given atomic species, be determined from numerical *ab initio* calculations as well as from photoassociation spectroscopy [146].

Inserting the potential (4.3) into Equation (4.2) yields the Hamiltonian

$$\hat{H} = \int d^3r \hat{\psi}^\dagger(\vec{r},t)\left(-\frac{\hbar^2}{2m}\Delta + V(\vec{r}) + \frac{U_0}{2}\hat{\psi}^\dagger(\vec{r},t)\hat{\psi}(\vec{r},t)\right)\hat{\psi}(\vec{r},t) \tag{4.5}$$

where the nature of the interaction is characterized by a single parameter, namely the s-wave scattering length a_s of the two-body collision process. It is quite obvious that the sign of a_s crucially determines the *stability* properties of a Bose-Einstein condensed state. A positive sign of a_s effectively induces a *repulsive* interaction within the condensate, what prevents the atoms from approaching each other too closely. At a negative sign of a_s, on the other hand, the atoms effectively *attract* each other. This enhances the probability for *three-body recombinations* (where two atoms form a molecule by transfering the binding energy to a third atom) and thereby reduces the lifetime of the condensate. Experiments with Bose-Einstein condensates are, as a consequence, preferrably performed with alkaline isotopes that exhibit a positive s-wave scattering length (such as ^{87}Rb or ^{23}Na).

To obtain an analytical description for the ground-state properties of a gas of N atoms within the trapping potential $V(\vec{r})$, we now make the *Hartree* ansatz by

assuming that all atoms share the same normalized single-particle orbital $\phi(\vec{r})$. Defining the *condensate wavefunction* by $\psi(\vec{r}) \equiv \sqrt{N}\phi(\vec{r})$ (where $|\psi|^2$ would consequently represent the density of condensed atoms), the variational principle for the optimal choice for ψ amounts to the minimization of the functional $\mathcal{H}[\psi] - \mu\mathcal{N}[\psi]$ with

$$\mathcal{H}[\psi] = \int d^3r \left(\frac{\hbar^2}{2m} |\vec{\nabla}\psi(\vec{r})|^2 + V(\vec{r})|\psi(\vec{r})|^2 + \frac{1}{2}U_0|\psi(\vec{r})|^4 \right) , \tag{4.6}$$

$$\mathcal{N}[\psi] = \int d^3r |\psi(\vec{r})|^2 - N \, . \tag{4.7}$$

This straightforwardly leads to the *Gross-Pitaevskii equation*

$$\left(-\frac{\hbar^2}{2m}\Delta + V(\vec{r}) + U_0|\psi(\vec{r})|^2 \right) \psi(\vec{r}) = \mu\psi(\vec{r}) \tag{4.8}$$

for the condensate wavefunction ψ. The Lagrange parameter μ can here be interpreted as the *chemical potential* of the condensate, i.e. the energy that would be required to add a single atom to (or remove it from) the condensate.

The minimization approach sketched here can be straightforwardly generalized to describe also *time-dependent* phenomena, such as the evolution of a condensate in presence of the time-dependent potential $V(\vec{r}, t)$ [147]. This leads to the time-dependent Gross-Pitaevskii equation

$$\mathrm{i}\hbar\frac{\partial}{\partial t}\psi(\vec{r}, t) = -\frac{\hbar^2}{2m}\Delta\psi(\vec{r}, t) + V(\vec{r}, t)\psi(\vec{r}, t) + U_0|\psi(\vec{r}, t)|^2\psi(\vec{r}, t) \tag{4.9}$$

which is the starting point for many theoretical investigations of the properties of a Bose-Einstein condensate [148]. Corrections to this lowest-order mean-field description of the condensate can be investigated by means of the well-known *Bogoliubov approach*, which is described in Refs. [149, 150] for the case of an inhomogeneous trapping potential. An alternative approach consists in the numerical integration of the equations of motion that describe the time evolution of cumulants which are associated with expectation values of products of the field operators $\hat{\psi}(\vec{r}, t)$ and $\hat{\psi}^\dagger(\vec{r}, t)$ [151, 152]. In lowest order, this approach yields again the Gross-Pitaevskii equation (4.9).

The above mean-field ansatz is clearly valid for harmonic confinement potentials, for which theoretical predictions of excitation modes and their frequencies on the basis of the Gross-Pitaevskii equation were found to be in good agreement with experiments [148]. It can also be applied to describe tunneling of Bose-Einstein condensates in symmetric double-well potentials [144, 153, 154]. In the simplest possible formulation of this process, two normalized and orthogonal wavefunctions $\phi_L(\vec{r})$ and $\phi_R(\vec{r})$ are introduced which are localized in the left and right well of the potential,

respectively, and which can be formally defined by the symmetric and antisymmetric linear combinations of the "even" and "odd" ground states of the double well potential. Within a two-mode approximation, the population of other single-particle orbitals is neglected, and the condensate wavefunction is written as

$$\psi(\vec{r},t) = \psi_L(t)\phi_L(\vec{r}) + \psi_R(t)\phi_R(\vec{r}) \tag{4.10}$$

with time-dependent amplitudes $\psi_L(t)$ and $\psi_R(t)$. Inserting this ansatz into the time-dependent Gross-Pitaevskii equation (4.9) yields the equations

$$\mathrm{i}\hbar\frac{d\psi_L}{dt} = [E_L + u_0 N_L(t)]\,\psi_L(t) - K\psi_R(t) \tag{4.11}$$

$$\mathrm{i}\hbar\frac{d\psi_R}{dt} = [E_R + u_0 N_R(t)]\,\psi_R(t) - K\psi_L(t) \tag{4.12}$$

where $N_{L/R}(t) \equiv |\psi_{L/R}(t)|^2$ corresponds to the instantaneous number of atoms in the left and right well, respectively. The energies E_L, E_R, u_0, and K are here defined by

$$E_{L/R} = \int d^3r \left(\frac{\hbar^2}{2m}|\vec{\nabla}\phi_{L/R}(\vec{r})|^2 + V(\vec{r})|\phi_{L/R}(\vec{r})|^2\right) \tag{4.13}$$

$$u_0 = U_0 \int d^3r |\phi_L(\vec{r})|^4 = U_0 \int d^3r |\phi_R(\vec{r})|^4 \tag{4.14}$$

$$K = -\int d^3r \left(\frac{\hbar^2}{2m}\vec{\nabla}\phi_L(\vec{r})\cdot\vec{\nabla}\phi_R(\vec{r}) + V(\vec{r})\phi_L(\vec{r})\phi_R(\vec{r})\right) \tag{4.15}$$

(assuming real wavefunctions $\phi_L(\vec{r})$ and $\phi_R(\vec{r})$), and nonlinear contributions to the coupling between ψ_L and ψ_R are neglected. E_L and E_R would be identical in the case of a perfectly symmetric double barrier potential, while a small bias of the wells would, in lowest order, introduce a finite splitting between those single-particle levels.

The system of equations (4.11,4.12) is most conveniently analyzed in terms of the fractional population imbalance

$$z(t) = \frac{N_L(t) - N_R(t)}{N} \tag{4.16}$$

where $N \equiv N_L(t) + N_R(t)$ is the total number of atoms in the double well potential, and the phase difference

$$\phi(t) = \arg[\psi_R(t)] - \arg[\psi_L(t)] \tag{4.17}$$

between the condensates in the left and right well. The time evolution of these two variables can be described by the effective pendulum-like Hamiltonian

$$H_{\mathrm{eff}}(z,\phi) = \frac{1}{2}\Lambda z^2 + \Delta\mathcal{E}z - \sqrt{1-z^2}\cos\phi \tag{4.18}$$

with $\Lambda \equiv Nu_0/(2K)$ and $\Delta\mathcal{E} \equiv (E_L - E_R)/(2K)$, and is given by

$$\frac{dz}{dt} = -\frac{\partial H_{\text{eff}}}{\partial \phi} = -\sqrt{1-z^2(t)}\sin\phi(t)\,, \tag{4.19}$$

$$\frac{d\phi}{dt} = +\frac{\partial H_{\text{eff}}}{\partial z} = \Delta\mathcal{E} + \Lambda z(t) + \frac{z(t)}{\sqrt{1-z^2(t)}}\cos\phi(t)\,. \tag{4.20}$$

In the limit of small values for Λ, this system of equations is equivalent to the tunneling dynamics of noninteracting atoms: two stable fixed points at $(z,\phi) = (0,0)$ and $(z,\phi) = (0,\pi)$ arise at zero bias $\Delta\mathcal{E} = 0$, corresponding to the two symmetric and antisymmetric eigenstates of the double well potential, and the oscillatory motion around those fixed points describes the time-dependence of Rabi oscillations between the wells.

The scenario is quite different for large values of Λ, i.e. when the interaction energy Nu_0 exceeds the coupling rate K between the quasi-modes of the two wells. In this case, the phase space generated by the Hamiltonian (4.18) closely resembles the one of a pendulum where the effective "momentum" variable is dynamically restricted to $-1 \leq z \leq 1$ (see the lower panels in Figure 4.1). Rabi oscillations between the left and right well (which can be seen as the matter-wave analog of current oscillations across superconducting Josephson junctions [143]) are then, at $\Delta\mathcal{E} = 0$, only possible in the immediate vicinity of the fixed point $(z,\phi) = (0,0)$, i.e. for small differences z in the relative occupation number. At large imbalances, on the other hand, the effective pendulum described by Equation (4.18) undergoes "rotational" motion, which implies that the major part of the population is not exchanged between the wells, but remains trapped on one side of the barrier.

This macroscopic quantum self-trapping phenomenon can be intuitively understood from the fact that the chemical potentials in the left and right well are, in presence of the interaction, enhanced by the mean-field energies u_0N_L and u_0N_R, respectively (see Equations (4.11,4.12)). A large difference $N_L - N_R$ in the occupation numbers therefore introduces an effective *asymmetry* to the double-well problem. As a consequence, the chemical potentials in the left and right wells do no longer match, and population transfer across the barrier is inhibited. Quite obviously, macroscopic quantum self-trapping is "overruled" in the true many-body dynamics of the bosonic system, which certainly allows for tunneling of the whole condensate from one side of the barrier to the other. It was shown in Ref. [155], however, that this "meta tunneling " process takes place on a time scale that increases exponentially with the total number of atoms in the condensate.

Clearly, applying a finite *bias* $\Delta\mathcal{E}$ to the double well potential allows one to compensate the interaction-induced mismatch of chemical potentials and to permit Josephson-like oscillations between the wells (see Figure 4.1). The number of atoms that can be transferred in this way, however, is rather limited, due to the fact that

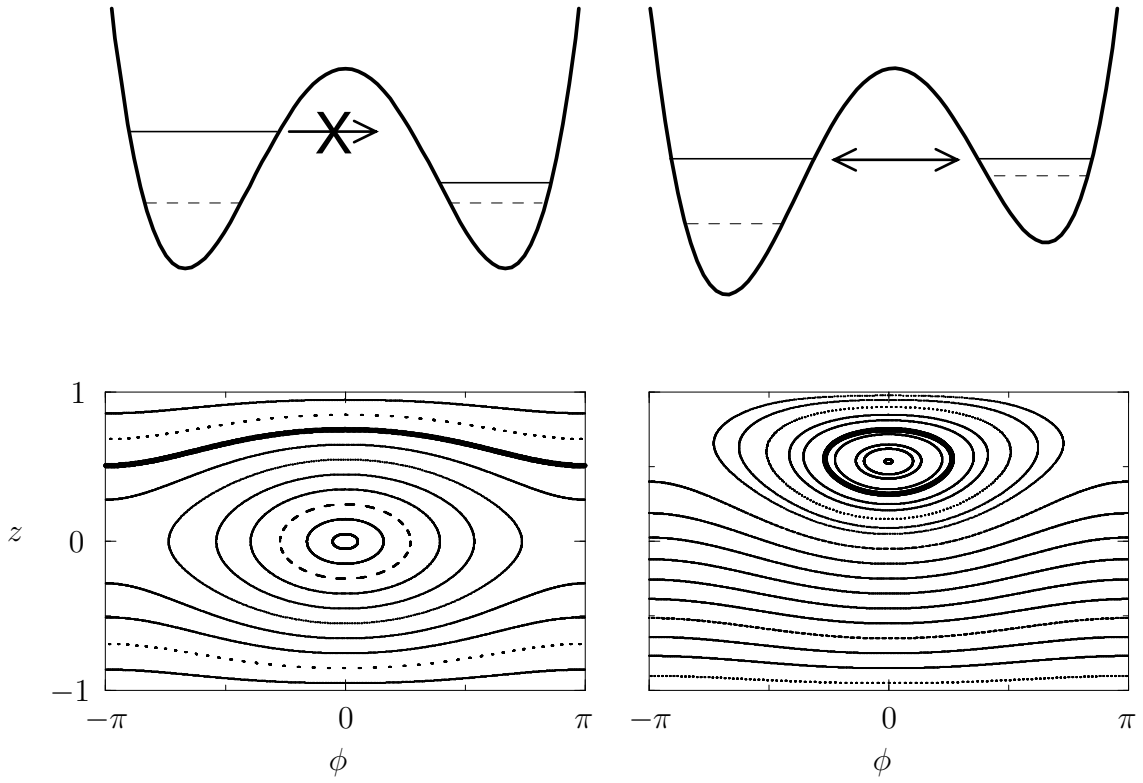

Figure 4.1: Macroscopic quantum self-trapping of a Bose-Einstein condensate in a double well potential. At zero bias between the wells (left column), a finite population imbalance leads to an unequal shift of the chemical potentials in the left and right wells (solid horizontal lines in the upper panels; the dashed lines indicate the unperturbed ground state energies $E_{L,R}$). A *mismatch* of levels consequently arises, and the transfer of atoms from the left to the right well is inhibited. This mismatch can be compensated by applying a finite bias to the system (upper right panel). The lower panels show the classical phase space generated by the effective pendulum Hamiltonian (4.18) at $\Lambda = 10$ in absence and in presence of the bias ($\Delta\mathcal{E} = -6$ in the lower right panel). Boldly marked are the orbits that correspond to the scenarios depicted in the upper panels.

the chemical potentials move out of resonance again as soon as the populations in the two wells start to approach each other (see Ref. [156]). This is illustrated in Figure 4.2 where we plot the relative number of atoms that would participate at the tunneling process between the wells at given values for Λ and $\Delta\mathcal{E}$ if initially all atoms were prepared in the left well. For strong interactions $\Lambda \gg 1$, this number is maximized at finite negative bias $\Delta\mathcal{E} < 0$, but remains rather limited compared

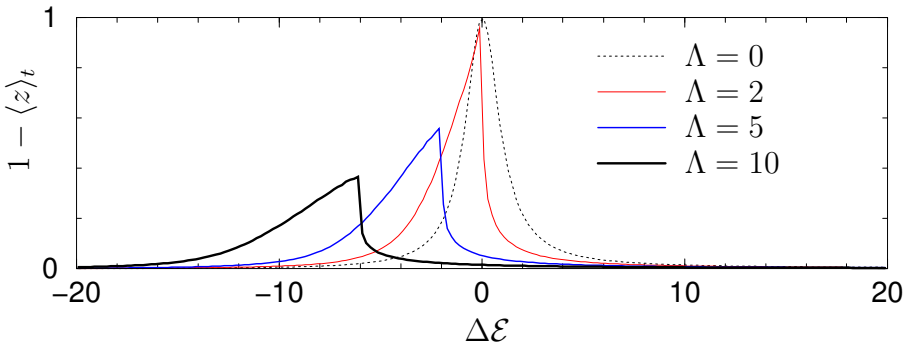

Figure 4.2: "Tunneling spectrum" of the double well potential, calculated by numerically integrating Equations (4.19,4.20) with the initial condition $z(0) = 0.999$ and $\phi(0) = 0$, and by computing the temporal average $\langle z \rangle_t$. The vertical axis therefore corresponds to the relative amount of atoms that participate at the transfer process between the wells, at given relative interaction strength Λ and given bias $\Delta\mathcal{E}$, if initially all atoms are prepared in the left well. While a perfect Lorentzian centred around $\Delta\mathcal{E} = 0$ is obtained in the noninteracting case $\Lambda = 0$, asymmetric peak shapes with sharp cuts arise at large interactions $\Lambda \gg 1$, where a finite bias is necessary in order to transfer a macroscopic amount of atoms through the barrier (see also Ref. [156]).

to the case of weak interactions $\Lambda \ll 1$ where essentially all atoms are transferred across the barrier. Similar phenomena can also be found in tilted optical lattices, where resonant tunneling between quasi-bound Wannier-Stark states is suppressed in presence of a finite atom-atom interaction [157].

It was recently suggested [158–160] that *coherent control* schemes could be applied in this context, in order to circumvent this limitation and to achieve complete population transfer. In a similar way as for coherent control in molecular systems [161], the desired transfer process would be realized by a suitable variation of the double well potential *during the time evolution of the condensate*, namely by adapting the relative difference $\Delta\mathcal{E}$ of the noninteracting ground state energies in such a way that the chemical potentials of the two wells equate each other during the whole transfer process [160]. This process would be experimentally realizable and can furthermore be used to generate mesoscopic entanglement in the double-well trap [160] (see also Ref. [162]). As we shall see in the following section, such a control approach can also be applied to the resonant tunneling of a Bose-Einstein condensate through a symmetric double barrier potential, where a similar "blocking" effect occurs due to the repulsive interaction between the atoms.

4.2 Resonant transport of Bose-Einstein condensates

In the following, we focus our attention on *open* systems and consider in particular the transport of Bose-Einstein condensates through *atomic quantum dots* in quasi one-dimensional waveguides. For cold atoms, such waveguides can be created either with optical techniques, e.g. by combining a red-detuned laser beam with an array of cylindrical microlenses [163], or on *atom chips* [164]. The latter consist of a suitable geometry of microscopic electric wires, typically made of gold or copper, which are mounted on top of an insulating substrate. Sending electric currents through the wires induces magnetic fields the superposition of which can be used to trap and guide cold atoms [165]. A matter-wave guide can, for instance, be realized by mounting three straight wires parallel to each other on the chip surface: At appropriate values for the electric currents through the wires (which should have opposite directions in the outer two wires as compared to the central one), a line of vanishing magnetic field would be induced at a certain distance above the surface. By applying, in addition, a weak external magnetic field parallel to the wires, this line can be transformed into a homogeneous harmonic waveguide for atoms that are in the "low field seeker state", i.e. the magnetic moment of which is antiparallel to the direction of the net magnetic field.

In a similar way, microscopic trapping potentials can be induced on atom chips, in which cold gases of bosonic alkaline atoms can be confined and evaporatively cooled down to condensation temperatures [166–168]. The resulting Bose-Einstein condensate (which may contain more than 10^5 atoms for suitable traps [167]) can then be released into the matter-wave guide structure, along which it can either freely propagate [169] or be transported in a controlled way by using additional wire geometries with alternating electric currents [168]. The inherent flexibility of the atom chip concept permits the realization of various waveguide geometries with beam splitters [170,171], Michelson interferometers [172], double well potentials [173], and one-dimensional magnetic lattices [174], and thereby opens a number of possibilities for atomic interference experiments that could serve as sensors for external gravitational or electromagnetic fields. It was furthermore suggested that inhomogeneities in microfabricated electric wires could sensitively be probed on atom chips, by measuring the density of atoms within waveguides that are induced on top of such wires, with distances of the order of a few microns [175–177].

The *mesoscopic* length scales that are typically encountered on atom chips suggest intriguing analogies to electronic transport physics in semiconductor heterostructures and nanostructures. In this context, atom chips are potentially interesting as they permit the preparation of scattering geometries in which the role of interaction at transport processes can be studied in a fairly clean and well-controlled way. The connection to electronic mesoscopic physics was first explored by Thywissen et al. with the attempt to generalize the concept of a "conductance" for noninter-

acting cold atoms [178]. Further research into this direction includes the determination and characterization of stationary transporting modes of an interacting Bose-Einstein condensate [179], the transmission of such a condensate through a potential step [180], as well as the generalization of the "Coulomb blockade" phenomenon to cold bosonic atoms [181]. In this latter work, the dynamics of a condensate was studied in a one-dimensional waveguide containing a symmetric double barrier potential, and it was shown that the transmission through this "atomic quantum dot" can be blocked in presence of a strong repulsive interaction between the atoms [181]. At weak interactions, on the other hand, this double-barrier potential would act as a *Fabry-Perot resonator* for the condensate, where similar nonlinear effects were predicted as for optical transmission problems with a nonlinear medium [182]. In practice, such double barrier potentials could, for instance, be realized by a pair of blue-detuned laser beams that are focused onto the waveguide.

The systematic study of the transport properties of Bose-Einstein condensates in presence of such atomic quantum dots is the main topic of this section. We consider here, for the sake of definiteness, a cylindrical harmonic waveguide with frequency $\omega_\perp$ onto which a sequence of two symmetric Gaussian barriers with width σ and distance L is superposed. The external potential for the atoms is then given by

$$V_{\text{ext}}(\vec{r}) = \frac{1}{2}m\omega_\perp^2(y^2+z^2) + V(x) \tag{4.21}$$

with

$$V(x) = V_0\left(e^{-(x+L/2)^2/\sigma^2} + e^{-(x-L/2)^2/\sigma^2}\right) \tag{4.22}$$

where x denotes the coordinate along the waveguide. We shall restrict ourselves to the so-called "1D mean field regime" [183] which is characterized by the condition

$$(a_s/a_\perp)^2 \ll n_{1D}a_s \ll 1 \tag{4.23}$$

for the longitudinal density n_{1D} along the waveguide, where a_s is the s-wave scattering length and $a_\perp = \sqrt{\hbar/(m\omega_\perp)}$ denotes the oscillator length of the transverse confinement (see also Ref. [179]). These inequalities ensure, on one hand, that the system does not enter the Tonks-Girardeau regime corresponding to a one-dimensional gas of impenetrable bosons [184] and, on the other hand, that nonlinear effects can be neglected in the transverse eigenfunctions of the waveguide. Assuming that only the transverse ground state $\phi_0(y,z)$ is populated in the scattering process, we can make the ansatz $\Psi(\vec{r},t) = \psi(x,t)\phi_0(y,z)e^{-\mathrm{i}\omega_\perp t}$ for the condensate wavefunction and obtain, in leading order in $n_{1D}a_s$, the one-dimensional Gross-Pitaevskii equation

$$\mathrm{i}\hbar\frac{\partial}{\partial t}\psi(x,t) = -\frac{\hbar^2}{2m}\frac{\partial^2}{\partial x^2}\psi(x,t) + V(x)\psi(x,t) + g|\psi(x,t)|^2\psi(x,t) \tag{4.24}$$

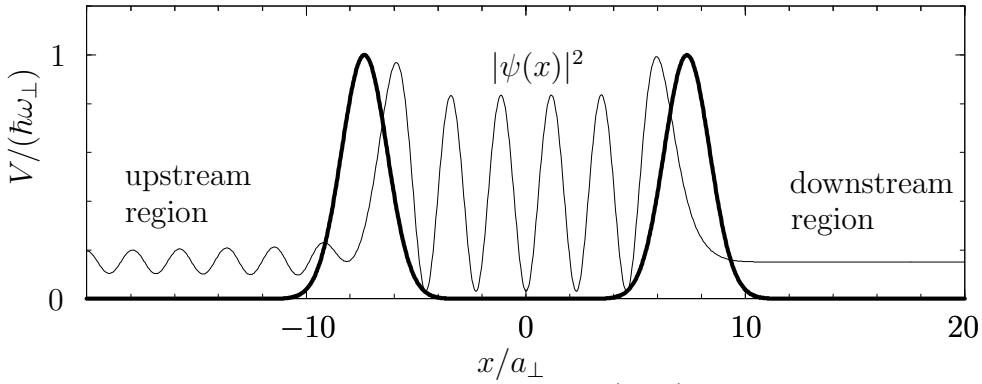

Figure 4.3: Plot of the double barrier potential (4.22) with $L = 10\,\sigma$. The thin solid line shows the probability density of a near-resonant scattering state which is injected from the "upstream" region and propagates towards the "downstream" region (on the left- and right-hand side of the quantum dot, respectively).

for the longitudinal component of the wavefunction, with the effective interaction strength [184]

$$g = 2\hbar\omega_\perp a_s\,. \tag{4.25}$$

A systematic study of the transport properties of the condensate in presence of a double barrier potential naturally invokes the concept of *stationary scattering states*. Such states correspond to stationary solutions $\psi(x,t) = \psi(x)e^{-\mathrm{i}\mu t/\hbar}$ of the longitudinal Gross-Pitaevskii equation (4.24), which satisfy the one-dimensional time-independent equation

$$-\frac{\hbar^2}{2m}\frac{d^2}{dx^2}\psi(x) + V(x)\psi(x) + g|\psi(x)|^2\psi(x) = \mu\psi(x) \tag{4.26}$$

at given chemical potential μ. They are furthermore characterized by *outgoing boundary conditions* on the "downstream" side of the quantum dot, which means that the wavefunction is given by a plane wave $\sim \exp(\mathrm{i}kx)$ with positive wavenumber k in the asymptotic spatial regime $x \gg L$ (we assume here that the condensate is injected from the left-hand side, i.e. at negative x, onto the double barrier potential). States with these properties would generally be expected to result from quasi-stationary propagation processes where matter waves are gradually injected into the initially empty waveguide (in a similar way as for the production of "atom laser" beams [185]).

Leboeuf and Pavloff pointed out [179] that such stationary scattering states can be straightforwardly calculated by inserting the ansatz $\psi(x) = A(x)\exp[\mathrm{i}\phi(x)]$ with real A and ϕ into the stationary Gross-Pitaevskii equation (4.26) and by separating the latter into real and imaginary parts. This yields the condition that the total

current

$$j_t \equiv \frac{\hbar}{m}\mathrm{Im}\left[\psi^*(x)\psi'(x)\right] = (\hbar/m)A^2(x)\phi'(x) \tag{4.27}$$

is independent of position (what is a consequence of the conservation of the integrated atomic density), and leads to the ordinary differential equation

$$-\frac{\hbar^2}{2m}\frac{d^2A}{dx^2} + \left(V(x) + \frac{m}{2}\frac{j_t^2}{A^4}\right)A + gA^3 = \mu A \tag{4.28}$$

for the amplitude $A(x)$. The latter can be numerically integrated from $x \to \infty$ to $x \to -\infty$ with the "initial condition" $A(x \to \infty) = \sqrt{n_0}$ and $A'(x \to \infty) = 0$, where the downstream density n_0 satisfies the relation

$$\mu = \frac{m}{2}\frac{j_t^2}{n_0^2} + gn_0 \tag{4.29}$$

for a given value j_t of the total current. As was pointed out in Ref. [179], Equation (4.29) exhibits a low-density (supersonic) and a high-density (subsonic) solution, where the transport is respectively dominated by the kinetic energy and by the mutual interaction of the atoms. Since in realistic propagation processes the waveguide is initially empty in the downstream region, we choose the low-density solution for the asymptotic value of A.

This description of the scattering process in terms of stationary states is quite convenient from the numerical point of view, but exhibits conceptual problems. On one hand, the *transmission coefficient* T, which is defined by the ratio of the total current j_t to the incident current j_i, cannot be directly extracted from the stationary wavefunction $\psi(x)$. In the absence of interaction, j_i is generally determined by decomposing the "upstream" part of the wavefunction (i.e., at $x \ll -L$) into an incident and a reflected component. This approach becomes invalid at finite $g > 0$, due to the absence of the superposition principle, and can only be justified in an approximate way in the limit of weak atomic densities or small back-reflections [180]. It is, however, possible to solve this problem, by considering the situation that the interaction strength g (4.25) is adiabatically decreased to zero for $x \to -\infty$ (which can, e.g., be achieved by decreasing the transverse confinement frequency $\omega_\perp$ of the waveguide). In the asymptotic region of vanishing interaction, the incident current j_i is given by

$$j_i = j_t + \mathcal{J}/(2\pi\hbar)\,. \tag{4.30}$$

where $\mathcal{J}$ denotes the effective "pseudo action"

$$\mathcal{J} = \frac{\hbar^2}{m}\int_{x_0}^{x_0+\Delta x}\left[A'(x)\right]^2 dx \tag{4.31}$$

that is integrated over the spatial period Δx of the upstream density oscillations (which would be given by $\Delta x = \pi/k$ in absence of interaction). Due to the theorem of adiabatic invariants [186], $\mathcal{J}$ remains *stationary* under a slow variation of g and can therefore be evaluated also at finite $x < -L$. This allows us to determine the transmission coefficient in the nonlinear spatial region [187].

A more severe problem is, on the other hand, the fact that the mere existence of a stationary scattering state does *not* necessarily imply that this state will be populated in the time-dependent scattering process. This is not only true for the propagation of finite wave packets (which obviously cannot be evolved by an expansion in terms of stationary solutions of the nonlinear Schrödinger equation (4.26) due to the absence of the superposition principle), but also concerns the limiting case of quasi-stationary propagation where the condensate is adiabatically injected into the waveguide. Indeed, as we shall see later on, different scattering states may exist at given chemical potential μ and given incident current j_i (which are the parameters that can be controlled in the experiment), and only one of them will be populated in the transport process while the others would be dynamically unstable.

In view of this complication, the numerical approach that we adopt to calculate the nonlinear transmission process is based on the *time-dependent* one-dimensional Gross-Pitaevskii equation (4.24). This equation is integrated in presence of an inhomogeneous *source term*, located at a position $x = x_S$ in the upstream region, which simulates the coupling of the waveguide to a reservoir of Bose-Einstein condensed matter at chemical potential μ. The effective nonlinear equation that governs the time evolution of the condensate wavefunction $\psi(x,t)$ is therefore given by

$$\begin{aligned} \mathrm{i}\hbar\frac{\partial}{\partial t}\psi(x,t) &= -\frac{\hbar^2}{2m}\frac{\partial^2}{\partial x^2}\psi(x,t) + V(x)\psi(x,t) + g|\psi(x,t)|^2\psi(x,t) \\ &\quad + S\delta(x-x_S)e^{-\mathrm{i}\mu t/\hbar} \end{aligned} \tag{4.32}$$

where the source amplitude S implicitly contains both the coupling strength as well as the wavefunction of the condensate in the reservoir. In practice, Equation (4.32) is integrated by representing $\psi(x,t)$ on a spatial grid and by using an implicit finite-difference scheme for the propagation (see Ref. [187] for technical details). We start with the initial condition $\psi(x,0) \equiv 0$ and adiabatically increase the source amplitude S up to a given maximum value during the propagation, in order to ensure that $\psi(x,t)$ remains, for all times t, close to a quasi-stationary scattering state with chemical potential μ. To avoid artificial back-reflections from the boundaries of the numerical grid, we employ *absorbing boundary conditions* [188] which are particularly suited for the calculation of one-dimensional transport problems.

We now apply this approach to the transport of a Bose-Einstein condensate of ^{87}Rb atoms through the double barrier potential (4.22) with the parameters $\sigma = 0.5$ μm, $L = 5$ μm, and $V_0 = \hbar\omega_\perp$ (see Figure 4.3). We consider here a waveguide with

the transverse confinement frequency $\omega_\perp = 2\pi \times 10^3$ s^{-1}, which yields the oscillator length $a_\perp \simeq 0.34$ μm and the effective one-dimensional interaction strength $g \simeq 0.034\,\hbar\omega_\perp a_\perp$. The transmission spectrum that results from the numerical integration of Equation (4.32) is shown in Figure 4.4 where we plot the transmission coefficient as a function of the chemical potential μ. This calculation was performed at fixed incident current $j_i = 10^4$ atoms/s, which determined the final value $S_0 \equiv S(t \to \infty)$ of the source amplitude according to

$$j_i = \frac{m|S_0|^2}{\hbar^3 k} \tag{4.33}$$

with k being self-consistently defined by

$$k = \sqrt{\frac{2m}{\hbar^2}\left(\mu - g\frac{m j_i}{\hbar k}\right)}\,. \tag{4.34}$$

This relation is essentially derived from the fact that j_i would be obtained as expectation value for the current operator in *absence* of the scattering potential, i.e. if Equation (4.32) was propagated at $V \equiv 0$.

In the linear case of noninteracting atoms, the transmission spectrum would display a sequence of Breit-Wigner peaks in the tunneling regime at $\mu < V_0$, corresponding to resonant tunneling through quasi-bound states of the double barrier potential. These peaks are *not* encountered in presence of the interaction, and only asymmetric remnants thereof can be identified in the transmission spectrum. Calculating all possible stationary scattering states that exhibit the above incident current $j_i = 10^4$ atoms/s reveals that the resonance peaks do exist also in the nonlinear case, but are strongly distorted towards positive values of the chemical potential and overlap with other branches of the spectrum. This is a typical *bistability* phenomenon which arises also in other areas of nonlinear science, such as the Duffing oscillator model [189], the transmission of laser light through resonators with nonlinear media [190], as well as the electronic transport through quantum wells [191–193] (see also Ref. [194] for an example in the context of superconductivity). The fact that the straightforward propagation process which is simulated by our numerical approach does not lead to resonant transport in the tunneling regime can be seen as an open-system analog of the self-trapping effect discussed in Section 4.1: With increasing population of the internal quasi-bound state, the corresponding resonance level is enhanced due to the repulsive interaction and shifts away from the external chemical potential μ, what makes the resonator intransparent (see also Figure 4.2).

It is apparent from Figure 4.4 how one should proceed in order to nevertheless achieve resonant transport at finite interaction: the chemical potential μ needs to be increased *during the propagation process*, e.g. from $\mu \simeq \hbar\omega_\perp$ to $\mu \simeq 1.12\,\hbar\omega_\perp$ in the case of Figure 4.4. In this way, it is possible to adiabatically move along the upper

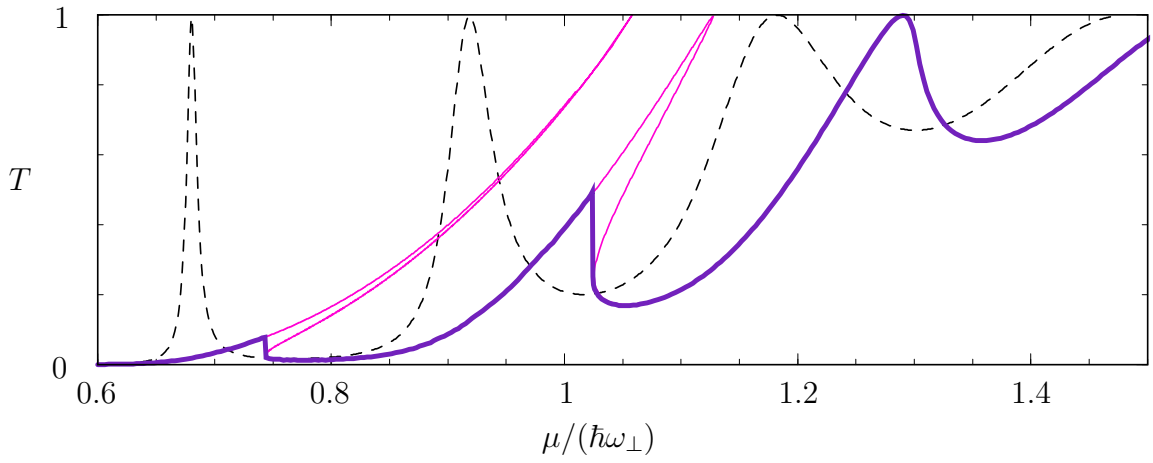

Figure 4.4: Transmission spectrum of the double barrier potential (4.22) at $V_0 = \hbar\omega_\perp$ and $L = 10\sigma = 14.7\ a_\perp$, for the effective interaction strength $g = 0.034\ \hbar\omega_\perp a_\perp$. The spectrum (thick solid line) was calculated at fixed incident current $j_i = 1.6\ \hbar\omega_\perp$, by integrating the time-dependent Gross-Pitaevskii equation (4.32) in presence of the source term. In contrast to the case of noninteracting atoms (dashed line), the spectrum does, for $\mu < V_0$, not exhibit Breit-Wigner peaks corresponding to quasi-bound states of the double barrier potential, but displays only asymmetric remnants thereof with sharp cuts. A calculation of all stationary scattering states that exist at the above value for the incident current (thin solid line) indeed reveals additional branches of the spectrum, and shows that the resonance peaks are strongly distorted towards positive values of μ. Such bistability phenomena arise in various areas of nonlinear science.

branch of the resonance peak around $\mu/(\hbar\omega_\perp) \simeq 1.1$ and to obtain nearly perfect transmission. In practice, the variation of μ could be experimentally realized by illuminating the scattering region with a weak red-detuned laser pulse, which effectively adds a constant negative offset to the external potential $V(x)$. This coherent control process is fairly analogous to the complete population transfer of an interacting Bose-Einstein condensate in a double well potential [160], where a similar temporal variation of the external bias field is applied in order to maintain the matching of chemical potentials during the transfer of atoms.

The numerical calculation of the propagation process in presence of this adiabatic variation of μ shows indeed that the resonance peak at $\mu \simeq 1.12\ \hbar\omega_\perp$ can be populated in this way [195]. Resonant transport through this peak cannot be maintained in a perfectly continuous way, since the associated resonant scattering state is *dynamically unstable* and decays to the low-transmission state that exists at the same chemical potential and the same incident current. However, the time scale at

which this decay takes place is calculated to be of the order of $\tau \sim 10$ ms [195], which should be long enough to allow for further experimental manipulations. One could, for instance, "close" the quantum dot during that time scale (e.g. by enhancing the barrier height) and thereby trap a part of the condensate within a interacting mean-field state that exhibits an unusually high number of nodes (see Figure 4.3). This specific application implicitly relies on a one-to-one correspondence between resonances in the transmission spectrum and decaying quasi-bound states of the double barrier potential in the nonlinear case of interacting atoms, which shall indeed be established in the following section.

4.3 Relation to the corresponding decay problem

In linear quantum mechanics, the transport of single particles through quantum-dot potentials is most conveniently described by means of the *scattering matrix approach* [196, 197]. This formalism employs the unitary operator

$$S = 1 - 2\pi \mathrm{i} W^\dagger \frac{1}{E - H_0 + i\pi W W^\dagger} W \tag{4.35}$$

that maps an incident wave in a given transverse eigenstate of the waveguide onto the resulting reflected and transmitted components (see also Ref. [198]). Here H_0 represents the "internal" Hamiltonian acting on local quasi-bound states within the resonator, and W describes the coupling of the external transverse channels onto the internal states. Evaluating the transmission coefficient within this formalism leads to the sequence of Breit-Wigner peaks that was also encountered in our numerical treatment of the nonlinear scattering problem in the limit of vanishing interaction (see Figure 4.4). We shall, in this section, rederive this essential result for a one-dimensional double-barrier geometry, in a way that permits the inclusion of interaction-induced nonlinear effects within the resonator, and that also allows one to study time-dependent issues related, e.g., to the question whether or not a given stationary scattering state can be populated in a propagation experiment.

As starting point, we introduce a subdivision of the Hilbert space $\mathcal{H}$ into a subspace $\mathcal{H}_0$ containing discrete bound states within the resonator, and two other subspaces $\mathcal{H}_{L/R}$ containing continuous states in the left and right "leads" of the waveguide. This subdivision can be formally achieved by means of the *Feshbach projection method* [199, 200], where those subspaces are defined by the projection operators $P_L = \theta(x_L - \hat{x})$, $P_R = \theta(\hat{x} - x_R)$, and $Q = 1 - P_L - P_R$. Here x_L and x_R are suitably chosen positions that mark the left and right boundaries of the resonator, and θ denotes the Heavyside step function. An essential ingredient of the Feshbach formalism is to impose different boundary conditions (i.e., of Dirichlet or Neumann type) within and outside the resonator. It is then possible to shift

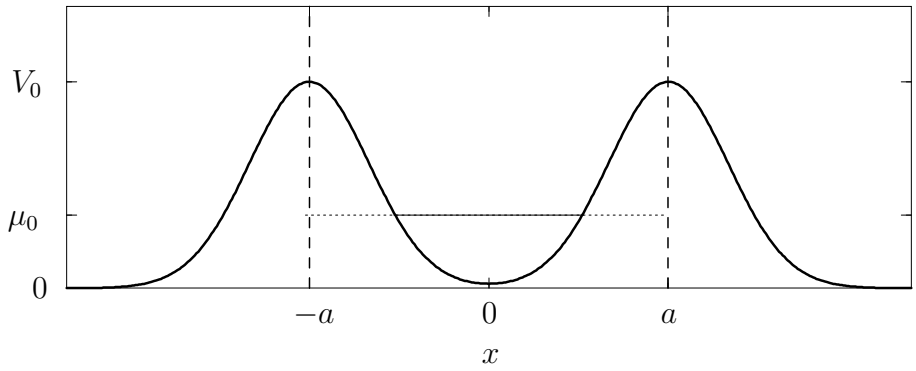

Figure 4.5: Plot of the double barrier potential (4.22) with $L \equiv 2a = 4.25\ \sigma$ and $V_0 = 1.1\ \hbar^2/(m\sigma^2)$. At these particular parameters, the atomic quantum dot exhibits only one quasi-bound state with a reasonably long lifetime, the chemical potential of which is indicated by the horizontal line. The vertical dashed lines mark the spatial cuts at $x = \pm a$ that are formally introduced by the Feshbach projection method.

the boundary contributions that result from the matrix elements of the Laplace operator to appropriate sides of the spatial cuts at $x = x_{L/R}$, in such a way that the operator T of the kinetic energy remains Hermitean within each subspace, but exhibits finite coupling matrix elements across the boundaries (see, e.g., Ref. [201] for more details). Choosing Dirichlet boundary conditions within the resonator and Neumann boundary conditions in the leads, these matrix elements would read

$$\langle \psi_R | T | \phi \rangle = \frac{\hbar^2}{2m} \psi_R^*(x_R) \phi'(x_R) \tag{4.36}$$

$$\langle \psi_L | T | \phi \rangle = -\frac{\hbar^2}{2m} \psi_L^*(x_L) \phi'(x_L) \tag{4.37}$$

for wavefunctions $\phi(x)$, $\psi_L(x)$, and $\psi_R(x)$ defined within the subspaces $\mathcal{H}_0$, $\mathcal{H}_L$, and $\mathcal{H}_R$, respectively.

We shall specifically focus on the symmetric double barrier potential (4.22) with $L = 4.25\ \sigma$ and $V_0 = 1.1\ \hbar^2/(m\sigma^2)$, which is plotted in Figure 4.5, and place the spatial cuts introduced by the Feshbach formalism at the positions of the maxima — i.e., $x_{R/L} = \pm a$ with $a \equiv L/2$. At these parameters, $V(x)$ exhibits, in the noninteracting case, only one quasi-bound state with a reasonably long lifetime (the local "ground state"), which is energetically well separated from other internal eigenstates within $\mathcal{H}_0$. It is therefore justified to neglect the contribution of those higher excited states of the resonator and to make the ansatz

$$\psi(x,t) = B(t)\phi_0(x) + \int_0^\infty dE \left(A_E^L(t)\phi_E^L(x) + A_E^R(t)\phi_E^R(x) \right) \tag{4.38}$$

for the wavefunction, where $\phi_0 \in \mathcal{H}_0$ denotes the above quasi-bound state and $\phi_E^{L/R} \in \mathcal{H}_{L/R}$ are the energy-normalized continuum eigenstates within the left and right lead, respectively. Inserting this ansatz into the Schrödinger equation given by Equation (4.24) with $g \equiv 0$, we obtain the equations

$$\mathrm{i}\hbar\frac{d}{dt}A_E^{L/R}(t) = EA_E^{L/R}(t) + V_E B(t) \tag{4.39}$$

$$\mathrm{i}\hbar\frac{d}{dt}B(t) = \mu_0 B(t) + \int_0^\infty dE\, V_E \left(A_E^L(t) + A_E^R(t)\right) \tag{4.40}$$

for the amplitudes A_E^L, A_E^R, and B, with the coupling matrix element

$$V_E = \frac{\hbar^2}{2m}\phi_0'(a)\phi_E^R(a) = -\frac{\hbar^2}{2m}\phi_0'(-a)\phi_E^L(-a) \tag{4.41}$$

that results from Equation (4.36,4.37). We assume here, without loss of generality, that the wavefunctions $\phi_0(x)$, $\phi_E^L(x)$, and $\phi_E^R(x)$ are real-valued and that the continuum eigenfunctions exhibit the symmetry-related property $\phi_E^R(x) = \phi_E^L(-x)$.

As appropriate initial state for the quasi-stationary scattering process, we consider a spatially broad Gaussian wave packet that is injected from the left-hand side onto the double-barrier geometry. This wave packet is explicitly written as

$$\psi(x, t_0) = \alpha \exp\left[-\frac{(x + x_\epsilon)^2}{2\sigma_\epsilon^2} + \mathrm{i}k\left(x + \frac{1}{2}x_\epsilon\right)\right] \tag{4.42}$$

with $x_\epsilon \equiv x_0/\epsilon^2$ and $\sigma_\epsilon \equiv \sigma_0/\epsilon$ where the positive length scales x_0 and σ_0 satisfy $x_0 \ll k\sigma_0^2$. Choosing the initial time t_0 in the asymptotic past according to $t_0 = -mx_\epsilon/(\hbar k)$, the wave packet will, in the limit $\epsilon \to 0_+$, evolve into the plane wave

$$\psi(x, t) = \alpha e^{\mathrm{i}(kx - \mu t/\hbar)} \tag{4.43}$$

at finite times t, with the incident chemical potential $\mu \equiv \hbar^2 k^2/(2m)$. Using the fact that the energy-normalized continuum eigenfunctions are, in the asymptotic spatial region $x \gg a$, given by

$$\phi_E^R(x) = \phi_E^L(-x) = \sqrt{\frac{2m}{\pi\hbar^2 k_E}}\cos(k_E x + \varphi_E) \tag{4.44}$$

with $k_E \equiv \sqrt{2mE}/\hbar$ and with a potential-dependent phase φ_E, we obtain the initial amplitudes

$$A_E^L(t_0) = \sqrt{\frac{m\sigma_\epsilon^2}{\hbar^2 k_E}}\alpha \exp\left[-\frac{1}{2}\sigma_\epsilon^2(k_E - k)^2 + \mathrm{i}x_\epsilon(k_E - k/2) + \mathrm{i}\varphi_E\right] \tag{4.45}$$

and $B(t_0) = A_E^R(t_0) = 0$.

Equation (4.39) can now be formally integrated yielding

$$A_E^{L/R}(t) = A_E^{L/R}(t_0)e^{-\mathrm{i}E(t-t_0)/\hbar} - \frac{\mathrm{i}}{\hbar}V_E \int_{t_0}^{t} B(t')e^{-\mathrm{i}E(t-t')/\hbar}dt' \,. \tag{4.46}$$

Inserting this expression into Equation (4.40) leads to the equation

$$\begin{aligned} \mathrm{i}\hbar\frac{d}{dt}B(t) &= \mu_0 B(t) - \frac{2\mathrm{i}}{\hbar}\int_0^\infty dE\, V_E^2 \int_{t_0}^{t} dt'\, B(t')e^{-iE(t-t')/\hbar} \\ &\quad + \int_0^\infty dE\, V_E A_E^{L/R}(t_0)e^{-\mathrm{i}E(t-t_0)/\hbar} \end{aligned} \tag{4.47}$$

for the bound component. In the limit $\epsilon \to 0$, the last term on the right-hand side of Equation (4.47) is evaluated as $Se^{-\mathrm{i}\mu t/\hbar}$ with the effective source amplitude

$$S = \sqrt{\frac{2\pi\hbar^2 k}{m}}V_\mu \alpha e^{\mathrm{i}\varphi_\mu} \,. \tag{4.48}$$

Hence, the time-dependence of the bound amplitude is, in the quasi-stationary case, dominated by the exponential factor $e^{-\mathrm{i}\mu t/\hbar}$, which permits the evaluation of the second term on the right-hand side of Equation (4.47) (see, e.g., Ref. [202]): we obtain

$$\mathrm{i}\hbar\frac{d}{dt}B(t) = \left(\mu_0 - \frac{\mathrm{i}}{2}\hbar\gamma_\mu\right)B(t) + Se^{-\mathrm{i}\mu t/\hbar} \tag{4.49}$$

with the rate $\gamma_\mu \equiv 4\pi V_\mu^2/\hbar$ [203].

The equation for B can now be straightforwardly integrated yielding

$$B(t) = \int_0^\infty dE \frac{V_E A_E^{L/R}(t_0)}{E - \mu_0 + \frac{\mathrm{i}}{2}\hbar\gamma_\mu}e^{-\mathrm{i}E(t-t_0)/\hbar} \tag{4.50}$$

$$\stackrel{\epsilon\to 0}{=} \frac{S}{\mu - \mu_0 + \frac{\mathrm{i}}{2}\hbar\gamma_\mu}e^{-\mathrm{i}\mu t/\hbar} \tag{4.51}$$

for $t \gg t_0$. Inserting this expression into the equation (4.46) for the transmitted component finally yields

$$A_\mu^R(t) = -2\pi\mathrm{i}\frac{V_\mu^2}{\mu - \mu_0 + \frac{\mathrm{i}}{2}\hbar\gamma_\mu}e^{-\mathrm{i}\mu(t-t_0)/\hbar}A_\mu^L(t_0) \tag{4.52}$$

while $A_E^R(t)$ would, for $E \neq \mu$, vanish in the limit $\epsilon \to 0$. We therefore obtain the transmission coefficient according to

$$T(\mu) \equiv \frac{|A_\mu^R(t)|^2}{|A_\mu^L(t_0)|^2} = \frac{(\hbar\gamma_\mu/2)^2}{(\mu - \mu_0)^2 + (\hbar\gamma_\mu/2)^2} \,, \tag{4.53}$$

which is in perfect agreement with the scattering matrix formalism (4.35). Provided γ_μ varies relatively slowly with μ within the range $\mu_0 - \hbar\gamma_{\mu_0} \lesssim \mu \lesssim \mu_0 + \hbar\gamma_{\mu_0}$ (which is generally the case for long-lived quasi-bound states), we can safely replace γ_μ by γ_{μ_0}, which corresponds to the rate at which the quasi-bound state decays through the barriers. The manifestation of this state in the transmission spectrum is then given by a Lorentzian peak with a width that is equivalent to its decay rate.

We now consider the presence of a finite but not too strong repulsive interaction between the atoms, which appreciably manifests within the double barrier potential, but can be neglected in the leads. In this case, Equation (4.49) needs to be modified according to

$$\mathrm{i}\hbar\frac{d}{dt}B(t) = \left(\mu_0 + g_0|B(t)|^2 - \frac{\mathrm{i}}{2}\hbar\gamma_\mu\right)B(t) + Se^{-\mathrm{i}\mu t/\hbar} \tag{4.54}$$

where g_0 is the effective interaction parameter that accounts for the nonlinearity in the Gross-Pitaevskii equation (4.24). This leads to a nontrivial modification of the transmission peak (4.53), due to the fact that the "center" of the peak now implicitly depends on the amplitude B of the quasi-bound state and thereby also on the incident chemical potential μ: As is displayed in Figure 4.4, the peak is distorted over a large range of incident chemical potentials μ, which implies that the replacement $\gamma_\mu \to \gamma_{\mu_0}$ can no longer be justified.

We shall show, however, that a fairly good reproduction of the distorted transmission peak can nevertheless be obtained through

$$T(\mu) \simeq \frac{[\hbar\gamma_0(N_0)/2]^2}{[\mu - \mu_0(N_0)]^2 + [\hbar\gamma_0(N_0)/2]^2} \tag{4.55}$$

where $\mu_0(N_0)$ and $\gamma_0(N_0)$ represent the chemical potential and the decay rate, respectively, of the interacting quasi-bound state at the population $N_0 \equiv |B|^2$. The latter can be related to the amplitude α and the chemical potential μ of the incident wave by inserting the ansatz $B(t) = |B|e^{-\mathrm{i}\mu t/\hbar}$ into Equation (4.54), replacing $\mu_0 + g_0|B(t)|^2$ by $\mu_0(|B|^2)$ and γ_μ by $\gamma_0(|B|^2)$. Together with Equation (4.48), this yields the equation

$$N_0 = \frac{\hbar^2\gamma_0(N_0)\sqrt{\mu/(2m)}|\alpha|^2}{[\mu - \mu_0(N_0)]^2 + [\hbar\gamma_0(N_0)/2]^2} \tag{4.56}$$

which can be self-consistently solved if $\mu_0(N_0)$ and $\gamma_0(N_0)$ are known.

The chemical potentials and decay rates of the interacting quasi-bound state can be calculated by the method of *complex scaling* [204–206], which is widely applied in atomic and molecular physics. This numerical method effectively amounts to a complex dilation $x \mapsto xe^{\mathrm{i}\theta}$ of the position operator, whereby quasi-bound states $\psi(x)$ with purely outgoing (Siegert) boundary conditions [207] — i.e., with the

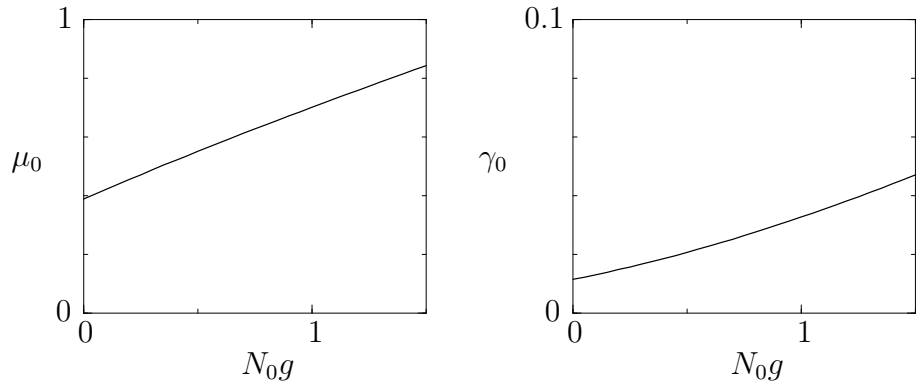

Figure 4.6: Chemical potential μ_0 and decay rate γ_0 of the quasi-bound state within the double barrier potential of Figure 4.5, calculated as a function of $N_0 g$ with N_0 the population of the quasi-bound state and g the effective one-dimensional interaction strength. In practice, μ_0 and γ_0 were computed at 30 equidistant values of $N_0 g$ within $0 \leq N_0 g \leq 1.5$, and cubic interpolation was employed to obtain intermediate values of μ_0 and γ_0 for the self-consistent solution of Equation (4.56). μ_0, $\hbar\gamma_0$, and g/σ are given in "natural" energy units of $\hbar^2/(m\sigma^2)$.

asymptotic behaviour $\psi(x) \longrightarrow \psi_0 \exp(\mathrm{i}k|x|)$ with $\mathrm{Re}(k) > 0$ and $\mathrm{Im}(k) > 0$ for $x \to \pm\infty$ — become square-integrable. We could recently show [208] that the complex-scaling approach can indeed be generalized to the calculation of decaying states of Bose-Einstein condensates within the nonlinear Gross-Pitaevskii equation. Such states are, in practice, obtained through a real-time propagation of the condensate wavefunction under the complex-scaled Gross-Pitaevskii Hamiltonian (which is *non-Hermitean* and thereby implicitly accounts for the decay of the condensate) where frequent renormalizations are employed in order to ensure that a given number N_0 of atoms would be encountered within the trapping potential [208]. The power of this technique was successfully demonstrated for one-dimensional traps with Gaussian barriers [208] as well as for tilted optical lattices [209].

The complex-scaling approach intrinsically exhibits the possibility to provide a conceptually clean access to decaying states of Bose-Einstein condensates, as it does not involve any *a priori* approximations. Its numerical implementation, however, requires great care since explicit evaluations of the wavefunction in the complex spatial domain (i.e., at $xe^{\mathrm{i}\theta}$) need to be performed. An alternative approach, which is somewhat more "dirty" from the conceptual point of view but easier to implement in practice, consists in the propagation of the condensate wavefunction under the time-dependent Gross-Pitaevskii equation (4.24) in presence of *complex absorbing potentials* (see Ref. [210]). The latter are imposed in the asymptotic spatial

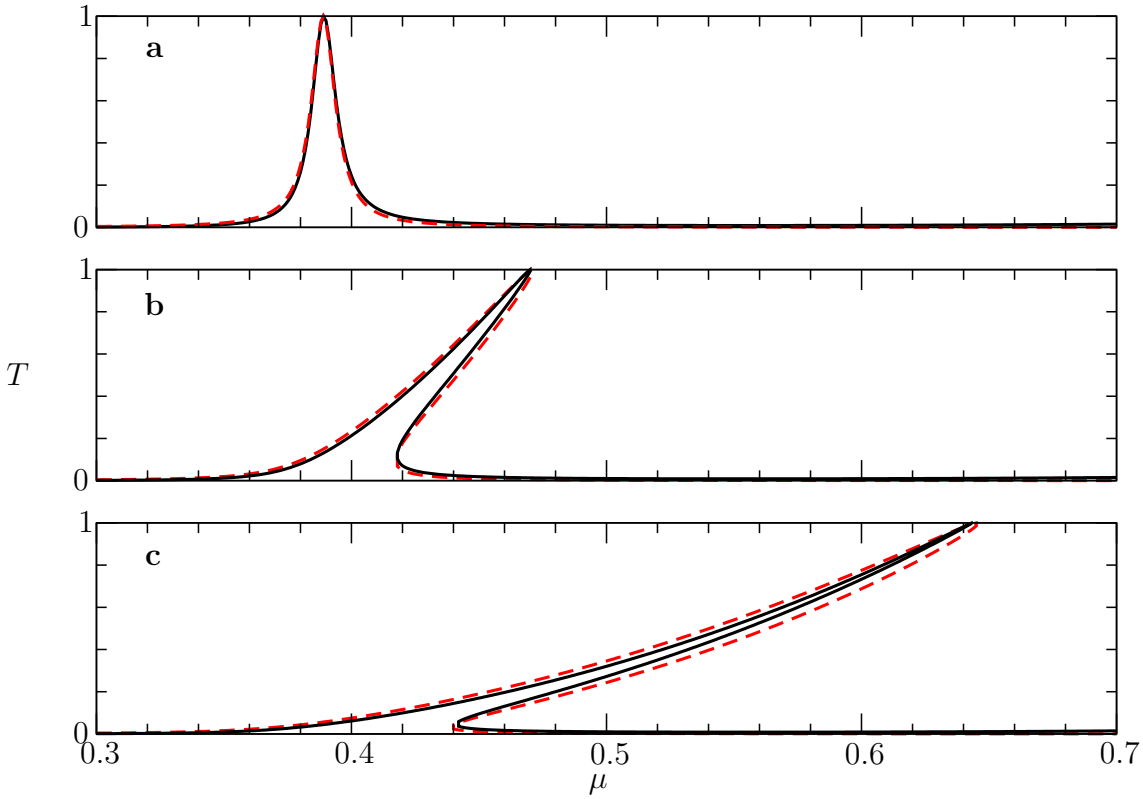

Figure 4.7: Transmission spectra of the double barrier potential of Figure 4.5 at the interaction strengths (a) $g = 0$, (b) $g = 0.002\ \hbar^2/(m\sigma)$, and (c) $g = 0.01\ \hbar^2/(m\sigma)$. The solid line shows the transmissions of all stationary scattering states, calculated by the "stationary" method based on Equation (4.28), that exist at the density $|\alpha|^2 = 1/\sigma$ of the incident matter-wave beam. The dashed line is obtained from self-consistent solutions of Equation (4.56) at the above value for $|\alpha|^2$, which are inserted in the expression (4.55) for the nonlinear transmission coefficient. The good agreement confirms the one-to-one correspondence between quasi-bound states of the atomic quantum dot and resonance peaks in the transmission spectrum.

region $x \to \pm\infty$ and "absorb" the outgoing current in order to avoid artificial back-reflection from the boundaries of the numerical grid. In a similar way as for the complex-scaling approach, the wavefunction is renormalized after each propagation step to satisfy the condition

$$\int_{-a}^{a} |\psi(x)|^2 dx = N_0 \tag{4.57}$$

for a given number N_0 of atoms within the trapping potential. The scaling factor

that is needed to perform this renormalization in the limit of large propagation times gives then rise to the decay rate $\gamma_0 = \gamma_0(N_0)$ of the quasi-bound state, while its chemical potential $\mu_0 = \mu_0(N_0)$ can be extracted from the expectation value of the nonlinear Gross-Pitaevskii Hamiltonian.

This method is now used in order to compute the chemical potentials $\mu_0(N_0)$ and decay rates $\gamma_0(N_0)$ of the quasi-bound state at a given population N_0 (see Figure 4.6). With this information, self-consistent solutions of Equation (4.56) can be calculated, yielding possible occupation numbers N_0 of the quasi-bound state that may exist at given density $|\alpha|^2 = 1/\sigma$ and given chemical potential μ of the incident matter-wave beam. These occupation numbers are then inserted in the expression (4.55) for the transmission coefficient. As a result, a distorted resonance peak is obtained for $g > 0$, which is compared in Figure 4.7 with the peak structure that would be formed through the transmission coefficients of all possible stationary scattering states that exhibit the above incident density. The agreement between the two approaches is fairly good, apart from a slight overestimation of the width of the resonance peak by the above self-consistent method.

In short summary, nonlinearly distorted resonance structures of transport processes through atomic quantum dots can not only be reproduced by the calculation of stationary scattering states within the waveguide, but also through the chemical potentials and decay rates of the interacting quasi-bound states within the quantum dot potential. The underlying approach, which was outlined in this section, is intrinsically suited to take into account time-dependent effects (see Equation 4.47), and might therefore be used to predict the outcome of a specific propagation experiment within an initially empty waveguide. This issue shall be investigated in more detail in a forthcoming publication [211].

Perspectives

In conclusion, two different aspects of complex quantum tunneling scenarios were studied in this thesis. We investigated, on one hand, the influence of classical non-integrability and chaos on the tunneling process (Chapter 2) for which no unified semiclassical theory is yet available. Special emphasis was put on the tunneling-induced level splittings between symmetry-related regular regions in phase space, which are separated from each other by a finite chaotic layer (Chapter 3). We could show that this dynamical tunneling process is dominantly governed by nonlinear resonances that manifest within the regular islands [86, 87, 97, 98]. The validity of this resonance-assisted tunneling mechanism was verified not only for periodically kicked model Hamiltonians, but also within more realistic systems such as the microwave-driven hydrogen atom [116] as well as the pendulum Hamiltonian that approximately describes the dynamics of cold atoms in periodically modulated optical lattices [101]. Further open issues in this context include the role of partial barriers and Cantori in the chaotic part of the phase space [104, 105] as well as the generalization of the resonance-assisted tunneling scheme to systems with two or more degrees of freedom [93].

On the other hand, nonlinear effects arising from a finite repulsive interaction between the atoms in a Bose-Einstein condensate were investigated (Chapter 4). We specifically focused on the transport of a condensate through a double barrier geometry, for which we could show that resonant transmission is strongly affected by the interaction-induced nonlinearity in the Gross-Pitaevskii equation [195]. This phenomenon is indeed analogous to nonlinear self-trapping in double well potentials [144, 153] and can also be understood in terms of the corresponding decay problem [211] in which the chemical potentials and decay rates of the quasi-bound states within the double barrier potential are appreciably enhanced due to the interaction [208, 209]. Similar conclusions were recently obtained in a related study on nonlinear resonant transport of condensates [212] where the resonator was defined by a piecewise constant potential.

It seems natural to *combine* these two aspects and to study tunneling in presence of both chaos *and* interactions. An interesting open question in this context would be, for instance, to which extent the scenario of resonance- and chaos-assisted tunneling is affected by a finite interaction-induced nonlinearity. Preliminary studies on this problem have indeed been carried out by Artuso and Rebuzzini [213] who found that tunneling-induced Rabi oscillations between left- and right-moving modes in a periodically driven optical lattice are suppressed in presence of the repulsive interaction between the atoms (which is quite similar to the breakdown of Bloch oscillations of a condensate in a tilted periodic potential [141]). In practice, however, the effect of interactions should be rather small in realistic experimental setups for dynamical tunneling of cold atoms in optical lattices, as was pointed out in Ref. [214].

The interplay between chaos and interaction can also be investigated from the complementary point of view, namely by studying how the nonlinear double-well scenario discussed in Section 4.1 is modified in presence of a periodic driving. This problem was indeed addressed in a number of publications (e.g., [156, 215–218]) focusing on different aspects of the nonlinear driven double-well scenario, such as photon-assisted tunneling of the condensate [156, 218], coherent control [158, 159], the assessment of chaos and unpredictability on the level of the "classical" mean-field theory of the condensate [216], as well as the possibility of dynamical (meta) tunneling between regular islands that are induced by nonlinear resonances of the driving [217]. Although a complete and coherent picture of the problem is still missing, the above studies already reveal interesting analogies with resonance- and chaos-assisted tunneling processes in "linear" quantum mechanics, with are worth a further exploration.

In the context of transport processes of Bose-Einstein condensates in atomic waveguides, classical chaos can be introduced also in a "static" way, namely by considering scattering through multidimensional quantum dot potentials that correspond to billiard geometries with nontrivial boundaries. Such setups exhibit new intriguing aspects, pertaining, e.g., to the qualitative and quantitative difference between regularity and chaos in the associated classical dynamics (which should somehow manifest in the transmission spectrum) as well as to the formulation of a semiclassical theory of the nonlinear scattering process in terms of billiard trajectories, which could possibly proceed along similar lines as in Refs. [219–221] and might provide interesting generalizations of the semiclassical transport physics for noninteracting particles [222,223]. An obvious question that arises in this context concerns the way how resonant transmission peaks, involving quasi-bound states which are semiclassically associated either with regular periodic orbits or with chaotic phase space regions, are affected by a finite nonlinearity. This question can be straightforwardly investigated by a multidimensional generalization of our numerical approach based on the inhomogeneous time-dependent Gross-Pitaevskii equation (4.32), which

was already implemented and applied to the transport through a three-dimensional symmetric double barrier potential [195].

Indeed, our numerical approach is sufficiently versatile to take into account also the influence of spatial and temporal *randomness*, which was completely excluded in this thesis. It would be interesting, for instance, to study the nonlinear resonant transport problem [195] in presence of external *noise*, which could be modelled by a stochastic temporal variation of the double barrier potential. Such an additional random component would probably affect the resonant transmission state shown in Figure 4.3 in a destructive way (see in this context also Refs. [224–226]), but might also play a *constructive* role when being combined with a suitable periodic driving of the quantum dot: In that case, a *stochastic resonance* might be induced [227], which would stimulate quasi-periodic transitions between low- and high-transmission scattering states that exist at the same chemical potential and the same incident current (e.g., at $\mu/(\hbar\omega_\perp) \simeq 1.1$ in Figure 4.4). Such an effect could, in practice, be implemented and observed on atom chips where external noise and weak AC components in the waveguide potential can be straightforwardly realized.

It is also interesting to investigate the influence of spatial *disorder* on the transport process of Bose-Einstein condensates. Such disorder is naturally present on atom chips, where inhomogeneities in the underlying electric wires induce random fluctuations in the waveguide potential [175–177]. An alternative and more controlled way to produce disorder for cold atoms can be achieved by superpositions of incommensurate optical lattices [228] or by means of *optical speckle potentials*, which arise from laser beams that are irradiated through a diffusive plate [229]. Recent experiments on the propagation of Bose-Einstein condensates in such optical disorder potentials [229–232] indeed revealed that the expansion process of the condensate is inhibited in presence of the disorder, and that the atomic cloud becomes trapped around prominent local minima of the external potential [230]. These findings represent an important step towards a clear-cut experimental signature of Anderson localization [233].

In Ref. [234], we applied our numerical approach to study the transport of a Bose-Einstein condensate through a one-dimensional disorder potential. The nature of this potential was inspired from the atom chip context [175–177] where smooth disorder with a finite Lorentzian-like spatial autocorrelation would generally be encountered. The central result of this investigation was that the transmission of the condensate exhibits, at finite repulsive interaction, a cross-over from an exponential (Anderson-like) to an algebraic (Ohm-like) decrease with the sample length [234] (which was also found in earlier studies focusing on the "fixed output" problem where the average transmission is determined from nonlinear stationary scattering states [235, 236]). This cross-over, which arises at a nonlinearity-dependent critical length of the disorder sample, is found to be strongly correlated to the occurrence of *permanently time-dependent scattering* of the condensate, that is, the integration

of the inhomogeneous Gross-Pitaevskii equation (4.32) in presence of an adiabatically increased source amplitude does, for sample lengths beyond that critical value, not result in a stationary scattering state, but leads to ongoing time-dependent variations of the condensate wavefunction [234]. This behaviour indicates that single atoms are scattered out of the condensed state during the propagation process, leading to a finite depletion of the condensate and to an incoherent transmission of the atomic cloud. We are, at present, investigating this depletion process by means of the "microscopic quantum dynamics" approach introduced by Köhler and Burnett [151, 152], where the condensate wavefunction is propagated together with cumulants that are associated with expectation values of products of the bosonic field operators. On the long-term scale, we plan to extend our calculations to the case of transport through two- and three-dimensional disorder, in order to study the effect of a nonlinear repulsive interaction onto the scenario of weak localization [237].

In general, we expect that the experimental and theoretical exploration of the propagation properties of cold bosonic (and fermionic) atoms will continue to provide new opportunities to investigate the interplay of chaos, disorder, interaction, and tunneling in mesoscopic transport physics. This comparatively young field of research constitutes a bridge between the physics of cold atoms and the mesoscopic science in the electronic context, what should lead to mutual benefits and inspirations for both areas.

Bibliography

[1] G. Binnig and H. Rohrer, *Scanning tunneling microscopy—from birth to adolescence*, Rev. Mod. Phys. **59**, 615 (1987).

[2] B. D. Josephson, *Possible new effects in superconductive tunnelling*, Phys. Lett. **1**, 251 (1962).

[3] L. L. Chang, L. Esaki, and R. Tsu, *Resonant tunneling in semiconductor double barriers*, Appl. Phys. Lett. **24**, 593 (1974).

[4] E. Y. Tsymbal, O. N. Mryasov, and P. R. LeClair, *Spin-dependent tunnelling in magnetic tunnel junctions*, J. Phys.: Condens. Matter **15**, R109 (2003).

[5] E. Merzbacher, *The Early History of Quantum Tunneling*, Physics Today **55**, no. 8, p. 44 (2002).

[6] S. Creagh, *Tunnelling in multidimensional systems*, in *Tunneling in Complex Systems*, edited by S. Tomsovic (World Scientific, Singapore, 1998), pp. 1–65.

[7] M. Grifoni and P. Hänggi, *Driven quantum tunneling*, Phys. Rep. **304**, 229 (1998).

[8] K. Takatsuka, H. Ushiyama, and A. Inoue-Ushiyama, *Tunneling paths in multidimensional semiclassical dynamics*, Phys. Rep. **322**, 347 (1999).

[9] C. Zener, *Non-adiabatic crossing of energy levels*, Proc. R. Soc. London **A 137**, 696 (1932).

[10] V. P. Maslov and M. V. Fedoriuk, *Semiclassical Approximations in Quantum Mechanics* (Reidel, Dordrecht, 1981).

[11] F. Hund, *On the explanation of molecular spectra I*, Z. Phys. **40**, 742 (1927).

[12] J. P. Gordon, H. J. Zeiger, and C. H. Townes, *The Maser—New Type of Microwave Amplifier, Frequency Standard, and Spectrometer*, Phys. Rev. **99**, 1264 (1955).

[13] U. Fano, *Effects of Configuration Interaction on Intensities and Phase Shifts*, Phys. Rev. **124**, 1866 (1961).

[14] G. Gamov, *The quantum theory of the atom nucleus*, Z. Phys. **51**, 204 (1928).

[15] D. N. Fittinghoff, P. R. Bolton, B. Chang, and K. C. Kulander, *Observation of nonsequential double ionization of helium with optical tunneling*, Phys. Rev. Lett. **69**, 2642 (1992).

[16] B. Walker, B. Sheehy, L. F. DiMauro, P. Agostini, K. J. Schafer, and K. C. Kulander, *Precision measurement of strong field double ionization of helium*, Phys. Rev. Lett. **73**, 1227 (1994).

[17] P. B. Corkum, *Plasma perspective on strong field multiphoton ionization*, Phys. Rev. Lett. **71**, 1994 (1993).

[18] J. B. Watson, A. Sanpera, D. G. Lappas, P. L. Knight, and K. Burnett, *Nonsequential Double Ionization of Helium*, Phys. Rev. Lett. **78**, 1884 (1997).

[19] A. Becker and F. H. M. Faisal, *Interpretation of Momentum Distribution of Recoil Ions from Laser Induced Nonsequential Double Ionization*, Phys. Rev. Lett. **84**, 3546 (2000).

[20] T. Weber, M. Weckenbrock, A. Staudte, L. Spielberger, O. Jagutzki, V. Mergel, F. Afaneh, G. Urbasch, M. Vollmer, H. Giessen, and R. Dörner, *Recoil-Ion Momentum Distributions for Single and Double Ionization of Helium in Strong Laser Fields*, Phys. Rev. Lett. **84**, 443 (2000).

[21] K. Richter, *Semiclassical Theory of Mesoscopic Quantum Systems* (Springer, Heidelberg, 2000).

[22] W. Liang, M. Bockrath, D. Bozovic, J. H. Hafner, M. Tinkham, and H. Park, *Fabry - Perot interference in a nanotube electron waveguide*, Nature **411**, 665 (2001).

[23] M. J. Davis and E. J. Heller, *Quantum dynamical tunneling in bound states*, J. Chem. Phys. **75**, 246 (1981).

[24] R. T. Lawton and M. S. Child, *Local model vibrations of water*, Mol. Phys. **37**, 1799 (1979).

[25] W. K. Hensinger, H. Häffner, A. Browaeys, N. R. Heckenberg, K. Helmerson, C. McKenzie, G. J. Milburn, W. D. Phillips, S. L. Rolston, H. Rubinsztein-Dunlop, and B. Upcroft, *Dynamical tunneling of ultracold atoms*, Nature **412**, 52 (2001).

[26] D. A. Steck, W. H. Oskay, and M. G. Raizen, *Observation of Chaos-Assisted Tunneling Between Islands of Stability*, Science **293**, 274 (2001).

[27] A. Mouchet, C. Miniatura, R. Kaiser, B. Grémaud, and D. Delande, *Chaos-assisted tunneling with cold atoms*, Phys. Rev. E **64**, 016221 (2001).

[28] A. Mouchet and D. Delande, *Signatures of chaotic tunneling*, Phys. Rev. E **67**, 046216 (2003).

[29] C. Dembowski, H.-D. Gräf, A. Heine, R. Hofferbert, H. Rehfeld, and A. Richter, *First Experimental Evidence for Chaos-Assisted Tunneling in a Microwave Annular Billiard*, Phys. Rev. Lett. **84**, 867 (2000).

[30] J. U. Nöckel and A. D. Stone, *Ray and wave chaos in asymmetric resonant optical cavities*, Nature **385**, 45 (1997).

[31] H.-J. Stöckmann, *Quantum Chaos: an introduction* (Cambridge University Press, Cambridge, 1999).

[32] I. C. Percival, *Regular and irregular spectra*, J. Phys. B **6**, L229 (1973).

[33] P. Schlagheck, *Das Drei-Körper-Coulombproblem unter periodischem Antrieb*, Dissertation, Technische Universität München, 1999.

[34] P. Schlagheck and A. Buchleitner, *Classical support for nondispersive two-electron wave packets in the driven helium atom*, J. Phys. B **31**, L489 (1998).

[35] P. Schlagheck and A. Buchleitner, *Stable classical configurations in strongly driven helium*, Physica D **131**, 110 (1999).

[36] P. Schlagheck and A. Buchleitner, *Nondispersive two-electron wave packets in the collinear driven helium atom*, Europhys. Lett. **46**, 24 (1999).

[37] P. Schlagheck and A. Buchleitner, *Nondispersive two-electron wave packets in driven helium*, Eur. Phys. J. D **22**, 401 (2003).

[38] J. Madroñero, P. Schlagheck, L. Hilico, B. Grémaud, D. Delande, and A. Buchleitner, *Decay rates of planar helium*, Europhys. Lett. **70**, 183 (2005).

[39] H. Friedrich, *Theoretical Atomic Physics*, 2nd ed. (Springer, Berlin, 1994).

[40] M. Abramowitz and I. A. Stegun, *Handbook of Mathematical Functions*, 10 ed. (National Bureau of Standards, Washington, 1972).

[41] W. F. Miller and T. F. George, *Analytic Continuation of Classical Mechanics for Classically Forbidden Collision Processes*, J. Chem. Phys. **56**, 5668 (1972).

[42] M. V. Berry and K. E. Mount, *Semiclassical approximations in wave mechanics*, Rep. Prog. Phys. **35**, 315 (1972).

[43] S. C. Creagh, *Tunnelling in multidimensional systems*, J. Phys. A **27**, 4969 (1994).

[44] A. J. Lichtenberg and M. A. Lieberman, *Regular and Stochastic Motion* (Springer-Verlag, New York, 1983).

[45] J. M. Greene and I. C. Percival, *Hamiltonian maps in the complex plane*, Physica **3D**, 530 (1981).

[46] M. Wilkinson, *Tunnelling between tori in phase space*, Physica **21D**, 341 (1986).

[47] J. Bardeen, *Tunnelling from a Many-Particle Point of View*, Phys. Rev. Lett. **6**, 201359 (1961).

[48] S. Takada and H. Nakamura, *Wentzel-Kramers-Brillouin theory of multidimensional tunneling: General theory for energy splitting*, J. Chem. Phys. **100**, 98 (1994).

[49] S. Takada, P. N. Walker, and M. Wilkinson, *Transfer-matrix approach to tunneling between Kolmogorov-Arnold-Moser tori*, Phys. Rev. A **52**, 3546 (1995).

[50] S. Takada, *Multidimensional tunneling in terms of complex classical mechanics: Wave functions, energy splittings, and decay rates in nonintegrable systems*, J. Chem. Phys. **104**, 3742 (1996).

[51] S. C. Creagh and M. D. Finn, *Evanescent coupling between discs: a model for near-integrable tunnelling*, J. Phys. A **34**, 3791 (2001).

[52] G. C. Smith and S. C. Creagh, *Tunnelling in near-integrable systems*, J. Phys. A **39**, 8283 (2006).

[53] M. C. Gutzwiller, *Chaos in Classical and Quantum Mechanics* (Springer, New York, 1990).

[54] S. C. Creagh and N. D. Whelan, *Complex Periodic Orbits and Tunneling in Chaotic Potentials*, Phys. Rev. Lett. **77**, 4975 (1996).

[55] S. C. Creagh and N. D. Whelan, *A Matrix Element for Chaotic Tunnelling Rates and Scarring Intensities*, Ann. Phys. **272**, 196 (1999).

[56] S. C. Creagh and N. D. Whelan, *Homoclinic Structure Controls Chaotic Tunneling*, Phys. Rev. Lett. **82**, 5237 (1999).

[57] A. Shudo and K. S. Ikeda, *Complex Classical Trajectories and Chaotic Tunneling*, Phys. Rev. Lett. **74**, 682 (1995).

[58] A. Shudo and K. S. Ikeda, *Stokes Phenomenon in Chaotic Systems: Pruning Trees of Complex Paths with Principle of Exponential Dominance*, Phys. Rev. Lett. **76**, 4151 (1996).

[59] A. Shudo and K. S. Ikeda, *Chaotic tunneling: A remarkable manifestation of complex classical dynamics in non-integrable quantum phenomena*, Physica D **115**, 234 (1998).

[60] A. Shudo, Y. Ishii, and K. S. Ikeda, *Julia set describes quantum tunnelling in the presence of chaos*, J. Phys. A **35**, L225 (2002).

[61] K. Takahashi and K. S. Ikeda, *Complex Semiclassical Description of Scattering Problem in Systems with 1.5 Degrees of Freedom*, Ann. Phys. **283**, 94 (2000).

[62] T. Onishi, A. Shudo, K. S. Ikeda, and K. Takahashi, *Tunneling mechanism due to chaos in a complex phase space*, Phys. Rev. E **64**, 025201 (2001).

[63] K. Takahashi and K. S. Ikeda, *Complex-classical mechanism of the tunnelling process in strongly coupled 1.5-dimensional barrier systems*, J. Phys. A **36**, 7953 (2003).

[64] K. Takahashi and K. S. Ikeda, *An intrinsic multi-dimensional mechanism of barrier tunneling*, Europhys. Lett. **71**, 193 (2005).

[65] W. A. Lin and L. E. Ballentine, *Quantum tunneling and chaos in a driven anharmonic oscillator*, Phys. Rev. Lett. **65**, 2927 (1990).

[66] F. Grossmann, T. Dittrich, P. Jung, and P. Hänggi, *Coherent destruction of tunneling*, Phys. Rev. Lett. **67**, 516 (1991).

[67] J. Plata and J. M. Gomez Llorente, *Classical-quantum correspondence for barrier crossing in a driven bistable potential*, J. Phys. A **25**, L303 (1992).

[68] R. Utermann, T. Dittrich, and P. Hänggi, *Tunneling and the onset of chaos in a driven bistable system*, Phys. Rev. E **49**, 273 (1994).

[69] O. Bohigas, S. Tomsovic, and D. Ullmo, *Manifestation of classical phase space structures in quantum mechanics*, Phys. Rep. **223**, 43 (1993).

[70] S. Tomsovic and D. Ullmo, *Chaos-assisted tunneling*, Phys. Rev. E **50**, 145 (1994).

[71] F. Leyvraz and D. Ullmo, *The level splitting distribution in chaos-assisted tunneling*, J. Phys. A **29**, 2529 (1996).

[72] R. Roncaglia, L. Bonci, F. M. Izrailev, B. J. West, and P. Grigolini, *Tunneling versus Chaos in the Kicked Harper Model*, Phys. Rev. Lett. **73**, 802 (1994).

[73] O. Bohigas, D. Boosé, R. Egydio de Carvalho, and V. Marvulle, *Quantum tunneling and chaotic dynamics*, Nucl. Phys. A **560**, 197 (1993).

[74] E. Doron and S. D. Frischat, *Semiclassical Description of Tunneling in Mixed Systems: Case of the Annular Billiard*, Phys. Rev. Lett. **75**, 3661 (1995).

[75] S. D. Frischat and E. Doron, *Dynamical tunneling in mixed systems*, Phys. Rev. E **57**, 1421 (1998).

[76] To be most precise, $|v_-\rangle$, $|v_+\rangle$ and $|v_c\rangle$ are assumed to result from separate pre-diagonalizations of the Hamiltonian in the regular and chaotic phase space regions, respectively, without taking into account the coupling between them.

[77] Without loss of generality, we restrict ourselves to time-reversal invariant systems. The matrix elements that arise in the Hamiltonian can therefore assumed to be real.

[78] V. Averbukh, S. Osovski, and N. Moiseyev, *Controlled Tunneling of Cold Atoms: From Full Suppression to Strong Enhancement*, Phys. Rev. Lett. **89**, 253201 (2002).

[79] F. Haake, *Quantum Signatures of Chaos*, 2nd ed. (Springer, Berlin, 2001).

[80] A. Bäcker, R. Ketzmerick, and A. G. Monastra, *Flooding of Chaotic Eigenstates into Regular Phase Space Islands*, Phys. Rev. Lett. **94**, 054102 (2005).

[81] R. S. MacKay, J. D. Meiss, and I. C. Percival, *Stochasticity and Transport in Hamiltonian Systems*, Phys. Rev. Lett. **52**, 697 (1984).

[82] L. Bonci, A. Farusi, P. Grigolini, and R. Roncaglia, *Tunneling rate fluctuations induced by nonlinear resonances: A quantitative treatment based on semiclassical arguments*, Phys. Rev. E **58**, 5689 (1998).

[83] T. Uzer, D. W. Noid, and R. A. Marcus, *Uniform semiclassical theory of avoided crossings*, J. Chem. Phys. **79**, 4412 (1983).

[84] A. M. Ozorio de Almeida, *Tunneling and the Semiclassical Spectrum for an Isolated Classical Resonance*, J. Phys. Chem. **88**, 6139 (1984).

[85] A. A. Stuchebrukhov and R. A. Marcus, *Perturbation theory approach to dynamical tunneling splitting of local mode vibrational states in ABA molecules*, J. Chem. Phys. **98**, 8443 (1993).

[86] O. Brodier, P. Schlagheck, and D. Ullmo, *Resonance-Assisted Tunneling in Near-Integrable Systems*, Phys. Rev. Lett. **87**, 064101 (2001).

[87] O. Brodier, P. Schlagheck, and D. Ullmo, *Resonance-Assisted Tunneling*, Ann. Phys. **300**, 88 (2002).

[88] P. Leboeuf, J. Kurchan, M. Feingold, and D. P. Arovas, *Phase-space localization: Topological aspects of quantum chaos*, Phys. Rev. Lett. **65**, 3076 (1990).

[89] P. Leboeuf, J. Kurchan, M. Feingold, and D. P. Arovas, *Topological aspects of quantum chaos*, CHAOS **2**, 125 (1992).

[90] M. Sheinman, S. Fishman, I. Guarneri, and L. Rebuzzini, *Decay of quantum accelerator modes*, Phys. Rev. A **73**, 052110 (2006).

[91] S. Keshavamurthy, *Dynamical tunneling in molecules: Role of the classical resonances and chaos*, J. Chem. Phys. **119**, 161 (2003).

[92] S. Keshavamurthy, *On dynamical tunneling and classical resonances*, J. Chem. Phys **122**, 114109 (2005).

[93] S. Keshavamurthy, *Resonance-assisted tunneling in three degrees of freedom without discrete symmetry*, Phys. Rev. E **72**, 045203(R) (2005).

[94] B. V. Chirikov, *A universal instability of many-dimensional oscillator systems*, Phys. Rep. **52**, 265 (1979).

[95] For the "direct" (arithmetic) average of ΔE, the cutoff of the probability distribution at large splittings $\Delta E \sim 2V_{\text{eff}}$ would have to be taken into account, since $\int \Delta E P(\Delta E) d(\Delta E)$ diverges for the Cuchy distribution (3.6).

[96] V. A. Podolskiy and E. E. Narimanov, *Semiclassical Description of Chaos-Assisted Tunneling*, Phys. Rev. Lett. **91**, 263601 (2003).

[97] C. Eltschka and P. Schlagheck, *Resonance- and chaos-assisted tunneling in mixed regular-chaotic systems*, Phys. Rev. Lett. **94**, 014101 (2005).

[98] P. Schlagheck, C. Eltschka, and D. Ullmo, *Resonance- and Chaos-Assisted Tunneling*, in *Progress in Ultrafast Intense Laser Science I*, edited by K. Yamanouchi, S. L. Chin, P. Agostini, and G. Ferrante (Springer, Berlin, 2006), pp. 107–131.

[99] B. Kramer and A. MacKinnon, *Localization: theory and experiment*, Rep. Prog. Phys. **56**, 1469 (1993).

[100] C. W. J. Beenakker, *Random-matrix theory of quantum transport*, Rev. Mod. Phys. **69**, 731 (1997).

[101] A. Mouchet, C. Eltschka, and P. Schlagheck, *Influence of classical resonances on chaotic tunnelling*, Phys. Rev. E, in press (2006).

[102] In the case of the driven pendulum that was studied in Ref. [27], the relevant resonance turned out to be located *outside* the regular island, i.e. within the chaotic domain. A quantitative prediction of the tunneling rates by our semi-classical approach, which is perturbative by nature and relies on the existence of well-preserved separatrix structures, was not possible for this case.

[103] R. Ketzmerick, L. Hufnagel, F. Steinbach, and M. Weiss, *New Class of Eigenstates in Generic Hamiltonian Systems*, Phys. Rev. Lett. **85**, 1214 (2000).

[104] T. Geisel, G. Radons, and J. Rubner, *Kolmogorov-Arnol'd-Moser Barriers in the Quantum Dynamics of Chaotic Systems*, Phys. Rev. Lett. **57**, 2883 (1986).

[105] N. T. Maitra and E. J. Heller, *Quantum transport through cantori*, Phys. Rev. E **61**, 3620 (2000).

[106] J. Zakrzewski, D. Delande, and A. Buchleitner, *Ionization via chaos-assisted tunneling*, Phys. Rev. E **57**, 1458 (1998).

[107] G. P. Berman and G. M. Zaslavsky, *Theory of quantum nonlinear resonance*, Phys. Lett. **61A**, 295 (1977).

[108] A. Buchleitner, *Atomes de Rydberg en champ micro-onde: regularité et chaos*, Thèse de doctorat, Université Pierre et Marie Curie, Paris, 1993.

[109] I. Bialynicki-Birula, M. Kaliński, and J. H. Eberly, *Lagrange Equilibrium Points in Celestial Mechanics and Nonspreading Wave Packets for Strongly Driven Rydberg Electrons*, Phys. Rev. Lett. **73**, 1777 (1994).

[110] A. Buchleitner and D. Delande, *Nondispersive Electronic Wave Packets in Multiphoton Processes*, Phys. Rev. Lett. **75**, 1487 (1995).

[111] J. Zakrzewski, D. Delande, and A. Buchleitner, *Nonspreading Electronic Wave Packets and Conductance Fluctuations*, Phys. Rev. Lett. **75**, 4015 (1995).

[112] M. Kaliński and J. H. Eberly, *New States of Hydrogen in a Circularly Polarized Electromagnetic Field*, Phys. Rev. Lett. **77**, 2420 (1996).

[113] A. Buchleitner, D. Delande, and J. Zakrzewski, *Non-dispersive wave packets in periodically driven quantum systems*, Phys. Rep. **368**, 409 (2002).

[114] H. Maeda and T. F. Gallagher, *Nondispersing Wave Packets*, Phys. Rev. Lett. **92**, 133004 (2004).

[115] H. Maeda, D. V. L. Norum, and T. F. Gallagher, *Microwave Manipulation of an Atomic Electron in a Classical Orbit*, Science **307**, 1757 (2005).

[116] S. Wimberger, P. Schlagheck, C. Eltschka, and A. Buchleitner, *Resonance-assisted decay of nondispersive wave packets*, Phys. Rev. Lett. **97**, 043001 (2006).

[117] G. Casati, I. Guarneri, and D. Shepelyansky, *Hydrogen Atom in Monochromatic Field: Chaos and Dynamical Photonic Localization*, IEEE J. Quant. Electron. **24**, 1420 (1988).

[118] A. Buchleitner, B. Grémaud, and D. Delande, *Wavefunctions of atomic resonances*, J. Phys. B **27**, 2663 (1994).

[119] M. H. Anderson, J. R. Ensher, M. R. Matthews, C. E. Wieman, and E. A. Cornell, *Observation of Bose-Einstein Condensation in a Dilute Atomic Vapor*, Science **269**, 198 (1995).

[120] C. C. Bradley, C. A. Sackett, J. J. Tollett, and R. G. Hulet, *Evidence of Bose-Einstein Condensation in an Atomic Gas with Attractive Interactions*, Phys. Rev. Lett. **75**, 1687 (1995).

[121] K. B. Davis, M.-O. Mewes, M. R. Andrews, N. J. van Druten, D. S. Durfee, D. M. Kurn, and W. Ketterle, *Bose-Einstein Condensation in a Gas of Sodium Atoms*, Phys. Rev. Lett. **75**, 3969 (1995).

[122] M. R. Andrews, C. G. Townsend, H.-J. Miesner, D. S. Durfee, D. M. Kurn, and W. Ketterle, *Observation of Interference Between Two Bose Condensates*, Science **275**, 637 (1997).

[123] D. S. Hall, M. R. Matthews, C. E. Wieman, and E. A. Cornell, *Measurements of Relative Phase in Two-Component Bose-Einstein Condensates*, Phys. Rev. Lett. **81**, 1543 (1998).

[124] D. S. Jin, J. R. Ensher, M. R. Matthews, C. E. Wieman, and E. A. Cornell, *Collective Excitations of a Bose-Einstein Condensate in a Dilute Gas*, Phys. Rev. Lett. **77**, 420 (1996).

[125] M.-O. Mewes, M. R. Andrews, N. J. van Druten, D. M. Kurn, D. S. Durfee, C. G. Townsend, and W. Ketterle, *Collective Excitations of a Bose-Einstein Condensate in a Magnetic Trap*, Phys. Rev. Lett. **77**, 988 (1996).

[126] M. R. Andrews, D. M. Kurn, H.-J. Miesner, D. S. Durfee, C. G. Townsend, S. Inouye, and W. Ketterle, *Propagation of Sound in a Bose-Einstein Condensate*, Phys. Rev. Lett. **79**, 553 (1997).

[127] O. M. Maragò, S. A. Hopkins, J. Arlt, E. Hodby, G. Hechenblaikner, and C. J. Foot, *Observation of the Scissors Mode and Evidence for Superfluidity of a Trapped Bose-Einstein Condensed Gas*, Phys. Rev. Lett. **84**, 2056 (2000).

[128] M. R. Matthews, B. P. Anderson, P. C. Haljan, D. S. Hall, C. E. Wieman, and E. A. Cornell, *Vortices in a Bose-Einstein Condensate*, Phys. Rev. Lett. **83**, 2498 (1999).

[129] J. R. Abo-Shaeer, C. Raman, J. M. Vogels, and W. Ketterle, *Observation of Vortex Lattices in Bose-Einstein Condensates*, Science **292**, 476 (2001).

[130] W. Ketterle, D. S. Durfee, and D. M. Stamper-Kurn, *Making, probing and understanding Bose-Einstein condensates*, in *Bose-Einstein condensation in atomic gases, Proceedings of the International School of Physics "Enrico Fermi", Course CXL*, edited by M. Inguscio, S. Stringari, and C. E. Wieman (IOS Press, Amsterdam, 1999), pp. 67–176.

[131] In the expression (4.1), the contribution of higher excited states is neglected. It is furthermore assumed that the spatial extension of the atom is much smaller than the laser wavelength.

[132] O. Morsch and M. Oberthaler, *Dynamics of Bose-Einstein condensates in optical lattices*, Rev. Mod. Phys. **78**, 179 (2006).

[133] M. Lewenstein, A. Sanpera, V. Ahufinger, B. Damski, A. Sen(De), and U. Sen, *Ultracold atomic gases in optical lattices: Mimicking condensed matter physics and beyond*, cond-mat/0606771 (2006).

[134] M. Greiner, O. Mandel, T. Esslinger, T. W. Hänsch, and I. Bloch, *Quantum phase transition from a superfluid to a Mott insulator in a gas of ultracold atoms*, Nature **415**, 39 (2002).

[135] D. Jaksch, C. Bruder, J. I. Cirac, C. W. Gardiner, and P. Zoller, *Cold Bosonic Atoms in Optical Lattices*, Phys. Rev. Lett. **81**, 3108 (1998).

[136] B. P. Anderson and M. A. Kasevich, *Macroscopic Quantum Interference from Atomic Tunnel Arrays*, Science **282**, 1686 (1998).

[137] E. E. Mendez, Agulló-Rueda, and J. M. Hong, *Stark Localization in GaAs-GaAlAs Superlattices under an Electric Field*, Phys. Rev. Lett. **60**, 2426 (1988).

[138] F. S. Cataliotti, S. Burger, C. Fort, P. Maddaloni, F. Minardi, A. Trombettoni, A. Smerzi, and M. Inguscio, *Josephson Junction Arrays with Bose-Einstein Condensates*, Science **293**, 843 (2001).

[139] O. Morsch, J. H. Müller, M. Cristiani, D. Ciampini, and E. Arimondo, *Bloch Oscillations and Mean-Field Effects of Bose-Einstein Condensates in 1D Optical Lattices*, Phys. Rev. Lett. **87**, 140402 (2001).

[140] A. Buchleitner and A. R. Kolovsky, *Interaction-Induced Decoherence of Atomic Bloch Oscillations*, Phys. Rev. Lett. **91**, 253002 (2003).

[141] D. Witthaut, M. Werder, S. Mossmann, and H. J. Korsch, *Bloch oscillations of Bose-Einstein condensates: Breakdown and revival*, Phys. Rev. E **71**, 036625 (2005).

[142] T. Anker, M. Albiez, R. Gati, S. Hunsmann, B. Eiermann, A. Trombettoni, and M. K. Oberthaler, *Nonlinear Self-Trapping of Matter Waves in Periodic Potentials*, Phys. Rev. Lett. **94**, 020403 (2005).

[143] K. K. Likharev, *Superconducting weak links*, Rev. Mod. Phys. **51**, 000101 (1979).

[144] A. Smerzi, S. Fantoni, S. Giovanazzi, and S. R. Shenoy, *Quantum Coherent Atomic Tunneling between Two Trapped Bose-Einstein Condensates*, Phys. Rev. Lett. **79**, 4950 (1997).

[145] C. J. Pethick and H. Smith, *Bose-Einstein Condensation in Dilute Gases* (Cambridge University Press, Cambridge, 2002).

[146] J. Weiner, V. S. Bagnato, S. Zilio, and P. S. Julienne, *Experiments and theory in cold and ultracold collisions*, Rev. Mod. Phys. **71**, 1 (1999).

[147] A. D. Jackson, G. M. Kavoulakis, and C. J. Pethick, *Solitary waves in clouds of Bose-Einstein condensed atoms*, Phys. Rev. A **58**, 2417 (1998).

[148] F. Dalfovo, S. Giorgini, L. P. Pitaevskii, and S. Stringari, *Theory of Bose-Einstein condensation in trapped gases*, Rev. Mod. Phys. **71**, 463 (1999).

[149] Y. Castin and R. Dum, *Low-temperature Bose-Einstein condensates in time-dependent traps: Beyond the U(1) symmetry-breaking approach*, Phys. Rev. A **57**, 3008 (1998).

[150] S. A. Morgan, S. Choi, K. Burnett, and M. Edwards, *Nonlinear mixing of quasiparticles in an inhomogeneous Bose condensate*, Phys. Rev. A **57**, 3818 (1998).

[151] T. Köhler and K. Burnett, *Microscopic quantum dynamics approach to the dilute condensed Bose gas*, Phys. Rev. A **65**, 033601 (2002).

[152] T. Köhler, T. Gasenzer, and K. Burnett, *Microscopic theory of atom-molecule oscillations in a Bose-Einstein condensate*, Phys. Rev. A **67**, 013601 (2003).

[153] G. J. Milburn, J. Corney, E. M. Wright, and D. F. Walls, *Quantum dynamics of an atomic Bose-Einstein condensate in a double-well potential*, Phys. Rev. A **55**, 4318 (1997).

[154] S. Raghavan, A. Smerzi, S. Fantoni, and S. R. Shenoy, *Coherent oscillations between two weakly coupled Bose-Einstein condensates: Josephson effects, π oscillations, and macroscopic quantum self-trapping*, Phys. Rev. A **59**, 620 (1999).

[155] S. Raghavan, A. Smerzi, and V. M. Kenkre, *Transitions in coherent oscillations between two trapped Bose-Einstein condensates*, Phys. Rev. A **60**, R1787 (1999).

[156] N. Tsukada, M. Gotoda, Y. Nomura, and T. Isu, *Laser-assisted coherent atomic tunneling between two trapped Bose-Einstein condensates*, Phys. Rev. A **59**, 3862 (1999).

[157] S. Wimberger, R. Mannella, O. Morsch, E. Arimondo, A. Kolovsky, and A. Buchleitner, *Nonlinearity induced destruction of resonant tunneling in the Wannier-Stark problem*, Phys. Rev. A **72**, 063610 (2005).

[158] M. Holthaus, *Towards coherent control of a Bose-Einstein condensate in a double well*, Phys. Rev. A **64**, 011601 (2001).

[159] M. Holthaus and S. Stenholm, *Coherent control of the self-trapping transition*, Eur. Phys. J. B **20**, 451 (2001).

[160] C. Weiss and T. Jinasundera, *Coherent control of mesoscopic tunneling in a Bose-Einstein condensate*, Phys. Rev. A **72**, 053626 (2005).

[161] W. S. Warren, H. Rabitz, and M. Dahleh, *Coherent control of quantum dynamics: the dream is alive*, Science **259**, 1581 (1993).

[162] A. Micheli, D. Jaksch, J. I. Cirac, and P. Zoller, *Many-particle entanglement in two-component Bose-Einstein condensates*, Phys. Rev. A **67**, 013607 (2003).

[163] R. Dumke, T. Müther, M. Volk, W. Ertmer, and G. Birkl, *Interferometer-Type Structures for Guided Atoms*, Phys. Rev. Lett. 89, 220402 (2002) **89**, 220402 (2002).

[164] R. Folman, P. Krüger, J. Denschlag, C. Henkel, and J. Schmiedmayer, *Microscopic atom optics: From wires to an Atom Chip*, Adv. At. Mol. Opt. Phys. **48**, 263 (2002).

[165] J. Denschlag, D. Cassettari, and J. Schmiedmayer, *Guiding Neutral Atoms with a Wire*, Phys. Rev. Lett. **82**, 2014 (1999).

[166] R. Folman, P. Krüger, D. Cassettari, B. Hessmo, T. Maier, and J. Schmiedmayer, *Controlling Cold Atoms using Nanofabricated Surfaces: Atom Chips*, Phys. Rev. Lett. **84**, 4749 (2000).

[167] H. Ott, J. Fortagh, G. Schlotterbeck, A. Grossmann, and C. Zimmermann, *Bose-Einstein Condensation in a Surface Microtrap*, Phys. Rev. Lett. **87**, 230401 (2001).

[168] W. Hänsel, P. Hommelhoff, T. W. Hänsch, and J. Reichel, *Bose-Einstein Condensation on a microelectronic chip*, Nature **413**, 498 (2001).

[169] H. Ott, J. Fortágh, S. Kraft, A. Günther, D. Komma, and C. Zimmermann, *Nonlinear Dynamics of a Bose-Einstein Condensate in a Magnetic Waveguide*, Phys. Rev. Lett. **91**, 040402 (2003).

[170] D. Cassettari, B. Hessmo, R. Folman, T. Maier, and J. Schmiedmayer, *Beam Splitter for Guided Atoms*, Phys. Rev. Lett. **85**, 5483 (2000).

[171] E. Andersson, T. Calarco, R. Folman, M. Andersson, B. Hessmo, and J. Schmiedmayer, *Multimode Interferometer for Guided Matter Waves*, Phys. Rev. Lett. **88**, 100401 (2002).

[172] Y.-J. Wang, D. Z. Anderson, V. M. Bright, E. A. Cornell, Q. Diot, T. Kishimoto, M. Prentiss, R. A. Saravanan, S. R. Segal, and S. Wu, *Atom Michelson Interferometer on a Chip Using a Bose-Einstein Condensate*, Phys. Rev. Lett. **94**, 090405 (2005).

[173] T. Schumm, S. Hofferberth, L. M. Andersson, S. Wildermuth, S. Groth, I. Bar-Joseph, J. Schmiedmayer, and P. Krüger, *Matter-wave interferometry in a double well on an atom chip*, Nature Physics **1**, 57 (2005).

[174] A. Günther, S. Kraft, M. Kemmler, D. Koelle, R. Kleiner, C. Zimmermann, and J. Fortágh, *Diffraction of a Bose-Einstein Condensate from a Magnetic Lattice on a Microchip*, Phys. Rev. Lett. **95**, 170405 (2005).

[175] J. Fortágh, H. Ott, S. Kraft, A. Günther, and C. Zimmermann, *Surface effects in magnetic microtraps*, Phys. Rev. A **66**, 041604(R) (2002).

[176] J. Estève, C. Aussibal, T. Schumm, C. Figl, D. Mailly, I. Bouchoule, C. I. Westbrook, and A. Aspect, *Role of wire imperfections in micromagnetic traps for atoms*, Phys. Rev. A **70**, 043629 (2004).

[177] D.-W. Wang, M. D. Lukin, and E. Demler, *Disordered Bose-Einstein Condensates in Quasi-One-Dimensional Magnetic Microtraps*, Phys. Rev. Lett. **92**, 076802 (2004).

[178] J. H. Thywissen, R. M. Westervelt, and M. Prentiss, *Quantum Point Contacts for Neutral Atoms*, Phys. Rev. Lett. **83**, 3762 (1999).

[179] P. Leboeuf and N. Pavloff, *Bose-Einstein beams: Coherent propagation through a guide*, Phys. Rev. A **64**, 033602 (2001).

[180] P. Leboeuf, N. Pavloff, and S. Sinha, *Solitonic transmission of Bose-Einstein matter waves*, Phys. Rev. A **68**, 063608 (2003).

[181] I. Carusotto, *Nonlinear atomic Fabry-Perot interferometer: From the mean-field theory to the atom blockade effect*, Phys. Rev. A **63**, 023610 (2001).

[182] I. Carusotto and G. C. La Rocca, *Modulated Optical Lattice as an Atomic Fabry-Perot Interferometer*, Phys. Rev. Lett. **84**, 399 (1999).

[183] C. Menotti and S. Stringari, *Collective oscillations of a one-dimensional trapped Bose-Einstein gas*, Phys. Rev. A **66**, 043610 (2002).

[184] M. Olshanii, *Atomic Scattering in the Presence of an External Confinement and a Gas of Impenetrable Bosons*, Phys. Rev. Lett. **81**, 938 (1998).

[185] I. Bloch, T. W. Hänsch, and T. Esslinger, *Atom Laser with a cw Output Coupler*, Phys. Rev. Lett. **82**, 3008 (1998).

[186] L. D. Landau and E. M. Lifschitz, *Lehrbuch der theoretischen Physik; Band I: Mechanik* (Akademie-Verlag, Berlin, 1976).

[187] T. Paul, *Transport von Bose-Einstein Kondensaten in mesoskopischen Strukturen*, Dissertation, Universität Regensburg, 2006.

[188] T. Shibata, *Absorbing boundary conditions for the finite-difference time-domain calculation of the one-dimensional Schrödinger equation*, Phys. Rev. B **43**, 6760 (1991).

[189] M. Lakshmanan and S. Rajasekar, *Nonlinear Dynamics* (Springer, Berlin, 2003).

[190] R. W. Boyd, *Nonlinear Optics* (Academic Press, London, 1992).

[191] V. J. Goldman, D. C. Tsui, and J. E. Cunningham, *Observation of intrinsic bistability in resonant tunneling structures*, Phys. Rev. Lett. **58**, 1256 (1987).

[192] C. Presilla, G. Jona-Lasinio, and F. Capasso, *Nonlinear feedback oscillations in resonant tunneling through double barriers*, Phys. Rev. B **43**, 5200 (1991).

[193] M. Y. Azbel', *Quantum turbulence and resonant tunneling*, Phys. Rev. B **59**, 8049 (1999).

[194] I. Zapata and F. Sols, *Supercurrent flow through an effective double-barrier structure*, Phys. Rev. B **53**, 6693 (1996).

[195] T. Paul, K. Richter, and P. Schlagheck, *Nonlinear Resonant Transport of Bose-Einstein Condensates*, Phys. Rev. Lett. **94**, 020404 (2005).

[196] C. Mahaux and H. A. Weidenmüller, *Shell-Model Approach to Nuclear Reactions* (North-Holland, Amsterdam, 1969).

[197] J. J. M. Verbaarschot, H. A. Weidenmüller, and M. R. Zirnbauer, *Grassmann integration in stochastic quantum physics: The case of compound-nucleus scattering*, Phys. Rep. **129**, 367 (1985).

[198] Y. V. Fyodorov and H.-J. Sommers, *Statistics of resonance poles, phase shifts and time delays in quantum chaotic scattering: Random matrix approach for systems with broken time-reversal invariance*, J. Math. Phys. **38**, 1918 (1997).

[199] H. Feshbach, *Unified theory of nuclear reactions*, Ann. Phys. (N.Y.) **5**, 357 (1958).

[200] H. Feshbach, *A unified theory of nuclear reactions. II*, Ann. Phys. (N.Y.) **19**, 287 (1962).

[201] C. Viviescas and G. Hackenbroich, *Field quantization for open optical cavities*, Phys. Rev. A **67**, 013805 (2003).

[202] C. Cohen-Tannoudji, J. Dupont-Roc, and G. Grynberg, *Atom-Photon Interactions* (Wiley, New York, 1992).

[203] In addition to the decay rate γ_0, the coupling to the continuum induces also a finite *shift* of the energy level μ_0 of the quasi-bound state. This shift is neglected in the following.

[204] E. Balslev and J. M. Combes, *Spectral properties of many-body Schrödinger operators with dilatation-analytic interactions*, Commun. Math. Phys. **22**, 280 (1971).

[205] W. P. Reinhardt, *Complex coordinates in the theory of atomic and molecular structure and dynamics*, Ann. Rev. Phys. Chem. **33**, 223 (1982).

[206] N. Moiseyev, *Quantum theory of resonances: calculating energies, widths and cross-sections by complex scaling*, Phys. Rep. **302**, 212 (1998).

[207] A. J. F. Siegert, *On the Derivation of the Dispersion Formula for Nuclear Reactions*, Phys. Rev. **56**, 750 (1939).

[208] P. Schlagheck and T. Paul, *Complex scaling approach to the decay of Bose-Einstein condensates*, Phys. Rev. A **73**, 023619 (2006).

[209] S. Wimberger, P. Schlagheck, and R. Mannella, *Tunnelling rates for the nonlinear Wannier-Stark problem*, J. Phys. B **39**, 729 (2006).

[210] N. Moiseyev, L. D. Carr, B. A. Malomed, and Y. B. Band, *Transition from Resonances to Bound States in Nonlinear Systems: Application to Bose-Einstein condensates*, J. Phys. B **37**, L193 (2004).

[211] T. Paul, M. Hartung, K. Richter, and P. Schlagheck, in preparation.

[212] K. Rapedius, D. Witthaut, and H. J. Korsch, *Analytical study of resonant transport of Bose-Einstein condensates*, Phys. Rev. A **73**, 033608 (2006).

[213] R. Artuso and L. Rebuzzini, *Effects of a nonlinear perturbation on dynamical tunneling in cold atoms*, Phys. Rev. E 68, 036221 (2003) **68**, 036221 (2003).

[214] W. K. Hensinger, A. Mouchet, P. S. Julienne, D. Delande, N. R. Heckenberg, and H. Rubinsztein-Dunlop, *Analysis of dynamical tunneling experiments with a Bose-Einstein condensate*, Phys. Rev. A **70**, 013408 (2004).

[215] F. K. Abdullaev and R. A. Kraenkel, *Coherent atomic oscillations and resonances between coupled Bose-Einstein condensates with time-dependent trapping potential*, Phys. Rev. A **62**, 023613 (2000).

[216] C. Lee, W. Hai, L. Shi, X. Zhu, and K. Gao, *Chaotic and frequency-locked atomic population oscillations between two coupled Bose-Einstein condensates*, Phys. Rev. A **64**, 053604 (2001).

[217] G. L. Salmond, C. A. Holmes, and G. J. Milburn, *Dynamics of a strongly driven two-component Bose-Einstein condensate*, Phys. Rev. A **65**, 033623 (2002).

[218] A. Eckardt, T. Jinasundera, C. Weiss, and M. Holthaus, *Analog of Photon-Assisted Tunneling in a Bose-Einstein Condensate*, Phys. Rev. Lett. **95**, 200401 (2005).

[219] M. Fliesser, A. Csordás, R. Graham, and P. Szépfalusy, *Classical quasiparticle dynamics in trapped Bose condensates*, Phys. Rev. A **56**, 4879 (1997).

[220] A. Csordás, R. Graham, and P. Szépfalusy, *Semiclassical wave functions and energy levels of Bose-condensed gases in spherically symmetric traps*, Phys. Rev. A **56**, 5179 (1997).

[221] M. Fliesser and R. Graham, *Classical quasiparticle dynamics and chaos in trapped Bose condensates*, Physica D **131**, 141 (1999).

[222] K. Richter and M. Sieber, *Semiclassical Theory of Chaotic Quantum Transport*, Phys. Rev. Lett. **89**, 206801 (2002).

[223] S. Heusler, S. Müller, P. Braun, and F. Haake, *Semiclassical Theory of Chaotic Conductors*, Phys. Rev. Lett. **96**, 066804 (2006).

[224] C. Henkel, S. Pötting, and M. Wilkens, *Loss and heating of particles in small and noisy traps*, Appl. Phys. B **69**, 379 (1999).

[225] C. Henkel, P. Krüger, R. Folman, and J. Schmiedmayer, *Fundamental limits for coherent manipulation on atom chips*, Appl. Phys. B **76**, 173 (2003).

[226] C. Schroll, W. Belzig, and C. Bruder, *Decoherence of cold atomic gases in magnetic microtraps*, Phys. Rev. A **68**, 043618 (2003).

[227] L. Gammaitoni, P. Hänggi, P. Jung, and F. Marchesoni, *Stochastic resonance*, Rev. Mod. Phys. **70**, 223 (1998).

[228] B. Damski, J. Zakrzewski, L. Santos, P. Zoller, and M. Lewenstein, *Atomic Bose and Anderson Glasses in Optical Lattices*, Phys. Rev. Lett. **91**, 080403 (2003).

[229] J. E. Lye, L. Fallani, M. Modugno, D. S. Wiersma, C. Fort, and M. Inguscio, *Bose-Einstein Condensate in a Random Potential*, Phys. Rev. Lett. **95**, 070401 (2005).

[230] C. Fort, L. Fallani, V. Guarrera, J. E. Lye, M. Modugno, D. S. Wiersma, and M. Inguscio, *Effect of Optical Disorder and Single Defects on the Expansion of a Bose-Einstein Condensate in a One-Dimensional Waveguide*, Phys. Rev. Lett. **95**, 170410 (2005).

[231] D. Clément, A. F. Varón, M. Hugbart, J. A. Retter, P. Bouyer, L. Sanchez-Palencia, D. M. Gangardt, G. V. Shlyapnikov, and A. Aspect, *Suppression of Transport of an Interacting Elongated Bose-Einstein Condensate in a Random Potential*, Phys. Rev. Lett. **95**, 170409 (2005).

[232] T. Schulte, S. Drenkelforth, J. Kruse, W. Ertmer, J. Arlt, K. Sacha, J. Zakrzewski, and M. Lewenstein, *Routes Towards Anderson-Like Localization of Bose-Einstein Condensates in Disordered Optical Lattices*, Phys. Rev. Lett. **95**, 170411 (2005).

[233] P. W. Anderson, *Absence of Diffusion in Certain Random Lattices*, Phys. Rev. **109**, 1492 (1958).

[234] T. Paul, P. Leboeuf, N. Pavloff, K. Richter, and P. Schlagheck, *Nonlinear transport of Bose-Einstein condensates through waveguides with disorder*, Phys. Rev. A **72**, 063621 (2005).

[235] P. Devillard and B. Souillard, *Polynomially decaying transmission for the nonlinear Schrödinger equation in a random medium*, J. Stat. Phys. **43**, 423 (1986).

[236] R. Knapp, G. Papanicolaou, and B. White, *Transmission of waves by a nonlinear random medium*, J. Stat. Phys. **63**, 567 (1991).

[237] *Mesoscopic quantum physics*, *Proceedings of the Les Houches Summer School, Session LXI*, edited by E. Akkermans, G. Montambaux, J.-L. Pichard, and J. Zinn-Justin (Elsevier Science B. V., Amsterdam, 1995).